

https://dspace.org/

The preparation and characteristics of cBN ceramics with Al-based binder phases

Sithebe, Humphrey Samkelo Lungisani

2008-12-09T08:47:10Z
http://hdl.handle.net/10539/5876

Downloaded from a DSpace repository. https://dspace.org/

THE PREPARATION AND CHARACTERISTICS OF cBN CERAMICS WITH AL-BASED BINDER PHASES

by

Humphrey Samkelo Lungisani Sithebe

A thesis submitted to the Faculty of Science,
University of the Witwatersrand,
Johannesburg
in partial fulfilment of the requirements for the degree of
Doctor of Philosophy (Physics)

Supervisors: Prof. D.S. McLachlan and Prof. I Sigalas

2007

DECLARATION

I declare that this thesis is my own, unaided work. It is being submitted for the Degree of Doctor of Philosophy in the University of Witwatersrand, Johannesburg. It has not been submitted before for any degree or examination in any other University.

(Signature of candidate)

---------- day of----------2007

ABSTRACT

The goal of this PhD thesis was to develop dense aluminium compound-cubic boron nitride composites with a high cBN content. To achieve this goal, two different strategies were used: infiltration of cBN preforms and hot pressing of cBN-Al mixtures. The particle size of the cBN and the amount of aluminium were systematically varied and the influence of these parameters on densification and selected properties was evaluated. A basic understanding of the product that was formed over certain temperatures and times provides information that can be used in optimizing the infiltration and hot pressing of cBN with Al. For this reason, the reaction kinetics between Al and cBN was initially investigated.

The reaction kinetics of the chemical interactions between Al and cBN was investigated in detail using X-ray diffraction (XRD) and scanning electron microscopy (SEM). The reaction was studied using samples containing 50 volume percent of Al and 50 volume percent of cBN (12 μm) hot pressed at 800 ^{o}C. The prepared samples were allowed to react isothermally at temperatures between 1 000 ^{o}C and 1 400 ^{o}C under nitrogen (N_2) and argon (Ar) atmospheres. It was found that the degree and rate of the reactions increased with increasing temperature in both N_2 and Ar atmospheres. The degree of aluminium nitride (AlN) formation was considerably higher under N_2 than under Ar. The difference in the formation of AlN between the two atmospheres was attributed to the reaction of N_2 gas with the sample due to the open porosity.

The infiltration of partially hexagonalized cBN matrix with molten Al was studied. The samples were found to have a density higher than 97% of the theoretical density. It was found that the amount of soft hBN phase present in the sample (due to hexagonalization) increases at temperatures higher than 1 300 ^{o}C, resulting in a hardness of the final material of H_v10 = 6.5 ± 4.8 GPa. Because of thie poor hardness this route was abandoned.

Cubic boron nitride powder (12 μm) without hexagonal boron nitride (hBN) was also infiltrated with aluminium. The infiltrated samples were found to exhibit a density higher than 96% of the theoretical density. The Al reacted with cBN and no hBN was observed at temperatures below 1 400 ^{o}C. The resulting product showed a Vickers hardness of H_v10 = 14.4 ± 1.6 GPa compared with H_v10 = 6.5 ± 4.8 GPa obtained with the partially hexagonalized cBN matrix. Infiltration of 3 μm cubic boron nitride increased the Vickers hardness to 22.0 ± 0.6 GPa. However, this infiltration was not very reproducible.

Al-cBN cermets were hot pressed at temperatures between 800 ^{o}C and 1 750 ^{o}C and at a pressure of 50 MPa in vacuum. The effect of the particle size of the starting powders, as well as the effect of the starting compositions and temperature, was investigated. The materials could only densify up to 80 – 92% of the theoretical density. After hot pressing at 800 ^{o}C, only Al and cBN could be observed by XRD, whereas higher hot-pressing temperatures resulted in the formation of AlN and AlB_2 which retard the densification. The microstructure of the hot-pressed materials was studied using SEM. It was observed that there are oxide layers at the interface between the Al and cBN phases. The presence of these oxide layers prevented the Al from spreading, thereby preventing full densification.

This thesis is dedicated to

My Mother: Tokozile

My sisters, brothers and especially to my son, Bheka.

ACKNOWLEDGEMENTS

The author received many valuable suggestions, and much help and encouragement from colleagues, family members and friends during the course of this research work. It is impossible to mention all of them individually, but special thanks are given to the following:

(i) My supervisors, Prof. D.S. McLachlan and Prof. I. Sigalas for their guidance, advice and comments which made this work possible.

(ii) Dr. M. Herrmann for all his help and comments throughout this work.

(iii) Element Six for sponsoring this work and for the use of their resources.

(iv) The National Research Foundation (NRF) for their financial assistance.

(v) My colleagues Aron, Keke, Thembinkosi, Zukile and others for all their contributions and the encouraging words they gave me.

(vi) Element Six staff: Nedret, Lucas, Emily, Hester, Brett, Thandeka and others for all the assistance they provided to me.

TABLE OF CONTENTS

DECLARATION ..... **ii**

Abstract ..... **iii**

Acknowledgements ..... **vi**

List of Figures ..... **x**

List of Tables ..... **xiv**

List of Tables ..... **xiv**

List of Abbreviations and Symbols ..... **xvi**

Chapter 1 Introduction **1**

Chapter 2 Literature review **3**

2.1 History and properties of boron nitride 3

2.2 Synthesis of cubic boron nitride 5

2.3 The hexagonalization of cBN powder 7

2.4 The preparation and properties of ceramic matrix, cBN reinforced composite materials 9

2.5 Properties of binderless cBN 14

2.6 Relationship of structure to properties in polycrystalline cBN 15

2.6.1 Effect of particle size on the strength of cBN materials 15

2.6.2 Effect of particle shape on the strength of cBN materials 15

2.6.3 Effect of particle size distribution on the strength of cBN materials 16

2.6.4 Effect of pores on the strength of cBN materials 16

2.6.5 Effect of microstructural homogeneity on the strength of cBN materials 17

2.6.6 Bonding between different phases in the cBN composite 17

2.6.7 Composition of binder materials 18

2.7 Wear of composite materials 18

2.8 Cubic BN materials produced at ambient pressure 19

2.8.1 Infiltration of BN 19

2.8.2 Hot pressing of BN with Al 21

2.9 Aluminium-boron-nitrogen ternary phase diagrams 22

Chapter 3 Motivation for the research objectives **26**

3.1 Background to the research objectives 26

3.2 Calculating the volume change 28

3.3 Calculation of the cBN to be used during reaction....29

Chapter 4 Experimental details....31

4.1 Starting materials and their characterization....31

4.2 Experimental apparatus....34

4.2.1 Turbular mixer....34

4.2.2 Attritor mill....35

4.2.3 Tube furnace....36

4.2.4 Uniaxial hot press....39

4.2.5 Thermal analysis technique....40

4.2.6 Polishing equipment....41

4.3 Powder processing....41

4.3.1 Preparation of green samples for infiltration....41

4.3.2 Preparation of powder mixtures for hot pressing....41

4.4 Densification and heat treatment....43

4.4.1 Infiltration....43

4.4.2 Hot pressing....44

4.4.3 Heat treatments....44

4.4.4 Reaction kinetics....45

4.5 Analysis of samples....45

4.5.1 Density measurements....45

4.5.2 X-ray diffraction phase analysis: qualitative and quantitative....47

4.5.3 Microstructural SEM-EDS analysis....51

4.5.4 Vicker's hardness determination....51

4.5.5 Thermal analysis....52

Chapter 5 Reaction kinetics of Al and cBN....55

5.1 Reaction kinetics in a nitrogen atmosphere....56

5.2 Reaction kinetics in an argon atmosphere....61

5.3 Calculating the initial amount of Al....65

5.4 Reaction kinetics of Al and single-crystal cBN....68

Chapter 6 Results of the infiltration of the BN samples....71

6.1 Infiltration of the hexagonal BN (hBN) samples....71

6.1.2 Phase composition of both infiltrated and reacted samples....72

6.1.3 Microstructure analysis of both infiltrated and reacted samples....76

6.2 Infiltration of the cubic BN (cBN) samples....81

6.2.1 Hexagonalization of the cBN particles 81
6.2.2 Infiltration of the hexagonalized cBN samples 89
6.2.3 Phase composition and microstructure of infiltrated samples 90
6.2.4 Hardness of the sample 92
6.3 Infiltration of the 12 μm cBN particles without previous hexagonalization 93
6.3.1 Phase composition and microstructure of the heat-treated samples 94
6.3.2 Vickers hardness of the sample 96
6.4 Infiltration of the 3 μm cBN particles 97
6.5 Discussion of the infiltration experiments 98

Chapter 7 Results for the hot-pressed sintered and heat-treated samples 101
7.1 Densification by hot pressing of 3 μm cBN 101
7.1.1 Phase composition and microstructure of the reacted samples 106
7.1.2 Vickers hardness of the sample 108
7.2 Densification of multimodal samples by hot pressing 109
7.3 Optimization of the hot pressing of multimodal cBN 114
7.3.1 Phase composition of the hot-pressed and heat-treated samples 118
7.3.2 Vickers hardness of the sample 120
7.3.3 Thermal properties 120
7.4 Densification by hot pressing of 12 μm cBN 122
7.5 Discussion of the results from hot pressing 123

Chapter 8 Conclusions and future work 131

Appendices 138
Appendix A 138
Raw data used to plot reaction kinetics graph shown in chapter 5. 138
Appendix C 145
Fundamental concepts explaining the meaning of the results obtained from the Mastersizer 2000. 145
Appendix D 147
Model multimodal powder compositions (combination of different grades) derived from the packing model program 147

LIST OF FIGURES

Figure 2.1: The structure of graphite, diamond, hBN and cBN 4

Figure 2.2: Comparison of the crystal structures of zink blende with wurtzite. 4

Figure 2.3: Schematic processes for the synthesis and preparation of products of PCD or cBN using ultra-high pressures and temperatures (Sumitomo*, 2000)* 6

Figure 2.4: Equilibrium phase boundary between hexagonal and cubic boron nitride (Fukunaga, 2000) 8

Figure 2.5: SEM image of Amborite surface after mechanical polishing (courtesy of Element Six (Pty) Ltd) 11

Figure 2.6: Knoop microhardness of the sintered specimens in cBN-Al system (Rong *et al.*, 1994) 12

Figure 2.7: Knoop microhardness (GPa) at a load of 500 g of the cBN-TiN-Al composite against mixing composition (Rong *et al.*, 2002). 13

Figure 2.8: Schematic diagram of infiltration sintering (Reed, 1995). 20

Figure 2.9: The contact angle in the Al-hBN system (Zhao et al, 1992) 21

Figure 2.10: Al-B binary system (Rogl and Schuster, 1992) 24

Figure 2.11: Isothermal section of the Al-B-N system at 900 ^{o}C under 10^{5} Pa argon 25

Figure 2.12: Isothermal section of ternary Al-B-N system at 1 500 ^{o}C 25

Figure 3.1: Schematic diagram of the experimental plan. 27

Figure 3.2: Reacted cBN and resulting hardness as a function of initial vol. % Al 29

Figure 4.1: SEM image of the hexagonal boron nitride powder 32

Figure 4.2: SEM image of the cubic boron nitride powder with an average size of 3 μm 32

Figure 4.3: SEM image of the cubic boron nitride powder with an average size of 12 μm 32

Figure 4.4: SEM images of ABN800 with a particle size of over 100 μm 33

Figure 4.5: Size distribution of grades 1, 2, 4 and 9 34

Figure 4.6: Schematic design of a rotary evaporator. 36

Figure 4.7: Schematic representation of the vertical tube furnace used during infiltration 38

Figure 4.8: The uniaxial hot press used 39

Figure 4.9: Typical temperature profile used during infiltration. 40

Figure 4.10: The furnace temperature profile for coating cBN with Aluminum. 43

Figure 4.11: A typical cBN particle coated with AlN. 43

Figure 4.12: Results obtained from the standards that were used to estimate the cBN/hBN ratio during the hexagonalization experiments 47

Figure 5.1: XRD results of the sample before and after hot pressing 56

Figure 5.2: Typical XRD results of the samples prepared to study the reaction kinetics of 50 vol. % Al with 50 vol. % cBN (12 μm) after 2 h at (a) 1 400 ^{o}C and (b) 1 100°C 57
Figure 5.3: Effect of holding time at a temperature of 1 100 ^{o}C in a N_2 atmosphere 59
Figure 5.4: Effect of holding time at a temperature of 1 200 ^{o}C in a N_2 atmosphere 59
Figure 5.5: Effect of holding time at a temperature of 1 300 ^{o}C in a N_2 atmosphere 60
Figure 5.6: Effect of holding time at a temperature of 1 400 ^{o}C in a N_2 atmosphere 60
Figure 5.7: Effect of varying temperature at constant time in a N_2 atmosphere 61
Figure 5.8: Effect of holding time at a temperature of 1 100 ^{o}C in an Ar atmosphere 63
Figure 5.9: Effect of holding time at a temperature of 1 200 ^{o}C in an Ar atmosphere 63
Figure 5.10: Effect of holding time at a temperature of 1 300 ^{o}C in an Ar atmosphere 64
Figure 5.11: Effect of holding time at a temperature of 1 400°C in an Ar atmosphere 64
Figure 5.12: Volume percent of AlN formed as a function of time at a temperature of 1 300 ^{o}C in both N_2 and Ar atmospheres 68
Figure 5.13: SEM image of the sample after 5 h in a N_2 atmosphere 69
Figure 5.14: SEM image of the sample after 5 h in an Ar atmosphere 69
Figure 5.15: SEM image of the sample after 2 h in a N_2 atmosphere 70
Figure 5.16: The very thin layer of AlN present after 30 min under N_2 70
Figure 6.1: Some of the XRD results for the hBN-26 sample 74
Figure 6.2: Some of the XRD results for the hBN-18 sample 75
Figure 6.3: Ratio of V_{AlN}/V_{hBN} (where the (100) peak of hBN was used) as a function of temperature for the hBN-18 sample 76
Figure 6.4a: Fracture surface SEM micrograph of the hBN-26 sample 77
Figure 6.4b: Fracture surface SEM micrograph of the hBN-26HT13 sample 77
Figure 6.4c: Fracture surface SEM micrograph of the hBN-26HT13 sample 78
Figure 6.5a: SEM micrograph of the hBN-18 sample 79
Figure 6.5b: SEM micrograph of the hBN-26HT13 sample 80
Figure 6.6: SEM micrograph of the hBN-24 sample 80
Figure 6.7: SEM micrograph of the hBN-19HT13 sample 81
Figure 6.8a: Results of the XRD measurements for the 12 μm cBN powder heated at 1 300 ^{o}C for different times using the Mo tube 83
Figure 6.8b: Results of the XRD measurements for the samples (i) cBN12HT14-12, (ii) cBN12HT13.5-12 and (iii) cBN12HT13-36 84
Figure 6.9a: SEM micrograph of sample cBN12HT14-12 85
Figure 6.9b: SEM micrograph of sample cBN12HT14-12 before annealing 85

Figure 6.10: Diffractograms of the samples (i) cBN3HT14-12, (ii) cBN3HT13.7-12, (iii) cBN3HT13.5-12 and (iv) cBN3HT13-12 at different temperatures for 12 hours 86
Figure 6.11a: Images of the cBN3HT14-12 samples taken at different magnification.....87
Figure 6.11b: SEM micrograph of sample cBN3-4 before annealing 88
Figure 6.11c: Heterogeneous nucleation in mould-wall cracks (Easter and Porterling,1992)....89
Figure 6.12: Diffractograms of the 40cBN12-36 sample heat treated at different temperatures. Mo-Kα radiation was used. 91
Figure 6.13: SEM micrograph of the 40cBN12-36HT13-1 sample 92
Figure 6.14: Diffractogram of the cBN12-42HT155-1 sample 95
Figure 6.15: SEM micrograph of the cBN12-42HT14-1HT700-3 sample.....96
Figure 6.16: Spore diameter distribution in green samples made of 3 μm (S5) and 12 μm cBN (S4). 98
Figure 6.17: Vickers hardness measured on the Al-infiltrated cBN samples.....99
Figure 7.1: DTA measurement for a sample consisting of 40 vol. % of Al and 60 vol. % of cBN 102
Figure 7.2: Schematic diagram showing how sinter forging of the cBN/Al composite pellets was done.....104
Figure 7.3: XRD results for cBN3-50-N1HT13-1 and cBN3-50-N1HT14-1 samples. 107
Figure 7.4: SEM micrographs at high and low magnification for the cBN3-50-N1HT13-1 sample. The additional phases indicated were proved by EDX analysis. 108
Figure 7.5: XRD results of the McBN30-N1 sample after heat treatment at (a) 800 ^{o}C, (b) 1 300 ^{o}C and (c) 1 350 ^{o}C in an Ar atmosphere 112
Figure 7.6: SEM micrograph of the McBN30-N1HT13-1 sample. 113
Figure 7.7: SEM micrograph of the McBN30-N1HT13-1 sample.....113
Figure 7.8: Particle size distribution of the grade 1 crushed cBN powder 115
Figure 7.9: Secondary electron and backscatter images of the McBN30-N5 sample 116
Figure 7.10: Photographs of samples (a) McBN30-N12, (b) McBN30-N11 and (c) McBN30-N4.....118
Figure 7.11: XRD results of the (a) McBN30-N5 and (b) McBN30-N7 samples.....119
Figure 7.12: Vickers hardnesses of the samples initially containing 50 vol. % Al and cBN (12 μm) heat treated at different temperatures and times.....123
Figure 7.13: The relationship between density and hot-pressing conditions when 30 vol.% Al was used with 3 μm cBN. 124
Figure 7.14: Graph showing the relationship between the density and Al concentration of the samples hot pressed at 800 ^{o}C for 30 min under 50 MPa 124

Figure 7.15: Graph of the densities of the samples containing 30 vol. % Al hot pressed under different conditions 125
Figure 7.16: Graph showing the densities as a function of Al concentration for both monomodal and multimodal cBN hot pressed at 800 ^{o}C for 30 min under 50 MPa. 126
(Samples name from left to right: McBN20-N1,cBN20-N2,McBN30-N1,cBN30-N3, McBN40-N1,cBN40-N3, McBN50-N2 and cBN50-N1) (NB: m = multimodal) 126
Figure 7.17: Vickers hardness measured on the hot-pressed samples annealed at 1 300 ^{o}C for 60 min..... 126
Figure 7.18: Contact angle curves of the Al/AlN [Fujii *et al.* (1993)] and Al/BN systems [Xue *et al.* (1992)]..... 128
Figure 7.19a: McBN30-N2 sample as hot pressed at 800 ^{o}C 129
Figure 7.19b: McBN30-N2 sample as hot pressed at 800 ^{o}C 129
Figure 7.20: McBN30-N2 sample as hot pressed at 800 ^{o}C 130

LIST OF TABLES

Table 2.1: Properties of cBN, PCD and diamond (Walmsley and Lang, 1987) 5

Table 2.2: Typical results of XRD peak intensity ratio as reported by Fukunaga (2000)..... 9

Table 2.3: Physical properties of the components of Amborite (Sumimoto, 2000)..... 10

Table 2.4: Crystallographic data on the elements and binary phases of the Al-B-N ternary system..... 23

Table 3.1: Data used to calculate the change in volume during the reaction 28

Table 3.2: Data used to calculate the change in volume during the reaction 28

Table 4.1: Materials used for processing..... 31

Table 4.2: Heat treatment conducted to study the reaction kinetics..... 45

Table 4.3: Some of the theoretical densities of the Al-cBN powder mixtures..... 46

Table 4.4: Structural data for phases involved 48

Table 4.5: Values required for the material phase analysis..... 49

Table 4.6: Absolute intensities normalized with regard to unit cell volume..... 50

Table 5.1: Results of the samples prepared to study the reaction kinetics of 50 vol. % Al with 50 vol. % cBN (12 μm) in a nitrogen atmosphere 58

Table 5.2: Results of the reaction kinetics study in an argon atmosphere of samples containing 50 vol. % Al with 50 vol. % cBN (12 μm)..... 62

Table 5.3: Data used to calculate Al before the reaction at 1 400 ^{o}C for 3 h 66

Table 5.4: Data used to calculate Al before the reaction at 1 300 ^{o}C for 3 h 67

Table 6.1: Al-infiltrated hBN samples after heat treatment at 800 ^{o}C for 30 min 71

Table 6.2: Al-infiltrated hBN samples after heat treatment at 1 300 ^{o}C for 60 min 72

Table 6.3: Samples heat treated during the hexagonalization experiments 82

Table 6.4: The partially hexagonalized cBN containing samples prepared by infiltration at 800 ^{o}C for 30 min..... 90

Table 6.5: The hBN containing samples containing Al after 60 min of heat treatment..... 90

Table 6.6: Some of the cBN samples prepared 94

Table 7.1: Samples prepared using the hot press under an Ar atmosphere..... 102

Table 7.2: Samples prepared using the hot press at 800 ^{o}C for 30 min under 50 MPa..... 105

Table 7.3: Samples heat treated at different temperatures in N_2 gas..... 106

Table 7.4: Calculated possible ratios of the cBN powders to obtain a maximum density... 109

Table 7.5: Green densities of cBN/Al mixture (model 1; refer to Table 7.4) as a function of pressure 110

Table 7.6: Samples prepared using multimodal powder mixtures (based on model 1) with their properties 111
Table 7.7: Samples prepared using multimodal powder mixtures (based on model 2) with their properties 116
Table 7.8: Phase quantification results for McBN50-N2HT13-1 sample 119
Table A.1: Data used to calculate the volume percentages shown in Table A.2 below 139
Table A.2: Volume percent of the different phases obtained after the heat treatment of the samples at a temperature of 1 200 ^{o}C (used to plot the graph in Figure 5.4) 140
Table A.3: Volume percent of the different phases obtained after the heat treatment of the samples at a temperature of 1 100 ^{o}C (used to plot the graph in Figure 5.3) 140
Table A.4: Volume percent of the different phases obtained from the heat treatment of the samples at a temperature of 1 300 ^{o}C (used to plot the graph in Figure 5.5) 141
Table A.5: Volume percent of the different phases obtained from the heat treatment of the samples at a temperature of 1 400 ^{o}C (used to plot the graph in Figure 5.6) 141
Table A.6: Volume percent of the different phases obtained from the heat treatment of the samples at a temperature of 1 100 ^{o}C (used to plot the graph in Figure 5.8) 142
Table A.7: Volume percent of the different phases obtained from the heat treatment of the samples at a temperature of 1 200 ^{o}C (used to plot the graph in Figure 5.9) 142
Table A.8: Volume percent of the different phases obtained from the heat treatment of the samples at a temperature of 1 300 ^{o}C (used to plot the graph in Figure 5.10) 143
Table A.9: Volume percent of the different phases obtained from the heat treatment of the samples at a temperature of 1 400 ^{o}C (used to plot the graph in Figure 5.11) 143
Table D1: Calculated possible ratios of the cBN powders to obtain a maximum density ... 147

LIST OF ABBREVIATIONS AND SYMBOLS

AlB_2	=	aluminium diboride
AlCu	=	aluminium copper
AlN	=	aluminium nitride
AMB	=	Amborite
BN	=	boron nitride
cBN	=	cubic boron nitride
CVD	=	chemical vapour deposition
DSC	=	differential scanning calorimetry
DTA	=	differential thermal analysis
DTGA	=	derivative thermogravimetric analysis
EDX	=	energy dispersive X-ray analysis
FEG	=	field emission gun
GPa	=	gigapascal
h	=	hour
hBN	=	hexagonal boron nitride
HP	=	hot-press(ing)
HPHT	=	high pressure, high temperature
ICSD	=	International Centre for Diffraction Data
min	=	minute
MPa	=	megapascal
Pa	=	pascal
PCD	=	polycrystalline diamond
s	=	second
SCS	=	differential scanning calorimetry
SEM	=	scanning electron microscopy
TEM	=	transition electron microscopy
TGA	=	thermogravimetric analysis
UHP	=	ultra-high pressure
wBN	=	wurtzite boron nitride
XRD	=	X-ray diffraction
μm	=	micron

CHAPTER 1 INTRODUCTION

Diamond and cubic boron nitride have exceptional properties, such as high hardness, thermal conductivity and excellent chemical and thermal stability. They are thus widely used in industry today. Both diamond and cBN have Vickers hardnesses of more than 40 GPa and as a result they are known as "superhard" materials (Wentorf and Bundy, 1980). The high hardness of these materials can be attributed (in part) to the strong covalent bonds by which these materials is held together, as well as to the high density of these bonds.

Cubic boron nitride (cBN) has a hardness of 45 GPa, which is half that of diamond. However, some of its properties are superior to those of diamond. cBN is less reactive than diamond with iron and iron alloys. This has opened a huge market for cBN and coated metal working tools (Bartl *et al.*, 1996). Cutting tools with a higher cBN content have displayed an excellent ability for cutting Ni- and Co-based superalloys and high-speed steel (Wentorf and Bundy, 1980). Other cBN based composites that have been formed recently under high pressure include cBN-WC-Co, cBN-TiN, cBN-AlN, cBN-Al and cBN-TiN-Al (Rong et al, 2002). Much research has been done on the sintering of cBN and cBN based materials. Since the atomic bonds of cBN, like those of diamond, are predominantly covalent and it is metastable at ambient pressures, the sintering of pure cBN samples requires high pressures (~7 GPa) to obtain a fully dense material (Wentorf, 1961). This difficulty led to research work dealing with the development of cBN composite materials. As early as 1974, Bundy and Wentorf (1980) developed cutting tools with a high cBN content, which were infiltrated by Al-Co (from a WC-Co substrate into a cBN layer) during high-pressure and high-temperature sintering.

The aim of the work described in this thesis was to develop dense Al-cBN composites with a high cBN content. To achieve this goal, two different strategies were used: infiltration of cBN preforms and hot pressing of cBN-Al mixtures. The grain size of cBN and the amount of Al were systematically varied and the influence of these parameters on densification and selected properties was evaluated.

An overview of the Al-cBN materials is presented in Chapter 2. The preparation and properties of cBN-based materials are also included in this chapter. At the end of this chapter some relevant phase diagrams (binary Al-B and ternary Al-B-N) are discussed.

Chapter 3 summarizes the findings of Chapter 2 and develops the strategy for the research on which this thesis is based.

Chapter 4 describes the powders, the equipment and the experimental techniques used.

The results of the investigation into the reaction kinetics of Al with cBN are given in Chapter 5, which includes the results of the investigation into the reaction between Al and a single crystal of cBN.

Chapter 6 summarizes the results of the infiltration experiments. It also includes some preliminary studies of the infiltration of hBN by Al. The infiltration of cBN with Al is presented and the infiltration results are discussed at the end of this chapter.

Chapter 7 summarizes the work carried out in the field of hot pressing and reaction sintering of cBN with Al. The results are discussed at the end of this chapter.

The conclusions and recommendations for necessary future work are presented in Chapter 8.

CHAPTER 2 LITERATURE REVIEW

2.1 History and properties of boron nitride

Boron nitride (BN) is a commercially important material with three well-known crystalline phases. These are the hexagonal boron nitride (hBN), cubic boron nitride (cBN) and wurtzite boron nitride (wBN) phases (McCulloch *et al.*, 2000). The first two of these are the most common forms. The first, hBN is a relatively soft material. Some of its properties resemble those of graphite. In the graphitic structure the B and N atoms have sp^2 p type bonding and the structure exhibits a single AaAa… stacking sequence such that the B atoms in one layer are placed directly below the N atoms in the next layer. The hexagonal structure has four atoms in the unit cell. This structure is very similar to that of graphite. The second most common form, cBN is a material with a zinc blende structure and properties resembling those of diamond. This structure is cubic close packed, with both types of atoms being 4-fold coordinated, and ½ of the terahedral sites of the unit cell are occupied. The nature of the chemical bond is sp^3 hybridised.

The structure of hBN, together with those of graphite, diamond and cBN, is shown in Figure 2.1. Figure 2.2 contrasts the crystal structure of zink blende with wurtzite. Again the nature of the bond in this BN allotrope is sp^3. The anion packing in this structure is hexagonal close packed, compared to cubic close packed for zink blende.

Boron nitride is commonly crystallized in a graphite-like form. It was only in 1957 that it was found that conditions of high pressure and high temperature, similar to those used for diamond synthesis, were suitable for the preparation of cBN from hexagonal boron nitride. This form of boron nitride was given the name “borazon” (Wentorf, 1961). Both synthetic cubic products (diamond and cBN) are produced at pressures (normally above 5.5 GPa) and temperatures appropriate to their thermodynamic stability by means of catalytic action upon the hexagonal material.

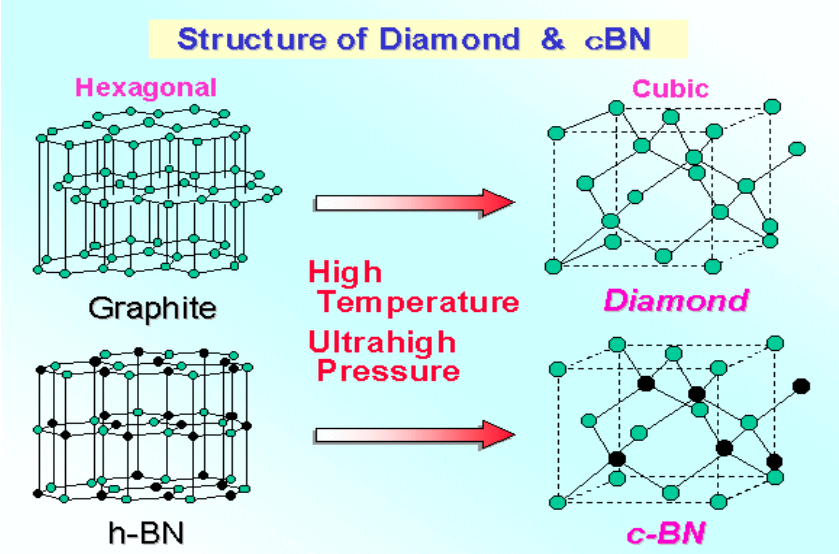

Figure 2.1: The structure of graphite, diamond, hBN and cBN

Conditions of high temperature and ultra-high pressures are required to convert hexagonal to cubic structures (Sumitomo, 2000)

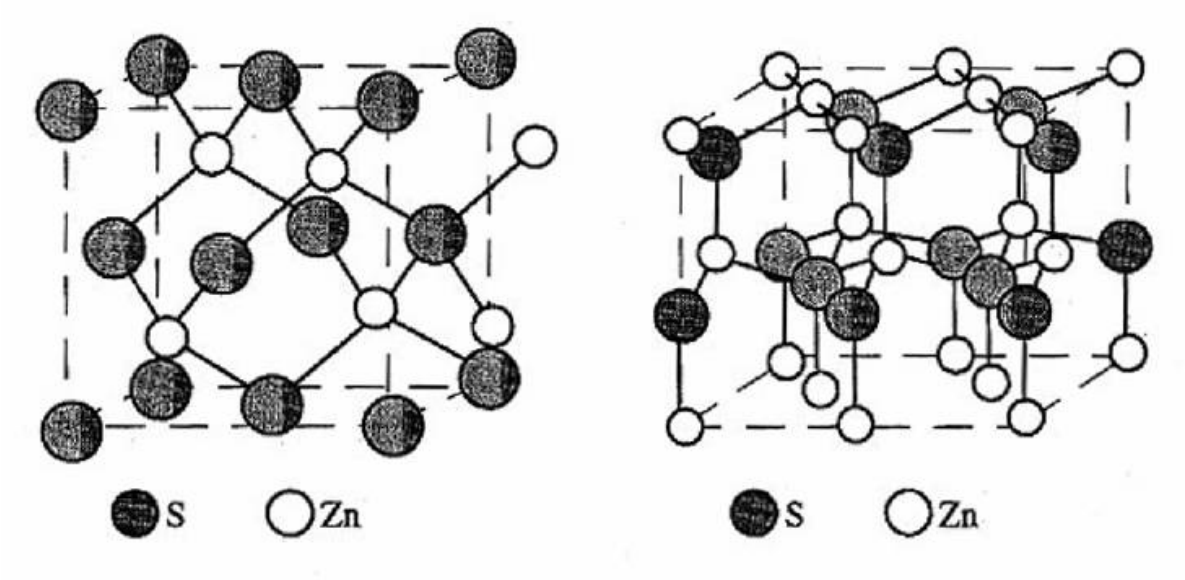

Zink blende Wurtzite

Figure 2.2: Comparison of the crystal structures of zink blende with wurtzite.

Diamond and cBN have exceptional properties, such as high hardness, thermal conductivity and excellent chemical stability. They are thus widely used in industry today. Diamond can be used in tools for the cutting and shaping of hard materials such as stone, concrete, glass, ceramics and other hard or abrasive materials that chemically react only slightly with the carbon at the cutting

edge. It cannot be used for ferrous materials as these are known to attack diamond chemically at the hot cutting edge, thereby causing diamond tools to deteriorate at an uneconomical rate (Wentorf and Bundy, 1980).

Cubic boron nitride has a hardness and thermal conductivity second only to that of diamond. It has a low reactivity with iron and its alloys. It has better chemical and thermal stability than diamond. Because of these properties, cBN has been widely used as the tool material best suited to the machining of Ni, grey cast iron, hardened steels, Co-based superalloys and also different composite materials (Bartl *et al.,* 1980). The mechanical properties of single-crystal cubic boron nitride, together with those of diamond and polycrystalline diamond (PCD) for comparison, are presented in Table 2.1. The term PCD used in this thesis refers to the high pressure high temperature sintered polycrystalline diamond material, where cobalt is used as a sintering aid and forms the basis of the resulting second phase in this material.

Table 2.1: Properties of cBN, PCD and diamond (Walmsley and Lang, 1987)

Property	**Diamond (natural)**	**PCD**	**cBN**
Density (g/cm^3)	3.5	4.0	3.48
Fracture toughness ($MPam^{0.5}$)	3.4	8	5
Knoop hardness (GPa)	57 – 104	50	43 – 46
Young's Modulus (GPa)	964	810	680
Thermal expansion ($10^{-6}K^{-1}$)	1.5 – 4.8	4.6	4.9
Thermal conductivity 20 $^oC(Wm^{-1}K^{-1})$	500 – 2000	760	100 – 600
Wear coefficient	2.1 – 5.5	4	2

2.2 Synthesis of cubic boron nitride

Diamond and cBN are synthesized industrially under high-pressure/high-temperature (HPHT) conditions and techniques. Figure 2.3 shows the schematic processes for the synthesis of PCD or cBN using ultra-high pressure and high temperature. cBN is usually obtained from the conversion of hBN to cBN at a temperature between 1 200 and 2 000 ^oC and at high pressure (2.5 – 7.5 GPa) in the presence of catalyst or solvent (Hao *et al*, 2001). Endo *et al.* (1981) obtained cBN by pyrolizing $Ca_3B_2N_4$ at high pressure (4.4 – 6.5 GPa) and high temperature (1 180 – 1 800 ^oC). cBN was also synthesized by the decomposition of Mg_3BN_3 under high pressure and high temperature. In this study carried by Nakano *et al.* (1992), the minimum

pressure for cBN synthesis was 4 GPa, which was 1 GPa lower than that of the conventional catalytic process.

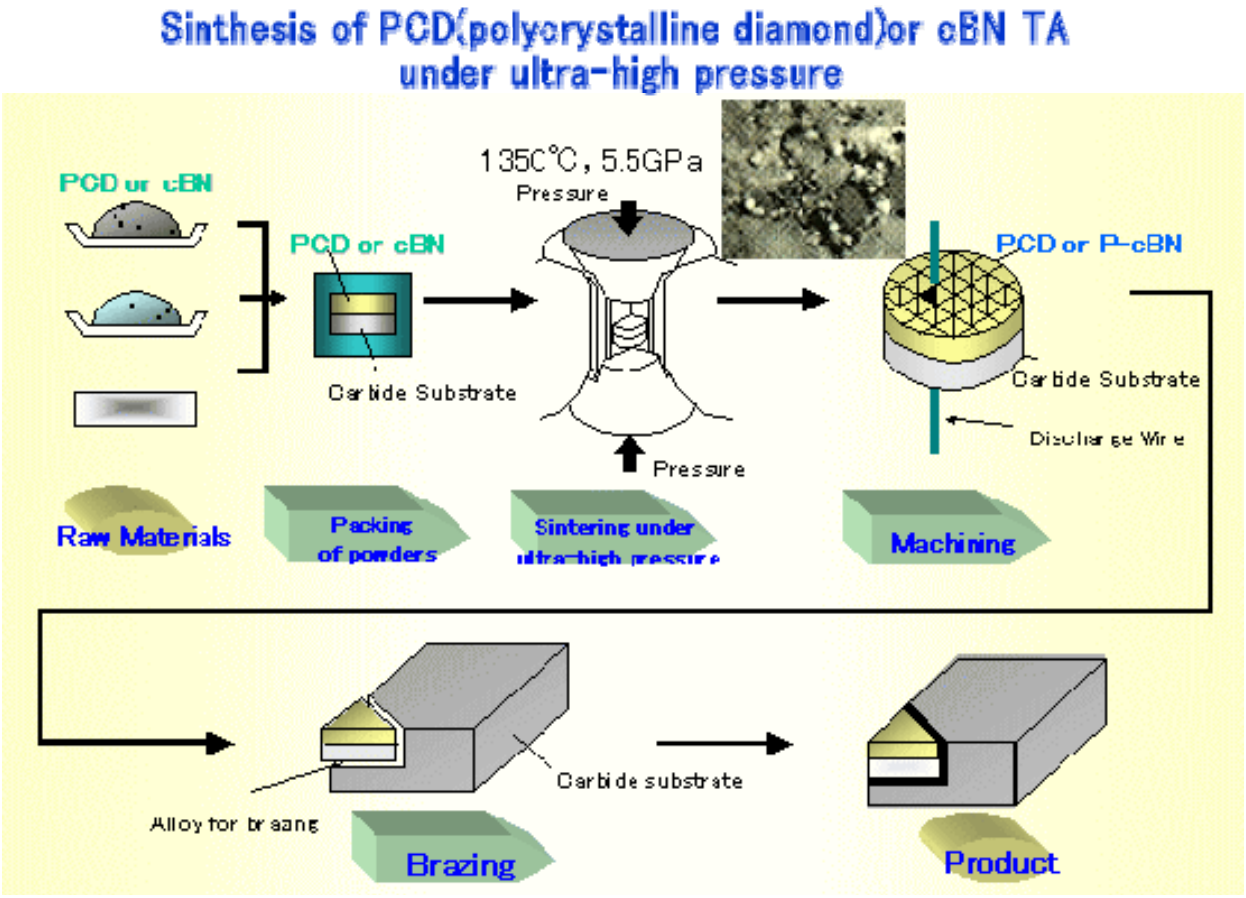

Figure 2.3: Schematic processes for the synthesis and preparation of products of PCD or cBN using ultra-high pressures and temperatures (Sumitomo, *2000)*

The extensive use of cBN-based materials has led to research concerning the synthesis of cBN under low-temperature and low-pressure conditions. There have been comprehensive reports on the success of synthesizing diamond by means of modified chemical vapour deposition (CVD); especially atomic hydrogen and radicals of hydrocarbon, and kinetic (not thermodynamic) effects are responsible for the synthesis of diamond from the gas phase. Pure polycrystalline, adherent diamond coatings and thick, free-standing layers can be produced on various substrates at reasonable costs (Bartl *et al.,* 1996). It has been a challenge to produce a similarly low-pressure synthesis process for cBN, permitting the formation of pure and well-crystallized cBN films by a CVD method. The nucleation of h-BN (which is the less dense phase) and its growth (since it is a metastable phase) is preferred as compared to c-BN, which is denser and the thermodynamically stable phase. In the carbon system the metastable diamond phase is favoured.

(Bartl *et al*, 1996). Zhang and Matsumoto (2000) have deposited a boron nitride film with cBN content higher than 85% ,where a growth rate of about 70 nm/min was achieved. The boron nitride films were synthesized on silicon substrates by radio frequency-bias-assisted direct current jet chemical vapour deposition in Ar-N_2-BF_3-H_2 system.

In the search for low-temperature and low-pressure synthesis of cBN, Hao *et al.* (2001) obtained a sample of BN nanocrystals, with the cubic BN phase as the dominant phase, at low temperature (480 ^oC) and ambient pressure. Boron nitride nanocrystals were synthesized in an autoclave with benzene as solvent.

2.3 The hexagonalization of cBN powder

Boron nitride has completely different diamond-like cubic (cBN) and graphite-like hexagonal (hBN) phases, with an extremely large change of volume ($\Delta V/V = 0.53$). Because of this large jump in volume, pronounced fragmentation and disordering of the substance between the two phases can develop. The direct diffusion-type transitions between the equilibrium phases of cBN and hBN have been studied. Many researchers have used high pressure and high temperature to obtain cBN from the hBN powder. More recently, hBN powder has been sintered under ultra-high pressure and temperature, which resulted in the sintering of binderless cBN with exceptional properties (Sumitomo, 2000) (refer to Section 2.4 of this thesis). Since cBN possesses exceptionally useful properties, more work has been done on understanding the conversion of hBN to cBN, but less work has been done on the reconversion of cBN to hBN. To bring cBN to the hBN state it is necessary to apply a certain pressure and, in addition, a certain temperature to overcome the activation barrier. The equilibrium phase boundary results of the earlier studies done by Bundy and Wentorf, reported by Eremets *et al.* (1998), showed that cBN "graphitizes" only at ~1 227 ^oC at ambient pressure. The lowest pressure for the direct transformation of hBN-cBN is about 8 GPa at a temperature of ~2 727 ^oC, and the transformation pressure increases with decreasing temperatures. As a result, if a cBN sample is heated under a pressure below ~8 GPa, it transforms to hBN and remains in this state under cooling (Eremets *et al.*, 1998).

The equilibrium phase boundary between hexagonal and cubic boron nitride has been determined over the pressure range 3 – 6 GPa and the temperature range 1 200 – 2 200 ^oC by Fukunanga, 2000). The summarized results of his study are presented in Figure 2.4 below. The

criterion used in determining the stable regions of cBN and hBN was that in the cBN stable region, cBN is formed from hBN and a catalyst (magnesium boron nitride) and cBN is not transformed to hBN. The boundary line below 3.8 GPa was determined using cBN powder or a mixture of cBN and Mg_3BN_3 by the criterion that the run products in the cBN stable region showed that the X-ray diffraction (XRD) peak intensity ratio was more than 3, whereas it is decreased to less than unity in the hBN stable region with increasing reaction time. The phase boundary line plotted can be expressed as P (GPa) = T (^{o}C)/465 + 0.79.

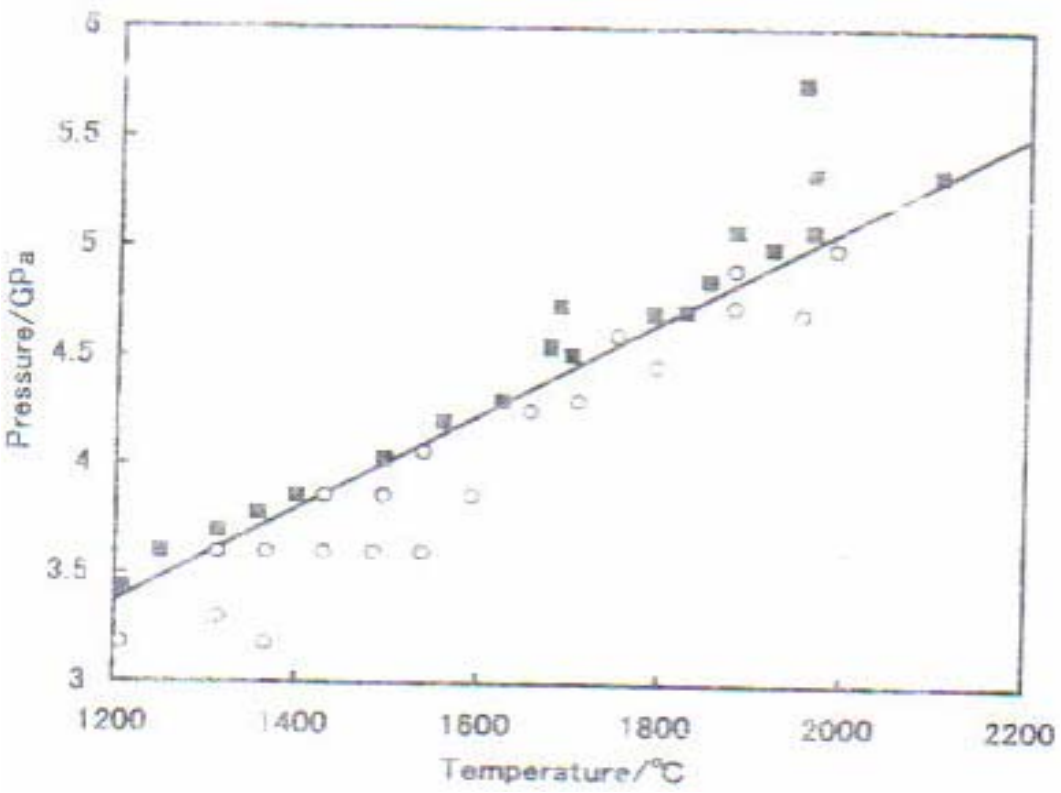

Figure 2.4: Equilibrium phase boundary between hexagonal and cubic boron nitride (Fukunaga, 2000)

Solid squares denote cBN stable points and open circles are hBN stable points

The transformation from cBN to hBN has been studied at normal pressures. The study by Fukunanga (2000) shows no hBN peaks for the run at 1 100 ^{o}C after heating for 48 h. The summarized results of his study presented in Table 2.2 below show the reaction period versus the XRD peak intensity ratio of cBN(111)/hBN(002). The ratio of the intensity of cBN to hBN was found to be 4 after heating at a temperature of 1 200 ^{o}C for 48 h and 0.3 after heating at 1 250 ^{o}C for 48 h. It was, however, found that the ratio increased to 18 after heating at a temperature of 1 300 ^{o}C for 5 h. This demonstrates that the phase transformation from cBN to hBN is very slow at lower temperatures.

Table 2.2: Typical results of XRD peak intensity ratio as reported by Fukunaga (2000)

Run No.	Pressure GPa	Temperature °C	Reaction time min	Starting materials	Ic/Ih	Phase
625	4.34	1207	40	cBN+ Mg_3BN_2	6.2	cBN
663	3.6	1250	480	cBN	7.9	cBN
660	3.78	1357	60	cBN	8.7	cBN
623	3.18	1207	60	cBN+ Mg_3BN_2	0	hBN
613	3.86	1431	30	cBN+ Mg_3BN_2	0.8	hBN
641	3.6	1431	60	cBN	0.2	hBN
642	3.3	1314	60	cBN	1.9	
645	3.3	1314	300	cBN	0.3	hBN
647	3.3	1314	600	cBN	0	hBN
j1201	0	1200	1440	cBN	35	
j1202	0	1200	2880	cBN	4	
j1251	0	1250	1440	cBN	3	
j1252	0	1250	2880	cBN	0.3	hBN
j1301	0	1300	300	cBN	18	

Magnesium boron nitride (Mg_3BN_2) was used as a catalyst.

2.4 The preparation and properties of ceramic matrix, cBN reinforced composite materials

There is great interest in the sintering of cBN composites. This interest has been generated as a result of their wide use as cutting tools for hardened steels. Since the atomic bonds of cBN, like those of diamond, are predominantly covalent, the sintering of highly pure cBN samples requires high pressure (~7 GPa) to obtain a fully dense material. This difficulty led to research work dealing with the development of cBN composite materials. As early as 1974, Bundy and Wentorf developed cutting tools with a high cBN content, the cBN layer being infiltrated with molten Al-Co during high-pressure and high-temperature sintering (Rong *et al.*, 2002). Other composites that have been formed recently include cBN-WC-Co (Rong and Fukunaga, 1993), cBN-TiN (Hara and Yazu, 1979), cBN-AlN (Bezhenar *et al.*, 1999), cBN-Al (Walnsley and Lang, 1987) and cBN-TiN-Al (Rong *et al.*, 2002). In this section composites of cBN-Al and cBN-TiN-Al will be discussed in detailed.

The reaction of cBN and aluminium has been reported previously (Walnsley and Lang, 1987), where aluminium powder was used as a binder in a compressed pellet. In that work, ultra-high pressures and high temperatures were used. The residual binder phase after sintering was found to be a mixture of aluminium nitride (AlN) and aluminium diboride (AlB_2). These two compounds protect the internal cBN surfaces from chemical attack, thereby giving excellent thermal stability. The resulting material is on the market under the trade name Amborite. Some of the physical properties of the three components of Amborite are listed in Table 2.3 below (Walnsley and Lang, 1987).

Table 2.3: Physical properties of the components of Amborite (Sumimoto, 2000)

Compound	**Knoop hardness ($kg.mm^{-2}$)**	**Melting point (low pressure)**	**Morphology**	**Lattice parameters (nm)**
AlB_2	960 100 g indenter load	1 928 K	Hexagonal platelets	a = 0.301 c = 0.326
AlN	1 200 100 g indenter load	3 273 K	Hexagonal platelets	a = 0.311 c = 0.498
CBN	4 050	-	Cubo-octahedral	a = 0.361

Amborite is strongly bonded, with a hardness of 30.8 GPa, and has an excellent toughness of 6.25 $MPam^{1/2}$ due to the presence of both AlN and AlB_2. A scanning electron micrograph (SEM) image of Amborite surface after mechanical polishing is shown in Figure 2.5 below. Some grains have broken into two or more pieces, between which the binder has penetrated. In regions between the larger distinct cBN grains, smaller cBN fragments are evident. Although it is clearly a composite material, its industrially relevant properties – hardness and wear resistance – are derived essentially from the original cBN particles (Bartl *et al.,* 1996).

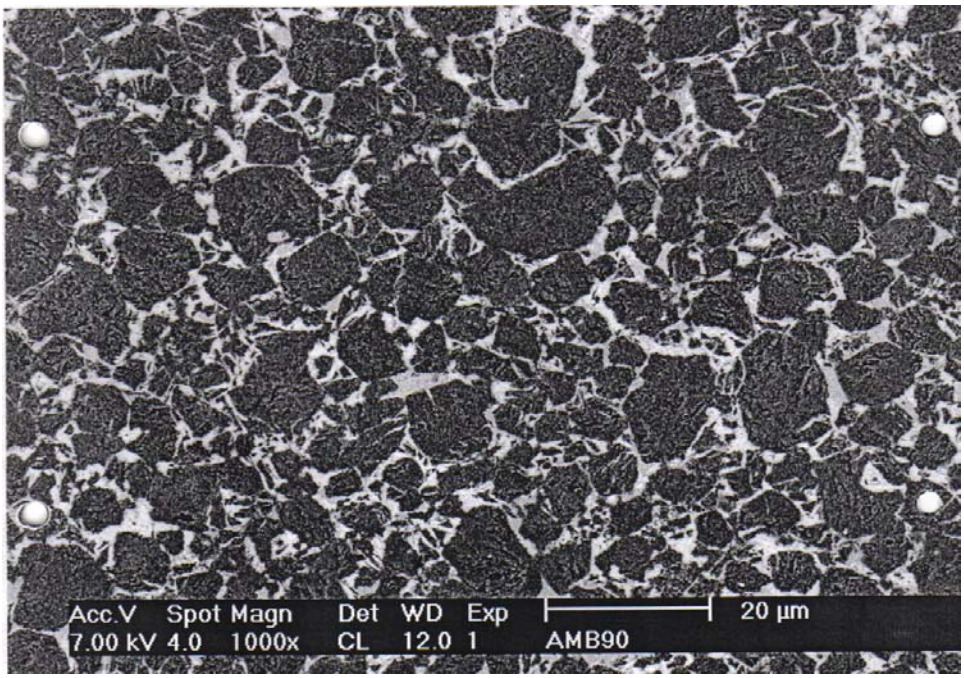

Figure 2.5: SEM image of Amborite surface after mechanical polishing (courtesy of Element Six (Pty) Ltd)

Rong and Fukunaga (1994) reported the sintering behaviour of the cBN-Al system and described reactions during ultra-high-pressure and high-temperature sintering. The starting materials were again cBN powder (particle size between 1.0 and 3.0 μm) and aluminium powder (particle size between 1.0 and 4.0 μm). In this work, mixtures containing cBN from 50 to 90 mol % were prepared and the balance phase was Al. According to this work, AlN, AlB_2 and α-AlB_{12} were formed through the reactions between solid cBN and molten Al, and rapid grain-growth of AlN and AlB_2 was observed during sintering. In their experiment, samples were sintered at 1 200 ^oC and 1 400 ^oC under a pressure of 5.75 GPa. Based on the XRD results, the following two reactions were suggested:

$$2BN + 3Al \text{----------} AlB_2 + 2AlN \quad (2.1)$$

$$12BN + 13Al \text{----------} \alpha\text{-}AlB_{12} + 12AlN \quad (2.2)$$

It was observed that for a small fraction of aluminium (10 mol % Al), the first reaction does not take place (Rong *et al.*, 1994).

The results of the Knoop microhardness testing of the sintered specimens measured on the polished surfaces are plotted in Figure 2.5 below. The two curves in the figure correspond to sintering at 1 200 ^oC (solid line) and at 1 400 ^oC (dotted line).

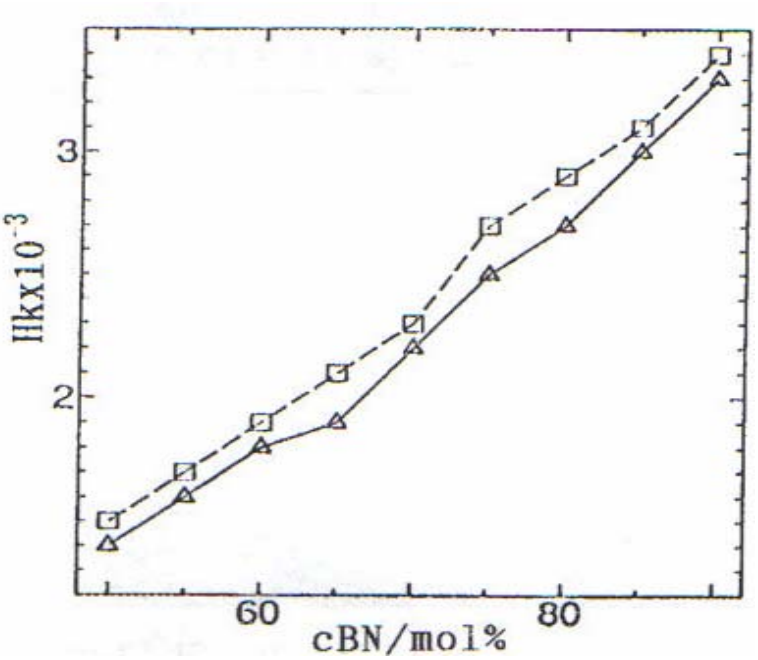

Figure 2.6: Knoop microhardness of the sintered specimens in cBN-Al system (Rong *et al.*, 1994)

The two lines in Figure 2.6 show that the hardness values of the materials sintered at 1 400 ^{o}C are higher than those of the materials sintered at 1 200 ^{o}C from 50 mol % cBN to 90 mol % cBN compositions. Both lines increase almost linearly with increasing cBN content. The highest hardness value of 33.4 GPa was obtained for the 90 mol % cBN composition sintered at 1 400 ^{o}C.

Investigation by transition electron microscopy (TEM) showed that the AlN phase exists around the cBN grain, while the AlB_2 phase and/or a α-AlB_{12} phase exist between AlN grains.

The rapid grain growth of AlN and AlB_2 in the cBN-Al system observed during sintering lowered the mechanical strength of the final material. To suppress this rapid grain growth, TiN as a secondary phase was added to the cBN-Al system. TiN has a thermal expansion coefficient intermediate between those of cBN and Al and can thereby prevent cracking in the microstructure. The grain size of the TiN powder used in the study by Rong *et al.*, 2002 was 1 μm, while the Al and cBN had the same grain size as in the cBN-Al system (Eremets *et al.*, 1998). The compositions of the starting materials ranged between 33 and 75 vol. % cBN, and the Al added to each mixture of cBN-TiN ranged between 14.8 and 12.3 vol. %. The compositions

of the mixtures are presented in Figure 2.7 below which shows the Knoop microhardness for samples sintered at 1 200 ^{o}C and 1 400 ^{o}C and at 5.75 GPa, and the load at which the microhardness was measured.

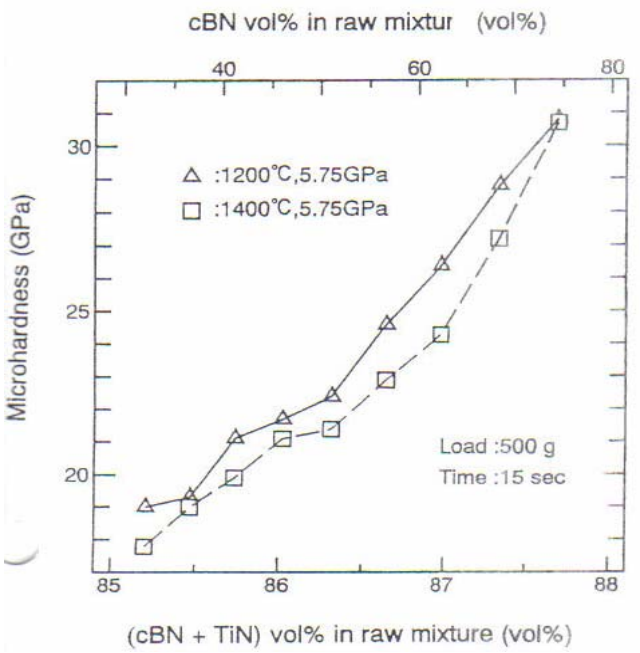

Figure 2.7: Knoop microhardness (GPa) at a load of 500 g of the cBN-TiN-Al composite against mixing composition (Rong *et al.*, 2002).

The microhardness values in Figure 2.7 increase with increasing amount of cBN in the raw mixture. Unlike in the cBN-Al system, the microhardnesses of the samples sintered at 1 200 ^{o}C show higher values than those of the samples sintered at 1 400 ^{o}C. The possible explanation for this difference was attributed to the crystallinity of the cBN phase. It was found (Rong *et al.*, 1994) that the crystallinity was not good in the composites sintered at 1 200 ^{o}C. It is presumed that due to the lack of Al, there is more residual cBN at the lower synthesis temperature, and as a result higher microhardness is to be expected since it has been observed that the microhardness of these composites is determined mainly by the amount of cBN. However, the highest microhardness of 30.7 GPa was obtained independently of the sintering temperature for the composition: 75 vol. % cBN, 13 vol. % TiN and 12 vol. % Al.

The microhardness in the cBN-Al system (Figure 2.6) was always lower than that of the cBN-TiN-Al system (Figure 2.7) at the same nominal cBN content. Due to the addition of relatively hard TiN particles, the microhardness of the binder phase was increased, especially in

the region of lower cBN compositions. The formation of significant amounts of AlB_2 at the lower cBN content in the cBN-Al system contributed to the resulting low hardness. In the cBN-TiN-Al system, XRD and microstructure analyses show that TiB_2 formed instead of AlB_2 (Benko *et al.*, 1997). The XRD analyses further revealed that TiB_2 and AlN formed with nearly the same relative amounts in all compositions.

2.5 Properties of binderless cBN

Conventional cBN sintered products are produced by sintering the mixture of cBN powder and binder materials under high temperature and high pressure. They have superior mechanical properties, and cutting tools made from them are being widely used for cutting hardened steels, cast iron and other materials. In order to improve the cutting performance of cBN's tool tips, tips made from products with different cBN contents and different crystalline grain sizes, and with different kinds of binders, are being produced by several manufacturers. The hardness of cBN is higher than that of the binder phases. Therefore, it is expected that products containing a higher volume fraction of cBN will show better cutting performance, at least in cases where abrasive wear is the dominant mechanism operation during machining. In this regard, binderless cBN sintered products, which contain neither a binder nor a sintering agent/catalyst, have been developed recently.

The method newly developed by Sumotomo Electrical Industries (SEI) uses as the raw material hBN (hexagonal boron nitride), which is completely converted to the cubic phase under high temperature and an extremely high pressure (~ 7 GPa). The converted particles of cBN are bonded together while the grain size is kept extremely fine (Sumitomo, 2000). The main advantageous features of the binderless cBN sintered product are as follows:

- It has high thermal conductivity as well as outstanding resistance to heat and thermal shock because it is a sintered product made of single-phase cBN.
- It is suitable for interrupted cutting, having superior mechanical properties, such as hardness and strength, because it is made of fine grains not larger than 0.5 μm that are solidly bonded to one another without a binder or a sintering agent/catalyst in the grain boundaries.
- It minimizes the possibility of thermal cracks and chipping occurring at the edge of the cutting tool in the extra-high-speed milling of cast iron: depending on machining conditions, tools provided with the binderless cBN sintered product can continue to

perform for more than 10 times longer than those provided with the conventional cBN sintered products containing binder materials.

- It can be cut and brazed to create desired shapes that will allow the production of inserts to be used for turning and milling, as well as the manufacturing of special brazing tools (Sumitomo, 2000).

2.6 Relationship of structure to properties in polycrystalline cBN

2.6.1 Effect of particle size on the strength of cBN materials

The sintering of cBN composites involves chemical reactions between the binder material(s) and the cBN particles (grains), resulting in strong chemical bond formation. The chemical reaction rate can be increased by increasing the surface area of both the cBN and the binder phase particles (Osipova *et al*, 1992). Therefore, decreasing the particle size increases sintering by promoting chemical interaction between the phases.

It appears certain that the decrease in the cBN grain size increases the strength of cBN composite materials. However, ultra-fine particles have a high tendency to form agglomerates in the matrix. Agglomerates of binder materials and cBN grains can act as defects in the microstructure, resulting in low-strength materials. Therefore, it is important to improve the mixing techniques when dealing with sub-micron particles in the composite materials in order to achieve uniform distribution of phases throughout the cBN composite matrix. Furthermore, the increases in the surface area of fine-grained materials increases their sensitivity to surface impurities such as oxygen, picked up from the atmosphere (USA patent No. 5 151 107). This results in difficulties when cleaning the sub-micron grains.

2.6.2 Effect of particle shape on the strength of cBN materials

The effect of particle shape on the strength may be explained in terms of the residual stress fields around the particles after sintering. The sintering of cBN composite materials requires the application of ultra-high pressure and high temperature which causes deformation and shrinkage of the composite. The deformation and thermal shrinkage rates of the composite constituents differ from one another and this results in the formation of various residual stress fields around each particle. Irregularly shaped particles tend to have high and low residual stress regions. High stress regions are more liable to initiate cracks under much lower stresses. Therefore, equiaxed or spherical particles are preferred to reduce localized regions of high stress within the micro-volumes of the cBN composite materials. Fine cBN particles that are obtained by crushing the

larger particles tend to have more equiaxed grains, which provides a more homogeneous stress distribution around each particle compared with uncrushed particles (Osipova *et al*, 1992)

Chemical reactions between cBN and binder materials are enhanced by the addition of aluminium. Aluminium reacts with cBN grains and, to a limited extent, it "rounds off" the particles, causing a reduction in possible stress raisers (Walnsley *et al*, 1987).

2.6.3 Effect of particle size distribution on the strength of cBN materials

Grain growth is associated with the consumption of small grains by the larger ones in order to lower the free energy by eliminating high energy regions, i.e. grain boundaries. Therefore, in the case of multi-modal particle size distributions, grain growth is enhanced. Grain growth has not been observed among cBN grains during high pressure and high temperature (HPHT) sintering (European Patent:EP 0598 140 A1), whereas binder materials are expected to suffer grain growth. Large grains in the microstructure of cBN composites are potential defects at which crack formation can occur. As a result, a narrow particle size range is preferred for binder materials, and a bi-modal or multi-modal particle size may be used in cBN composites to improve toughness (Vaben *et al*, 1995). However, depending on the relative amount and distribution of large cBN particles, composite strength may decrease substantially.

2.6.4 Effect of pores on the strength of cBN materials

The existence of micro- and macropores due to poor sintering in a ceramic composite has been found to decrease strength substantially. The reason for the resulting poor strength is because pores can act as crack-initiating sites, as well as providing little resistance to crack propagation, which leads to catastrophic failure. Pores may exist in the microstructure for various reasons and they can be eliminated by optimizing the sintering conditions (Avner, 1974). Sintering under high pressure (~ 5 GPa) and high temperature provides suitable conditions to facilitate mass transfer and hence bonding between phases in cBN composites. However, cBN-based materials generally contain ceramic binder phases (e.g. TiB_2) which have low atomic mobility due to covalent bonding. Therefore, the amount and distribution of aluminium in the matrix must be optimized to achieve a high degree of pore-free bodies after sintering.

It is important to avoid the formation of oxides on the surface (USA patent No: 5 151 107). These oxides inhibit the mass transfer required for sintering. The amount of oxide phases in a given volume can be increased by an increase in the surface area. Since high-strength composite

materials require very fine particles, which means a high surface area, extreme care must be taken to prevent oxidation of the starting materials.

2.6.5 Effect of microstructural homogeneity on the strength of cBN materials

The homogeneity of the composite matrix within microvolumes is the most important parameter affecting the strength. Based on the Griffiths law of brittle fracture, agglomerated cBN and/or binder phase particles will exhibit less resistance to crack initiation (Bhaumik *et a*l, 1993). Therefore, materials with a fine particle size, and uniform, well-distributed hard particles are favoured to increase strength.

The agglomeration of particles is generally associated with the milling and mixing of fine and ultra-fine particles. Since mixing efficiency decreases with decreasing particle size, the tendency towards agglomeration may be prevented by the addition of suitable dispersant agents to the milling slurry. It has been found that attritor milling of ultra-fine cBN particles and binder phase materials gives a more homogeneous microstructure compared with planetary ball milling. Therefore, homogeneous distribution of particles in a cBN composite matrix can be achieved, even for sub-micron particles, by improving the mixing techniques.

2.6.6 Bonding between different phases in the cBN composite

Good bonding between cBN and the binder phase usually occurs when the hard phase has a small amount of solubility in the binder phase. Therefore, aluminium or pre-reacted aluminium alloys are generally mixed with cBN particles to improve the bonding between phases before reactive-liquid phase sintering. It has been reported (Osipov *et al*, 1992) that if the aluminium content exceeds 20 wt % of the binder material, the hardness will be significantly reduced. Therefore, sub-stoichiometric Ti-containing phases are also added to further enhance the chemical reaction with cBN and to form TiB_2 and TiN, both of which are harder than AlN. TiB_2 is seen as a material that provides high junction strength with cBN and the binder phase (Yazu *et al*).

The mechanical wear resistance of cBN materials can be increased by increasing the bonding strength between the cBN particles and the binder phase. Therefore, a TiN or TiN/ TiB_2 coating on cBN particles was proposed to increase bonding between the binder phase and cBN. The coating of cBN particles can be accomplished by chemical vapour deposition techniques or by

dipping the cBN particles into a molten salt which contains the desired coating materials. The resultant microstructure is claimed to have fewer micropores at the cBN/binder interface, with a very homogeneous microstructure (USA Patent: PCT/US96/07014).

2.6.7 Composition of binder materials

Aluminium is added to almost all cBN composites to improve sintering. It can be added either in powder form, by admixing with other binder materials, or in pre-reacted form (Schmid, 1993). In the latter case, aluminium-containing alloys or compounds dissociate and form liquid metal during sintering. The addition of aluminium to cBN composites has many advantages:

- It is a low-melting metal and thus melts readily at low temperatures and transmits pressure evenly, restricting cBN to hBN transformation.
- It is very reactive and provides a high degree of sintering in a short time.
- It is compatible with cBN and binder materials, leading to the formation of high-strength cBN-to-binder, bonding.
- It reacts with hBN and cBN, as a result of which irregularly shaped cBN grains become rounded off.
- The addition of the proper amount of aluminium results in the formation of AlN, which has high thermal conductivity and increases the thermal shock resistance of the composite.

There are also some main disadvantages of aluminium addition, such as its high affinity for oxygen, and the addition of aluminium in excessive amounts can reduce substantially the strength and hardness of the composite (Sumitomo Patent: EP 0386 338 A1).

To improve the strength of the cBN-based materials, other binders, including TiN, have been used.

2.7 Wear of composite materials

Composites containing hard phases embedded in a softer matrix may be advantageous in applications requiring resistance to abrasive wear. The reason may be that a suitable combination of harder phases in a softer matrix can provide a good combination of hardness and toughness. Cemented carbides and high-speed steels are examples of commonly used wear-resistant materials of the multiphase type (Larsson *et al*, 1999). It has been argued that the wear resistance

of multiphase materials to abrasion or erosion depends on the dimensions of the surface damage caused by the wearing particles relative to the size of the reinforcing hard phase. Depending on the size of the hard particles and the contact zone of the abrasive particles, the composite will respond like either a homogeneous or a heterogeneous material. The latter case can lead to blunting or cracking of the abrasive particles under the interaction with the hard second phase. A combination of homogeneous and heterogeneous material responses may provide the highest possible abrasive wear resistance. The wear resistance also depends strongly on the strength of the interface between the hard phase and the matrix.

In erosive wear of ceramics, material is generally removed by the formation and intersection of cracks. Reinforcement by a harder phase in a ceramic matrix may increase the toughness by crack deflection, crack bowing and microcrack formation. The homogeneity of the binder phase content has been found to be important in the erosion resistance of ceramic composites (Larsson *et al*, 1999).

2.8 Cubic BN materials produced at ambient pressure

The conventional form of sintering is the one consisting of heating the original powder compact to a high temperature, but below its melting point, in a protective atmosphere known as "solid phase sintering". Solid-phase sintering of cBN requires ultra-high pressure and high temperature. The conditions of high pressure and high temperature facilitate mass transfer and hence bonding between the phases in cBN composites.

2.8.1 Infiltration of BN

During sintering under nearly ambient pressure (hot pressing, hot isostatic pressing), no solution, diffusion and precipitation would need to take place because all dissolved cBN would precipitate as hBN or as a reaction product. This could be possible if the product did not form very strong bonds between the cBN particles and could sinter at ambient temperature within a period during which the cBN did not convert. Forming composite structures has proved to be the solution. Composite structures prepared by mixing powders of boron nitride and metal aluminium, followed by compressing into pellets and sintering at various high temperatures and high pressures (~ 5 GPa), have been reported (Rong *et al.*, 2002). Although the infiltration of molten aluminium into a porous cBN matrix has not been reported, it could be a possible way of producing such materials. The main benefit of infiltration methods is the elimination of porosity with minimal dimensional change (Rong and Fukunaga, 1994).

Infiltration is a two-step process that wicks a molten phase into the pores of a porous structure of cold-pressed pellets. The liquid is added from an external reservoir in a process as illustrated in Figure 2.8 (Reed, 1995), using a separate cycle or a high-temperature transition at the end of the sintering cycle. Pore filling relies on liquid wetting the pores; a liquid with a low contact angle is spontaneously drawn into the open pore structure. In non-wetting systems, such as SiC-Al and cBN-Al, an external pressure is required to force the liquid into the pores. This process is termed "pressure casting". The sample is first evacuated to remove trapped gases. Pressure is applied to the melt to force it into the open pores, with the larger pores being filled at the lower pressures.

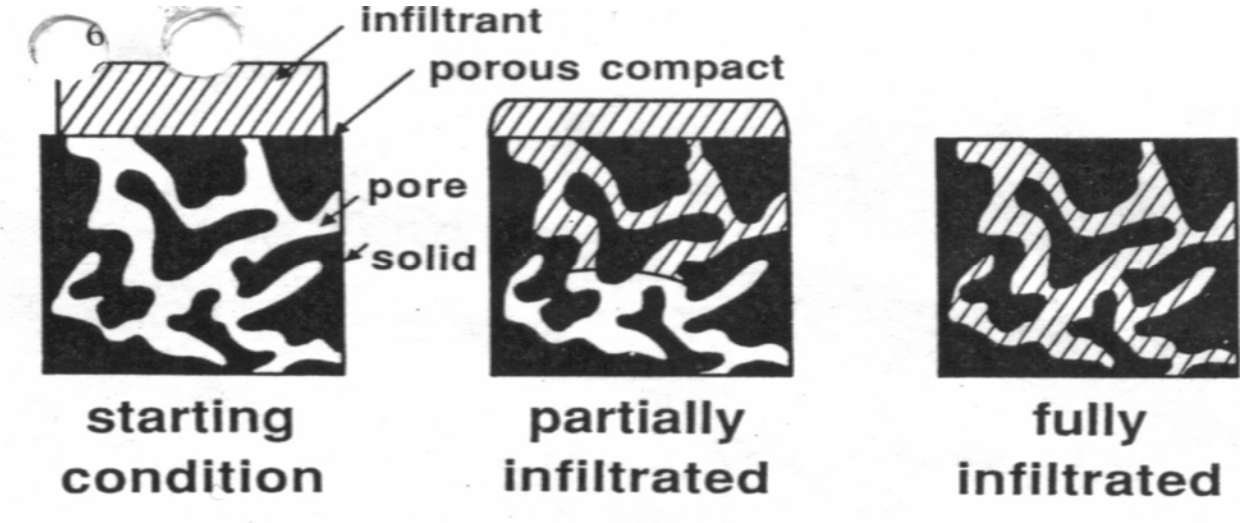

Figure 2.8: Schematic diagram of infiltration sintering (Reed, 1995).

The wetting angle in the Al-hBN system has been measured by Zhao *et al.* (1992) as a function of temperature. A summary of these results is presented graphically in Figure 2.9 below. There are no data available about the wetting of cBN by Al, but in a first approximation we assume that the wetting angles are similar. The graph shows that the wetting angle at 1 073K is about 140°. The angle decreases as the temperature increases. The infiltration of Al into BN will presumably begin to take place spontaneously when the wetting angle becomes less than 90° at temperatures above 950 ^{o}C.

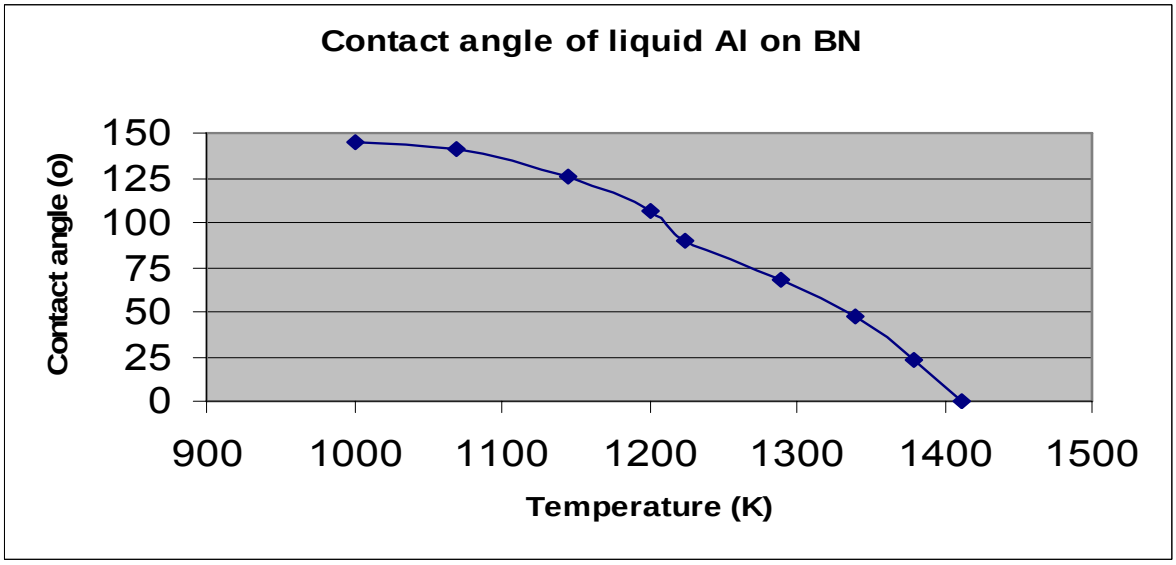

Figure 2.9: The contact angle in the Al-hBN system (Zhao et al, 1992)

A relation between pressure and pore size can be derived assuming cylindrical pores; the pressure, p, required to infiltrate a liquid into the pores relates to the contact angle, θ, the pore diameter, d_p, and the surface energy, γ, as follows:

$$p = \frac{-4\gamma\cos\theta}{d_p} \qquad (2.3)$$

For example, for a cylindrical pore structure with d_p = 1 μm, θ = 141° and γ(German, 1996) = 1.14 J/m^2, the pressure required is 3.5 MPa, whereas a pore diameter of 10 μm will reduce this pressure to 0.35 MPa.

2.8.2 Hot pressing of BN with Al

Hot pressing consists of applying an external pressure as well as high temperature (below the melting point of the main component of the material). In hot pressing, both high pressure and high temperature are imposed upon the powder mass, but they are both lower than the temperature and pressure that would be required if they were applied alone. The combination of both results in fast densification because both plastic deformation and diffusion are facilitated by high temperature.

Liquid-phase sintering consists of applying a temperature high enough for one or more of the components of the material to remain liquid during all or part of the sintering process. This

method is used for materials that would not achieve full densification by conventional solid-state sintering. It occurs through three stages: particle rearrangement, dissolution and reprecipitation , and coalescence.

In the first stage, the particles of the components that do not become liquid rearrange themselves in the liquid, leading to considerable densification. It is necessary that the liquid 'wets' the solid so that surface tension forces pull the particles together.

In the second stage, the solid particles partly dissolve into the liquid. The smaller particles dissolve preferentially. When the solution is saturated, reprecipitation occurs simultaneously, onto the large particles, which leads to a coarsening process and reduces the solid-liquid interfacial area and energy.

In the final stage, the solid particles that are not completely wetted by the liquid form bonds which leads to the formation of the skeleton of the solid (Luckyx, 2004).

The microstructure of BN sintered with Al by high-pressure (10 MPa) hot pressing has been studied by Benko *et al.* (1997). In their study they also measured the Knoop hardness of the sintered material before and after annealing. Boron nitride and Al with the same grain size (between 3 and 5 μm) were mechanically mixed in ethyl alcohol and then pressed under a pressure of 10 MPa and at a temperature of 1 750 ^{o}C. In this paper the data about density, heating rate and time was not reported. This was followed by annealing of the sample at a temperature of 950 ^{o}C in a vacuum of 3 MPa for 1 h. The prepared samples had a molar ratio of 9:1 (BN:Al). TEM micrographs show the presence of AlB_{10} and AlB_{12} after thermal treatment, and the hardness increased from 10 GPa to 20 GPa. Their studies led Benko *et al.* (1997) to the conclusion that the AlN grains nucleate at the Al-BN interface and that they then grow into the metal area. The significant increase in the hardness after annealing can be attributed to the formation of the AlN phase from Al. The presence of Al before annealing therefore affected the hardness of the composite.

2.9 Aluminium-boron-nitrogen ternary phase diagrams

To fully understand the densification of the Al-cBN composite, a detailed understanding of the relevant phase diagrams is necessary. The phase diagrams for the binary boundary systems Al-B,

Al-N and B-N have been studied sufficiently (Rogl and Schuster, 1992). Crystallographic data on the elements and binary phases that occur in the Al-B-N system are listed in Table 2.4.

Table 2.4: Crystallographic data on the elements and binary phases of the Al-B-N ternary system

Compound	Structure type	Lattice parameters (nm)
Al	Cu	a= 0.4048
α-B	B	-
β-B	B	a= 1.0925, c= 2.3814
β-B	B	a= 0.88, c= 0.505
AlB_2	own	a= 0.3005,c= 0.3257
AlB_{10}	own	a= 0.5690, b= 0.8881, c= 0.910
α-AlB_{12}	own	a= 1.0116, c= 1.4283
β-AlB_{12}	-	a= 1.234, b= 1.2663, c= 1.061
γ-AlB_{12}	own	a= 1.6623, b= 1.754, c= 1.018
AlB_{31}	own	a= 1.0955, c= 2.3868
AlN	ZnS	a= 0.311, c= 0.498
AlN	-	a= 0.4104
BN	C	a= 0.25039, c= 0.6612
BN	ZnS	a= 0.3615
BN	ZnS	a= 0.255, c= 0.424

The Al-B binary system (shown in Figure 2.10) contains AlB_2 and AlB_{12} as the only binary phases (Rogl and Schuster, 1992). The solid solubility of B in Al is less than 0.025% B at the (Al)+AlB2 eutectic temperature at 659.7 ^oC. Included in the diagram is the compound Al_2B_3 which has been recently reported from ion-implantation experiments and is claimed to be stable at least up to 525 ^oC (Rogl and Schuster, 1992). The phase diagram given by Bodkin (2005) shows a peritectic reaction of L+ β-AlB_{12} to form AlB_{10} at 1 850 ^oC. However, Rizzoli *et al.* (2002) in their study found no reliable data supporting the existence of both AlB_{10} and β-AlB_{12} compounds in the Al-B binary system. The Al-N binary system contains only one compound, namely AlN.

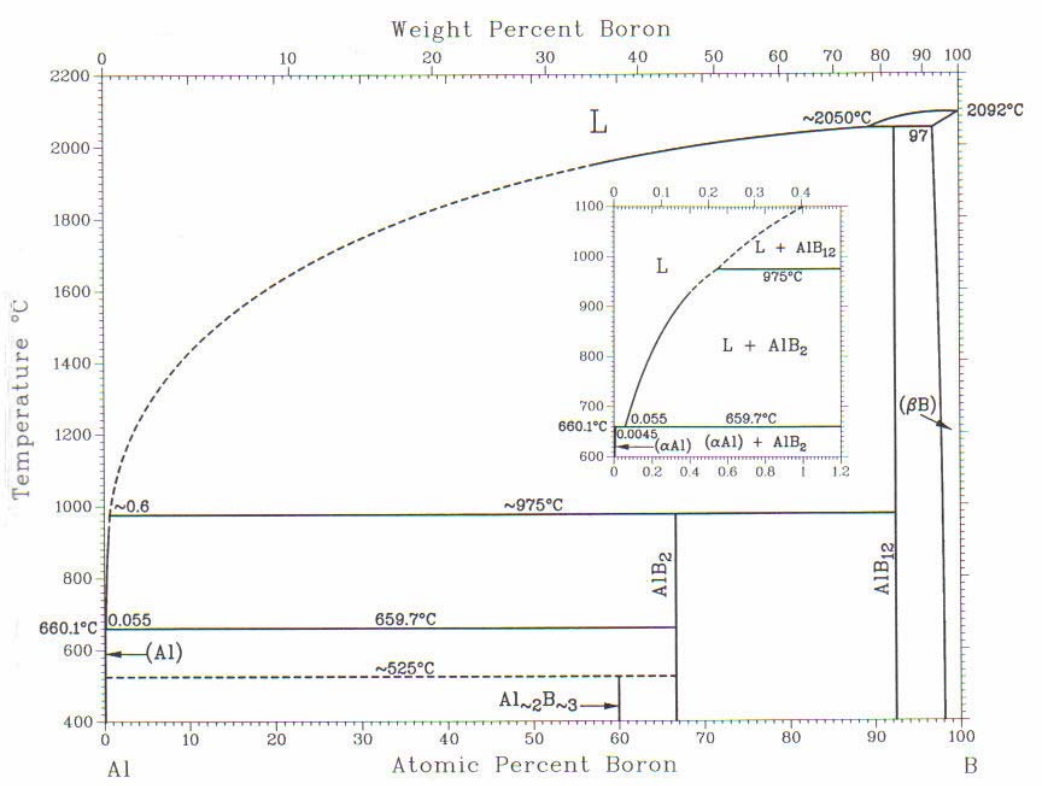

Figure 2.10: Al-B binary system (Rogl and Schuster, 1992)

Isothermal sections of the Al-B-N systems at 900 ^{o}C and 1 500 ^{o}C are presented in Figure 2.11 (Rogl and Schuster, 1992) and Figure 2.12 (Rizolli *et al.*, 2002) respectively below. In both cases, no external nitrogen was used. The binary boundary systems at 1 500 ^{o}C confirmed the existence of the AlB_{12}, AlN and BN compounds. In the study by Rizzoli *et al.* (2002), the sample of $Al_{33.3}B_{66.7}$ composition ("AlB_2") was found to contain two phases, namely Al and AlB_{12}. There was no evidence for the existence of the AlB_{10}, β- and γ-AlB_{12} and AlB_2 compounds at this temperature. However, the binary boundary systems at 900 ^{o}C show the existence of the AlB_2 compound. This compound decomposes to form both Al and AlB_{12} at high temperatures. No ternary compounds were observed at either temperature.

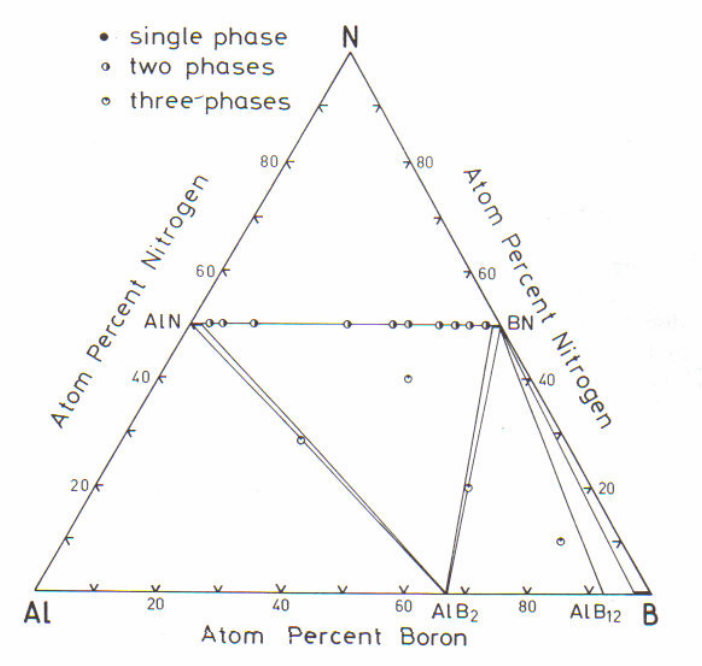

Figure 2.11: Isothermal section of the Al-B-N system at 900 ^{o}C under 10^{5} Pa argon

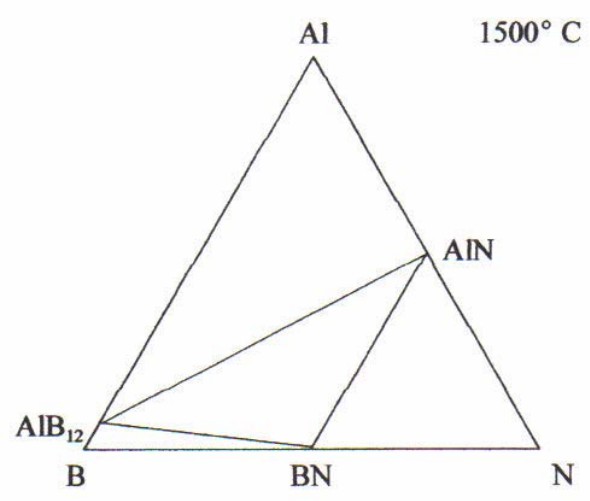

Figure 2.12: Isothermal section of ternary Al-B-N system at 1 500 ^{o}C

CHAPTER 3 MOTIVATION FOR THE RESEARCH OBJECTIVES

3.l Background to the research objectives

The combination of two or more phases to produce a composite is a common method for meeting the special requirements of advanced engineering materials. By combining ceramics and metals, a composite with, for instance, good mechanical and electrical properties at high temperature can be achieved. Cermets are an example of composites whose properties have been optimized for a specific application.

Polycrystalline diamond (PCD) materials are established materials in cutting and drilling applications. Although they are very hard and extremely wear-resistant, poor thermal stability of the diamonds generally causes their decomposition. The cobalt that is normally used as solvent during manufacturing leads to chemical instability of the PCD material at temperatures above 700 ^{o}C. This poor thermal stability can be improved by removing the metal binder phase after synthesis. The resulting material will exhibit a porous structure and therefore, whilst being relatively stable, it will be prone to internal oxidation. Therefore, in some instances the porous structure is infiltrated by liquid silicon.

SiC-diamond materials have been manufactured by the infiltration of porous diamond/carbon bodies with molten silicon in vacuum at 1 550 ^{o}C for a duration of about 10 min (Skeleton technologies,2000). To ensure sufficient formation of SiC and to minimize the amount of residual silicon, the volume fraction of the initial phases and the amount of porosity in the "green body" are usually 60 vol. % diamonds, 10 vol. % carbon and 30 vol. % porosity. The prepared composite was found to have a Knoop hardness of more than 55 GPa and a fracture toughness of at least 6 MPam$^{1/2}$. The test done on this composite revealed that the bonding between the diamonds and the SiC matrix is strong enough to withstand both the abrasion and erosion tests (*Larsson*, 1992). In this study there were no signs of the removal of entire diamonds from the matrix or crushing of the whole particles. The test also revealed that the composites containing fractions of both smaller and larger diamonds were better in the abrasion than in the erosion test.

The success of the SiC-diamond composite prepared by Skeleton Technologies (2000) led to speculation that a similar cBN-based composite could be obtained. Instead of silicon, aluminium could be used, which would lead to the formation of aluminium nitride (which has good thermal

conductivity) and some borides. The cBN particles were initially heated to higher temperatures to allow some surface hexagonalization. The hBN formed was expected to play a similar role as that of graphite added in the skeleton material (Skeleton technologies, 2000) i.e it was envisaged that Al will react more readily with hBN than cBN. An important aspect of this material is that it can be manufactured in any shape or size. The method is called "near-net-shaping", meaning that the shape of the sintered part has very nearly the final dimensions required for that part, with no or little subsequent expensive finishing operations being necessary. On the other hand, it is difficult but not impossible to produce PCD and other similar materials in non-flat shapes. In such cases the final shape is produced only by costly cutting, and joining.

The objective of this project was to develop dense Al-cBN composites with 40-50 vol% cBN content. To achieve this goal, two different strategies were used: infiltration of cBN preforms and hot pressing of cBN-Al mixtures. The particle size of cBN and the amount of Al were systematically varied and the influence of these parameters on densification and selected properties was evaluated. In the initial experiments hBN powder was used. The purpose was to learn and understand the Al/hBN system before experimenting with the expensive cBN powder. The whole experimental programme followed in this work is presented in Figure 3.1:

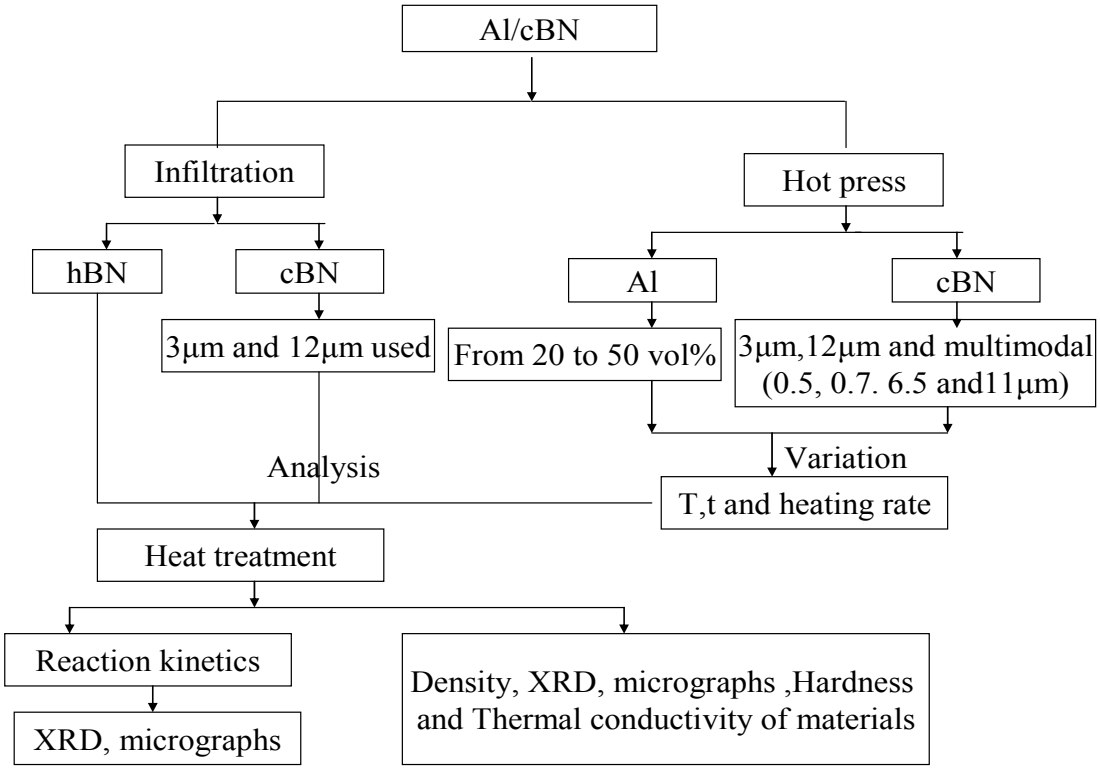

Figure 3.1: Schematic diagram of the experimental plan.

It is important to calculate the change in volume during the reaction. As discussed previously, the reaction between Al and BN was expected to produce AlN, AlB_2 and/ or AlB_{12} as products. The aim was to use up all the Al metal and have most of the cBN phase left unreacted.

3.2 Calculating the volume change

Two equations were expected:

Assume the reaction $3Al+2BN \longrightarrow 2AlN+AlB_2$ (3.1)

Table 3.1: Data used to calculate the change in volume during the reaction

	Al	**BN**	**AlN**	**AlB_2**
Mr (g/mol)	26.982	24.818	40.989	48.604
M (g)	80.95	49.64	81.978	48.604
P (g/cm^3)	2.702	3.48	3.25	3.19
V (cm^3)	29.96	14.264	25.224	15.236

The total volume of reactants is 44.224 cm^3/mol and the total volume of products is 40.46 cm^3/mol. Therefore, the change in the volume due to contraction is 8.5%.

The other reaction is $13Al+12BN \longrightarrow 12AlN+\alpha\text{-}AlB_{12}$ (3.2)

Table 3.2: Data used to calculate the change in volume during the reaction

	Al	**BN**	**AlN**	**AlB_{12}**
Mr (g/mol)	26.982	24.818	40.989	48.604
M (g)	350.766	297.816	491.868	156.714
P (g/cm^3)	2.702	3.48	3.25	2.55
V (cm^3)	129.82	85.58	151.34	49.13

The total volume of the reactants is 215.4 cm^3/mol and the total volume of products is 200.47 cm^3/mol. Therefore, the change in volume due to contraction is 7.0%.

In both reactions there is a large change in volume, which could cause either porosity or large tensile stresses. Both are undesirable for the material.

3.3 Calculation of the cBN to be used during reaction

Assume the reaction $3Al+2BN \longrightarrow 2AlN+AlB_2$ (3.3)

$$V_{BN} = \frac{2}{3}\left(\frac{\rho_{Al} \times V_{Al} \times M_{BN}}{M_{Al} \times \rho_{BN}} \right) \quad (3.4)$$

where M is the molar mass of each phase and V_{BN} is the volume of BN consumed during the reaction. For 50 vol. % Al, calculation gives 25.8 vol. % cBN reacted and hence only 24.2 vol. % of the cBN phase is expected to be present in the final material. A simple first approximation of the hardness can be made on the assumption of the volume mixture:

$$\begin{aligned} H_v &= 24.2\% \times H_v(cBN) + 75.8\% H_v(AlN) \\ \text{Expected hardness} \quad &= 0.242 \times 45 + 0.758 \times 12 \\ &= 20GPa \end{aligned} \quad (3.5)$$

The calculation assumes insignificant amount of the borides AlB_2 and/or AlB_{12}. Similar calculations were done using different amounts of the starting materials. The results are presented graphically in Figure 3.2.

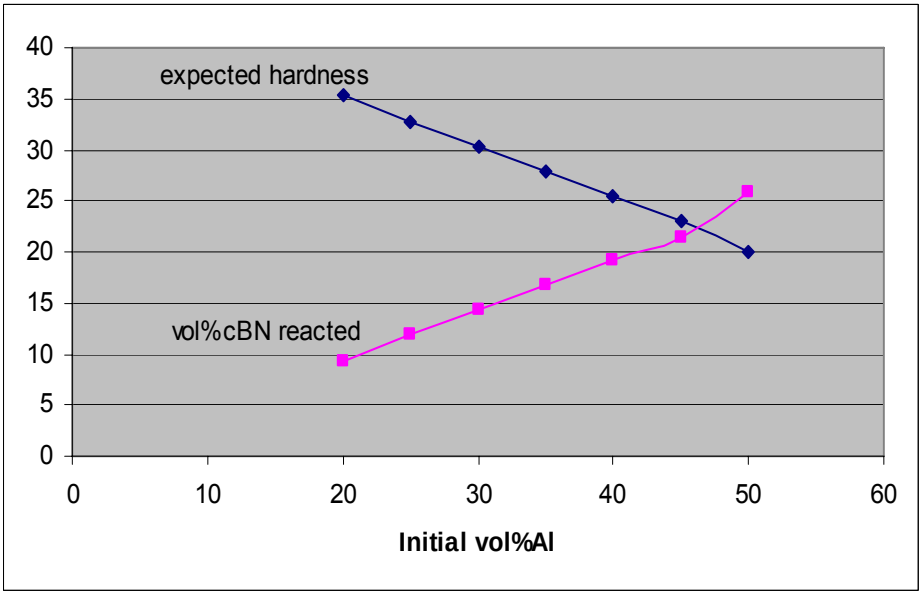

Figure 3.2: Reacted cBN and resulting hardness as a function of initial vol. % Al
Both graphs were constructed based on the theoretical calculations done as described above.

The graphs in Figure 3.2 show that as the initial vol. % of Al is increased, the vol. % of cBN required during reaction also increases. The decrease in the cBN phase in the final material results in a decrease in hardness, as shown by the dark blue line in the graph. The results above can be interpreted as follows: when 20 vol. % Al was used, about 10 vol. % cBN was used during the reaction and this led to the hardness of approximately 35 GPa.

CHAPTER 4 EXPERIMENTAL DETAILS

In this chapter the experimental techniques, materials, apparatus and procedures will be described.

4.1 Starting materials and their characterization

All the powders and chemicals used are given in Table 4.1.

Table 4.1: Materials used for processing

Material	Particle size (μm)	Company
hBN	40	H.C. Starck
cBN (two)	3 and 12	Element Six
cBN (grades 1, 2, 3 and 4)	0.52, 0.70, 6.52 and 11.4	Element Six
ABN800	~200 μm	Element Six
Al	5	Saarchem, 99.9%
Commercial Al foil	Thickness 20	Good Fellow Metals (UK)
Al sheet (99.999% purity)	Thickness 250	Good Fellow Metals (UK)
AlB_{12}	2 – 5	Poly Metals SA, 98%
AlN	5	H.C. Starck
Argon (UHP 99.999%)	–	Afrox
Nitrogen (UHP 99.999%)	–	Afrox
Hexane	–	Saarchem, 99.9%
Water	–	Distilled and deionised

The starting materials used in this work were hexagonal boron nitride (average particle size 40 μm), cubic boron nitride (average particle size 12 and 3 μm), crushed cubic boron nitride: grades 1, 2, 4 and 9 (average particle sizes 0.52, 0.70, 6.52 and 11.40 μm respectively), commercial aluminium foil (thickness = 20 μm), aluminium sheet (99.999% Al with thickness = 250 μm) and aluminium powder (average particle size 5 μm).

For the analysis of the particle shapes, SEM images were used. The SEM images of the hexagonal boron nitride and cubic boron nitride powder particles used in this work are shown in Figures 4.1, 4.2 (3 μm) and 4.3 (12 μm) respectively. Hexagonal boron nitride particles show plate-like shapes and are white in colour. The 3μm cubic boron nitride powder consisted of fine, well faceted particles. Figure 4.3 shows an irregular shaped particle of the 12μm powder. The irregular shape is the result of crushing of bigger grains in order to produce this grade.

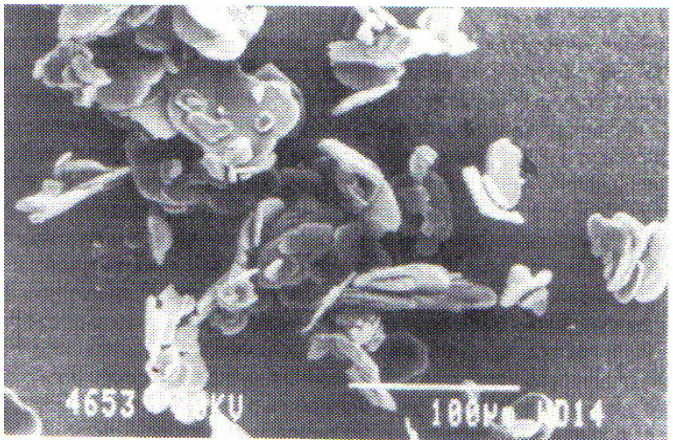

Figure 4.1: SEM image of the hexagonal boron nitride powder

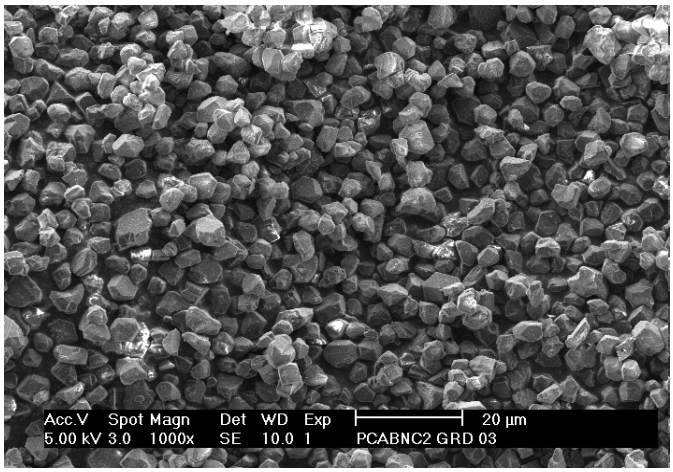

Figure 4.2: SEM image of the cubic boron nitride powder with an average size of 3 µm

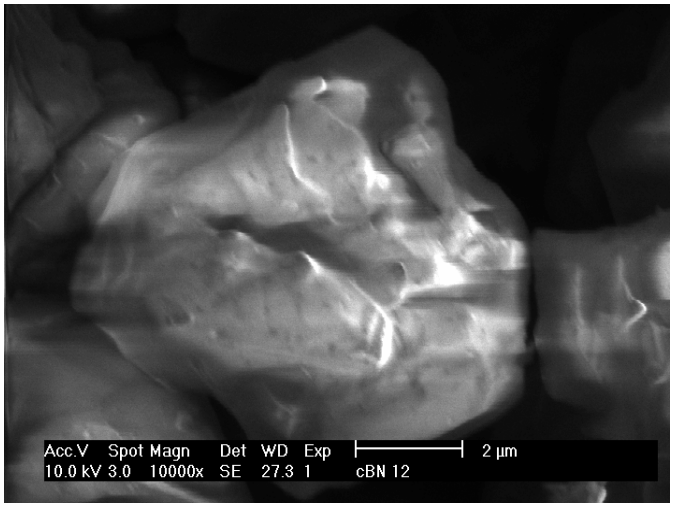

Figure 4.3: SEM image of the cubic boron nitride powder with an average size of 12 µm

Figure 4.4 shows a micrograph of ABN800 particles. ABN800 is a commercial name under which Element Six (Pty) Ltd market a particular grade of cBN abrasive grit. The particles of cBN belonging to this grade are dark brown in colour, strong and very thermally stable. (Element Six, 2000) These particles are sharp and angular, with a predominantly trancated tetrahedral morphology. The size of the particles shown in Figure 4.3 is above 0.1 mm.

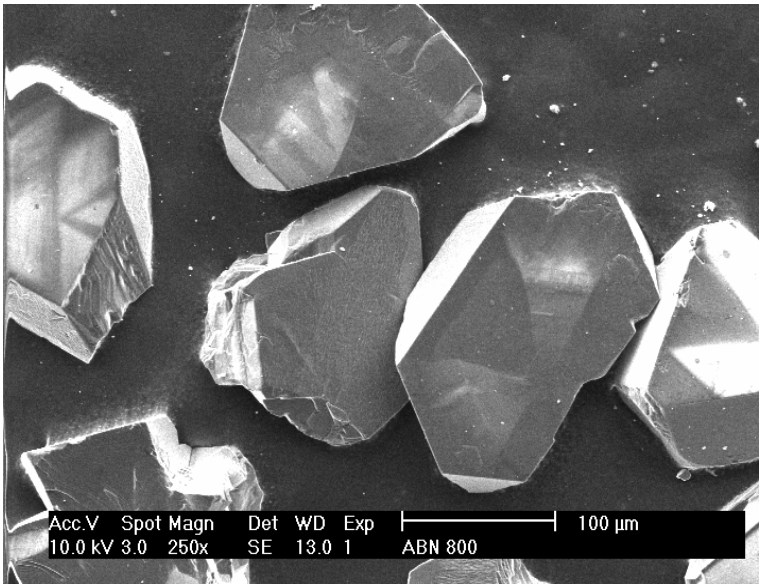

Figure 4.4: SEM images of ABN800 with a particle size of over 100 µm

The particle size was analysed using a Mastersizer 2000 (Malvern), with water used as the medium to disperse particles. Mastersizer 2000 instrument used to measure particle size and particle size distribution in this work relies on the principle of the Laser Diffraction Technique (Reed, 1995). There are many theories and models that the modern particle size analyst can use to predict the way particles scatter and absorb light. The accepted theory which accurately predicts the light scattering behaviour of all materials under all conditions is known as the Mie theory. Mie theory was developed to predict the way light is scattered by spherical particles and deals with the way light passes through, or is adsorbed by, the particle. This theory is more accurate, but some specific information, such as particle refractive index and absorption need to be known. From such theories, knowing the size of the particle and other details about its structure, it is possible to accurately predict the way it will scatter light. Each size of particle will have its own characteristic scattering pattern, like a fingerprint, that is unlike any other size of particle. The Mastersizer works backward from such theories by using the optical unit to capture the actual scattering pattern from a field of particles. Then, using the above theory, it can calculate the size of particles that created that pattern.

The Mastersizer measurement is fundamentally a measurement of the volume distribution (such as that of the crushed cBN powders given in Figure 4.5), however the results can be transformed into a surface length or number distribution by using a mathematical process which might amplify any error in the original result. To understand the meaning of the results given in Figure 4.5 some fundamental concepts are explained in appendix C. All the grades in Figure 4.5 show a narrow particle size distribution, except grade 2 which shows a bimodal distribution.

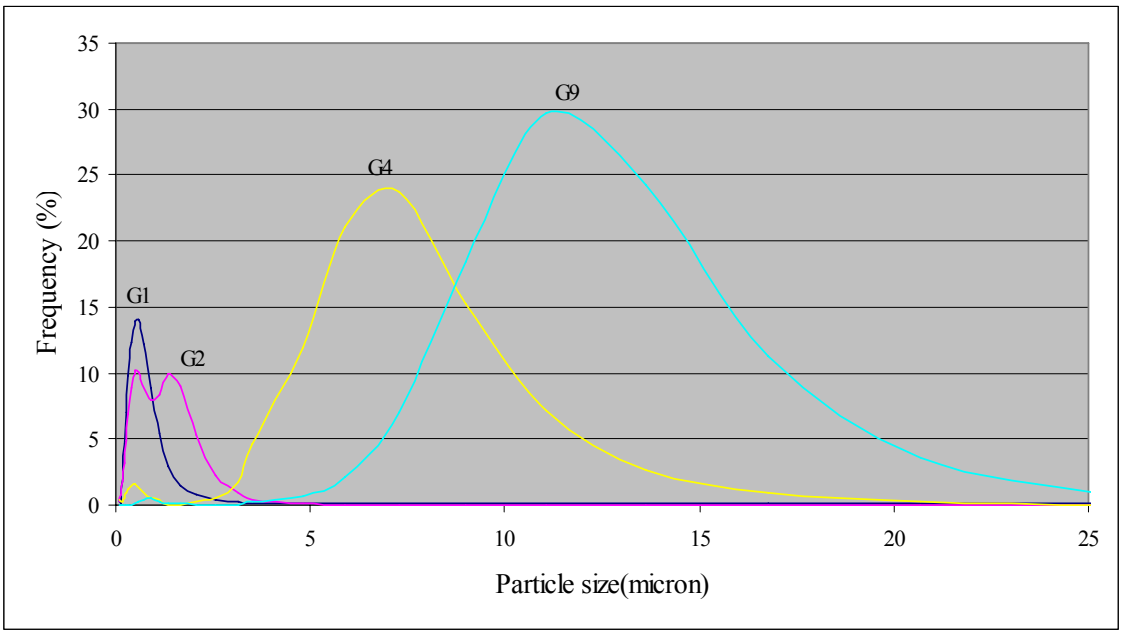

Figure 4.5: Size distribution of grades 1, 2, 4 and 9

In addition to the above materials, hexane was used during the mixing of powders and when measuring the samples' density, following Archimedes principle. Argon gas and/or vacuum was used during sintering; however, nitrogen gas was used as a reaction atmosphere for the heat treatment at high temperatures.

4.2 Experimental apparatus

4.2.1 Turbular mixer

A turbular mixer was used to facilitate the dry mixing of powders to prepare them for hot pressing. Stainless steel balls with a diameter of 5 mm were used as a milling medium during mixing. The number of balls used depended on the amount of powder that was mixed. The mixing was normally done for 60 min.

4.2.2 Attritor mill

An attritor mill was used to facilitate the wet mixing of powders, using hexane as a solvent. To mix the powders, balls were not used; instead, an impellor disc made of stainless steel was used with a rotating speed of 1 500 r/min. During mixing, about 1 wt % of polyisobutylene succinimide (commercial name Lubrizol, marketed by the Lubrizol Corporation) was added as a surfactant. This was necessary to avoid agglomeration of the fine cBN powders.

The mixed powders were dried in a rotary evaporator. Rotary evaporator is the equipment used for thermal separation of mixtures of materials. Whenever two liquids are being separated, the process is called distillation and when a liquid is being separated from a solid, the process is known as drying. Rotary evaporator was used to separate hexane liquid from the solid cBN powder mixture. The process of drying is based on the principle that different materials have different vapour pressures. The mixture is heated until it evaporates and then is re-condensed. The substance with the higher vapour pressure (hexane) converts to vapour and accumulates in the condensate The schematic diagram of a rotary evaporator is shown in Figure 4.6 below. It contains three parts ,that is, the heating bath (A) that supplies the energy, the support frame (B) that holds the parts together and accommodates the jack (1), the rotary motor (2), the control device (3), The glass assembly in which the process of drying takes place consists of the evaporation flask (4), the sealing system (5), the glass condenser (6), and the receiving flask (7). When the drying process is complete, the hexane is collected in the receiving flask (7), while the cBN powder is left in the evaporation flask (4). To attain complete dryness, the work must be done at low pressures. During the drying process the flask is rotated, thus ensuring that the various solid components of the powder being dried do not separate.

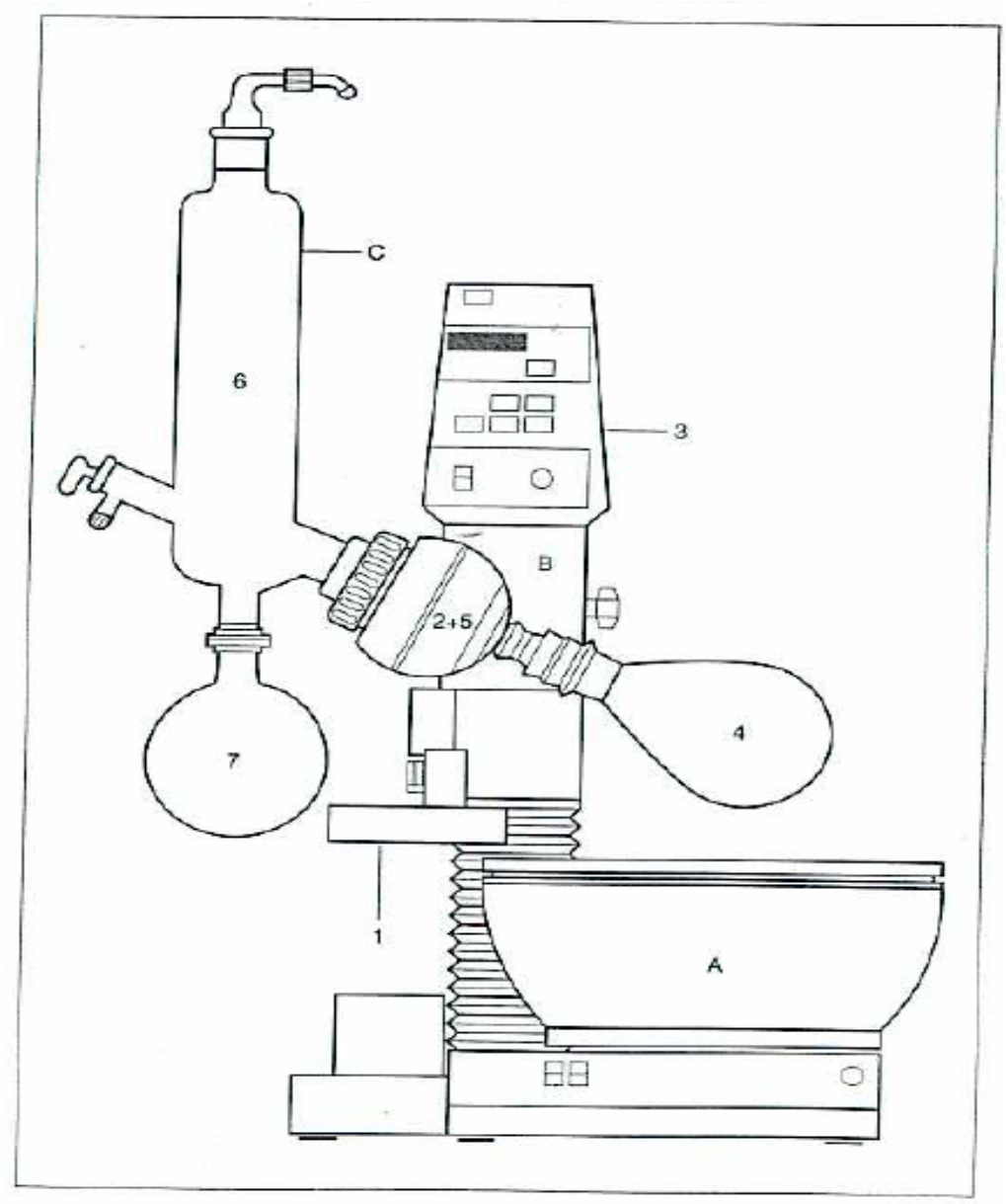

Figure 4.6: Schematic design of a rotary evaporator.

4.2.3 Tube furnace

The tube furnace used for this research work for the hexagonalization of cBN and for some heat treatment experiments was a normal horizontal tube furnace made by Carbolite. The tube furnace can reach a maximum temperature of 1 600°C and is water cooled. The work tube was an aluminium oxide tube (inner diameter: 7.10 cm; outer diameter: 7.40 cm; length: 115.9 cm). Both sides of the tube could be sealed from air with lids made of brass. O-rings were used to effect a seal at the point of contact of the brass cap with the Al_2O_3 tube. One of the sides was kept closed, while the other could be opened to allow the loading of the sample. Rectangular alumina crucibles were normally used as the sample holders. The furnace had an ("on" and

"off") Eurotherm microprocessor that controlled the heating rate and kept the temperature constant in the hot zone of the furnace. The furnace temperature was measured by a standard Pt-Rh thermocouple, which was connected to the microprocessor. The experiments were done in atmospheres of either argon or nitrogen.

The tube furnace used during infiltration was a typical vertical tube furnace which was also made by Carbolite. This tube furnace allowed the introduction of low uniaxial pressure (maximum 15 MPa) from the top. A stainless steel tube was used to load the sample into the graphite die. This tube was then inserted inside the tube furnace and sealed at the top with a lid made of stainless steel. Figure 4.7 shows how the sample was loaded in the stainless steel tube and how the pressure was applied. The furnace was evacuated using a rotary pump and then flushed with argon gas. The chamber was evacuated again after 3 min and backfilled with argon before heating up to 300 ^{o}C at 5 ^{o}C/min in the furnace. At 300 ^{o}C, the rotary pump was started again while heating to 800 ^{o}C at 5 ^{o}C/min and the furnace was held at this temperature for 30 – 60 min. The furnace was then cooled at 10 ^{o}C/min to ambient conditions; however, the cooling rate below 600 ^{o}C was slower than the programmed cooling rate.

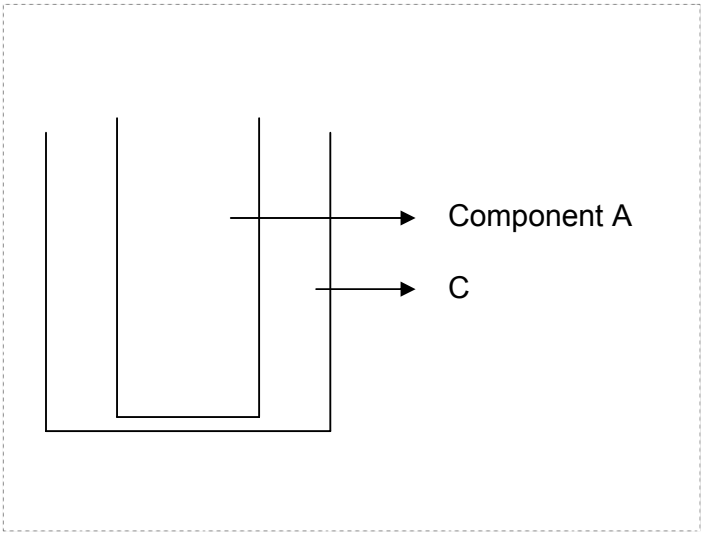

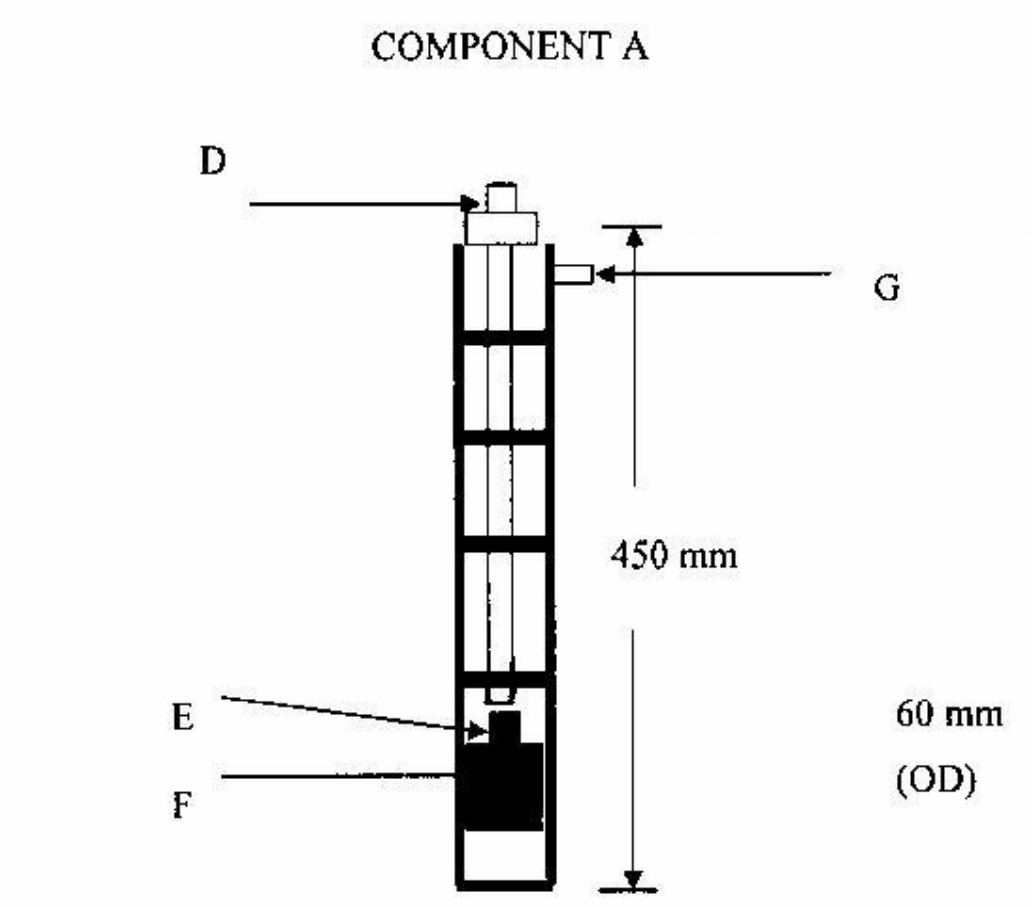

Figure 4.7: Schematic representation of the vertical tube furnace used during infiltration

Key to Figure 4.7

A. Sample holder, B. Steel furnace, D. Stainless steel rod where pressure was applied, E. Graphite punch, F. Graphite die, and G. Vacuum pump /argon gas

4.2.4 Uniaxial hot press

The uniaxial hot press used in this research work for sintering and heat treatment was purchased from Thermal Technology Industries. The furnace is heated by carbon elements. It can reach a maximum temperature of 2 200 ^{o}C and it is water cooled. A maximum pushing force of 100 000 N can be applied to compacts during the furnace cycle. The force is applied through graphite punches uniaxially from the bottom graphite punch. A rotary vacuum pump is attached to the press and can reach vacuum levels of 10 millitorr. Figure 4.8 below shows a photograph of the hot press. As can be seen in the photograph, the furnace is connected to a personal computer (PC) which helps the user to follow the key parameters during sintering cycle. The computer programme outputs graphs of load against time, temperature against time, and displacement against time.



Figure 4.8: The uniaxial hot press used

The all graphite components that are to be in the hot zone of the furnace need to be coated with an hBN suspension that is stabilized with polyvinyl pyrolidone. The suspension is made using the following components: 2 g of polyvinyl pyrolidone, 37 g of hBN and 100 ml of water. All the components of the suspension are stirred together vigorously using a magnetic stirrer bar until the constituency of the entire suspension is uniform. The suspension is then applied with a small paint brush to the clean hot (≈ 80 ^{o}C) surface prepared for coating. The graphite components placed in the hot zone include two graphite punches, an outer graphite die and

insert, and an inner graphite die (which holds the sample) of a fixed diameter; dies with inner diameters of 18.9 mm and 14.5 mm were used.

A general furnace programme was used to prepare the samples. The furnace was evacuated using the rotary pump to pressures of less than 200 mtorr and then flushed with argon gas. The chamber was evacuated again after 3 min and the furnace temperature cycle started under vacuum. The furnace was heated to 670 ^{o}C at 5 ^{o}C/min and held there for 20 min to allow the liquid phase (aluminium) to form and infiltrate into the pores of the BN preform. During the holding time, the load was applied to the sample and the furnace was allowed to heat up to 800 ^{o}C at 10 ^{o}C/min and held at this temperature for 30 or 60 min. In addition, other temperatures and heating rates were used as described in Chapter 7. The furnace was then cooled at 20 ^{o}C/min to room temperature; however, at temperatures below 600 ^{o}C the furnace cooled down at a slower cooling rate than the programmed cooling rate. Figure 4.9 below shows the typical temperature profile used during sintering. At 300 ^{o}C the load was removed from the sample and the chamber was refilled with argon. The sample was only removed from the die inside the furnace at temperatures below 80 ^{o}C.

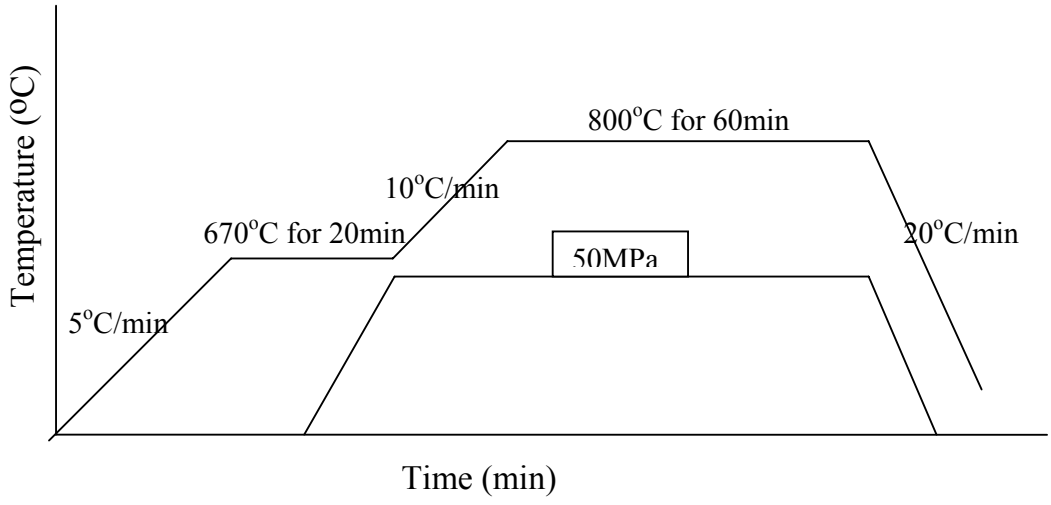

Figure 4.9: Typical temperature profile used during infiltration.

4.2.5 Thermal analysis technique

Thermal analysis studies are concerned with the measurement of heat and weight changes in a system when it is heated or cooled in a predetermined manner. These studies provide insight into the physical nature of the system, the chemical reactivity in a given environment and the behaviour during heating, e.g. phase-change reactions. They also provide kinetic data for

reaction rate studies. Thermal analysis techniques include differential thermal analysis (DTA), differential scanning calorimetry (DSC), thermogravimetry (TGA) and derivative TGA (DTGA). In this work DTA and TGA were used in a nitrogen atmosphere.

4.2.6 Polishing equipment

The prepared samples needed to be polished for SEM analysis and to perform mechanical testing. The samples to be polished were first mounted in a hot mounting press in Lucite powder. The mounting of each sample took about 35 min. The sample was then lapped for about 20 min on a standard lapping wheel, using 350 μm diamond grit. Additional lapping of the sample with 120 μm diamond grit was done for about 10 min.

The flat sample was then subjected to metallographic polishing. The normal procedure is as follows: polish for 20 min with 9 μm diamond grit at 200 r/min, with -6 μm diamond grit for 20 min using the same speed, with -6 μm diamond grit on a Textmet wheel for 10 min at 250 r/min and finally, for -5 min with a 1 μm diamond grit at 300 r/min.

4.3 Powder processing

4.3.1 Preparation of green samples for infiltration

The hexagonal boron nitride powders were pressed, using a stainless steel die, into pellets of 26 mm diameter under a pressure of 30 to 60 MPa at room temperature. The porosities of the samples were evaluated by comparing the green densities with the theoretical density. Aluminium sheet was cut into discs using a stainless steel punch with a diameter of 26 mm. The amount of Al to be added depended on the porosity of each sample, since the Al was added to fill the pores in the BN skeleton.

The partially hexagonalized cBN powder was also prepared using the same procedure described above for hBN. The same method did not work for pure cBN since the particles could not be pressed together to form a green compact.

4.3.2 Preparation of powder mixtures for hot pressing

Initially, some aluminium powder was added to the cBN powder and mixed together using the turbular mixer in order to form a green compact. In this case, the aluminium was acting as a binder holding the cBN particles together.

The crushed cBN powders (multimodals containing three to four different grades (described in detail in Chapter 7) were pressed, using the stainless steel die, into pellets of 18.9 mm diameter under a pressure of 30 to 200 MPa at room temperature. The porosities of the samples were evaluated by comparing the green densities with the theoretical density. The amount of Al added to the mixed cBN grades was between 20 and 50 vol. % of the total mixture.

4.3.3 Coating procedure

The Ammonium Chloride is mixed together with the the Aluminum powder according to the desired volume fraction. This is done in a 100ml plastic container. Six medium sized steel balls are added to the container to speed up the mixing process. The component powders are mixed together for an hour using the turbular mixer. The cBN is added to the mixture at a ratio of 1 to 4 by volume, of Al/NH_4CL to cBN. These components are further mixed together for another hour. The resulting mixture (cBN/Al/ NH_4Cl) is poured into alumina boats, and alumina pebbles are placed on top of the mixture. The alumina pebbles act as inert fillers and capture some of the gases being released in the furnace; thus preventing the clogging of the exhaust pipe of the tube furnace. The experiments were conducted at different temperatures and different dwelling times in the furnace to determine the temperature profile at which maximum coating of the cBN particles could be obtained. The final coating arrangement used a ratio of 30/70 for Al/NH_4Cl and the temperature profile shown in Figure 4.10 below. The alumina boat containing the mixture (cBN/Al/ NH_4Cl) was placed in the tube furnace, and heated up to 350 ^oC, at a rate of 10 ^oC/min. The formation of $AlCl_3$ and release of gases occur at around 350 ^oC, therefore there was a dwelling point of 1hour at this temperature. During that period, the following reaction takes place:

$$Al(s) + 3NH_4Cl\ (s) \rightarrow AlCl_3\ (s) + 3/2\ H_2\ (g) + 3NH_3\ (g) \quad \text{.....(4.1)}$$

A second dwelling time of 5hrs at 1000 ^oC was introduced in order to allow for a complete coating process, and followed by cooling, at a rate of 10 ^oC/min. The coated cBN powder contained aluminium nitride. Aluminium boride (AlB_2) phase was not detected. The boride phase is expected to form; however, it was probably too low in quantity to be detected. The method of acid digestion was used to quantify the thickness of the coating.

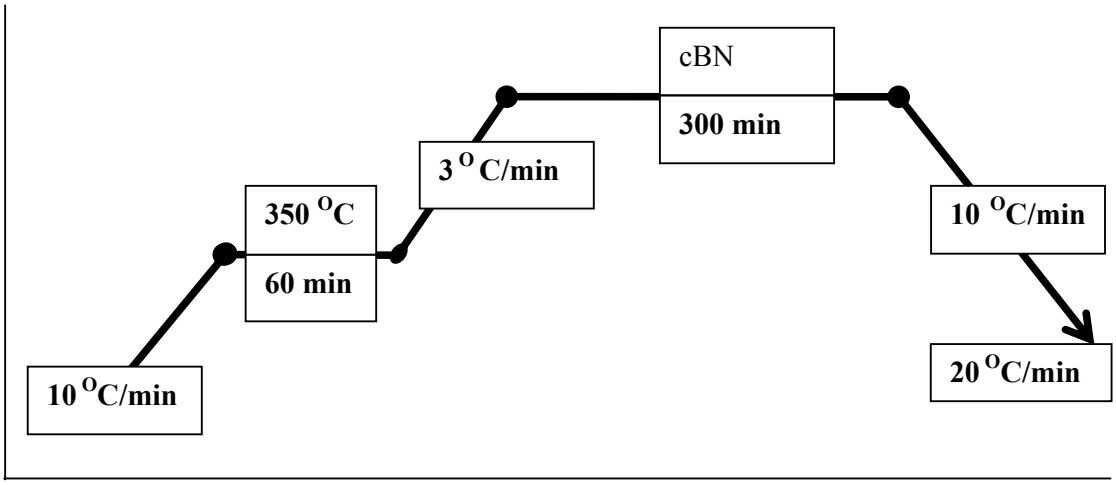

Figure 4.10: The furnace temperature profile for coating cBN with Aluminum.

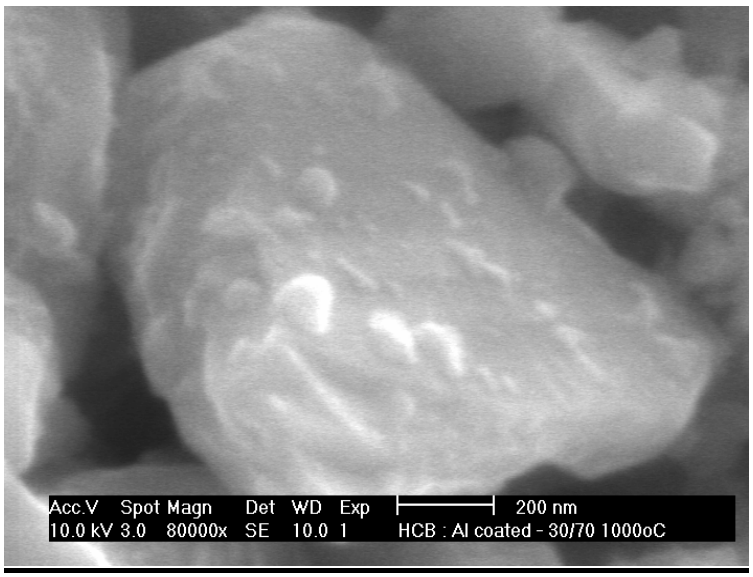

Figure 4.11: A typical cBN particle coated with AlN.

4.4 Densification and heat treatment

4.4.1 Infiltration

The infiltration process has been described in Section 2.8.1 of this thesis. However, an infiltrant, which in this case was aluminium, was placed at the bottom instead of the top, as shown in Figure 2.8.

For the infiltration, a graphite die (with an outer diameter of 60 mm and an inner diameter of 26.1 mm) and a 26 mm diameter punch were used. The Al discs were placed at the bottom of the die cavity. The the BN pellet was placed on top of the aluminium discs. A copper washer was placed on top of the BN pellet. Finaly, the die was closed at the top with a graphite punch. The copper washer was used to stop the aluminium from escaping from the die cavity by climbing up the inner die walls because of the applied pressure and through capillary action. It was found that at 800 ^{o}C, copper would expand enough relative to the tube walls, to stop the aluminium from moving up the sides of the punch. However, at a later stage a tantalum washer was used instead of the copper one (section 6.1.3 provides detailed explanation for the use of a refractory metal washer). The loaded sample was then put into the designed equipment (chamber) made of stainless steel. The infiltration was carried out as explained in Section 4.2.3.

After infiltration, the samples were removed from the graphite die and were cut into eight pieces with a diamond saw. The cut pieces of a particular sample were then heat-treated at different temperatures to find the appropriate temperature for the reaction between Al and BN.

4.4.2 Hot pressing

Hot pressing (HP) of either the green compacts or the powder containing Al and cBN was carried out as described in Section 4.2.4. The treatment of the sample after hot pressing was similar to that described below in Section 4.4.3. The samples from the hot press had a smaller diameter compared to samples from the infiltration furnace and hence they were cut into only four pieces instead of eight pieces.

4.4.3 Heat treatments

Heat treatments were performed after infiltration at 800 ^{o}C. They were done to allow the reaction between aluminium and boron nitride to take place. Temperatures above 1 400 ^{o}C proved to be detrimental to the samples due to the conversion of cBN to hBN. Therefore, the maximum temperature used for heat treatment was 1 400 ^{o}C. Most heat treatments were done using the hot press under nitrogen. However, some were done in the tube furnace under argon. The normal heating rate for heat treatments was 10 ^{o}C/min and the cooling rate was 20 ^{o}C/min.

4.4.4 Reaction kinetics

The Al powder, 50 vol. % (particle size < 5 μm) was mixed with cBN, 50 vol. % (particle size ~12 μm) using the turbular mixer. The mixed powder was hot pressed following the temperature profile shown in Section 4.2.4, Figure 4.9. The hot-pressed samples were cut and then heated to higher temperatures to allow the reaction between Al and BN to take place. Heat treatments were performed in both argon and nitrogen atmospheres. Table 4.2 below shows different temperatures and holding times used during the heat treatment experiements.

XRD analysis was used for phase identification and phase quantification.

Table 4.2: Heat treatment conducted to study the reaction kinetics

Temperature (^{o}C)	Holding time (min)
1100	30,60.120,180
1200	30,60.120,180
1300	30,60.120,180
1400	30,60.120,180

4.5 Analysis of samples

4.5.1 Density measurements

The density of the samples was measured using the Archimedes principle. The samples were immersed in water and later in hexane, and the solvent with the sample was boiled for 3 h in order to displace air from the pores in the sample. After boiling, the sample solvent with the sample inside was allowed to cool to room temperature.

The density of the material was calculated by measuring the weight of the boiled sample in hexane (water), W_w. The sample was then removed from the solvent and lightly dried using some cloth or paper to remove excess solvent on the surface of the sample. The weight of the sample is designated W_i while W is the weight before boiling the sample. The sample was then allowed to dry in the oven and cooled to room temperature, and the dry weight, W_d, was measured. These measured quantities were then used to calculate the densities and porosities of the samples. The equation used for the determination of the density is given in equation 4.2, the open porosity, P_o, in equation 4.3 and the porosity (open and closed), P, in equation 4.3.

$$\rho = \frac{W_d}{V} = \frac{W_d \rho(solvent)}{(W - W_w)_i} \tag{4.2}$$

$$\rho(hexane) = 0.6603 g.cm^{-3} and \rho(H_2O) = 1.0017 g.cm^{-3}$$

$$P_o = \frac{100(W_i - W_d)}{(W - W_{wi})} \quad \text{in percent} \tag{4.3}$$

$$P = [1 - (\frac{\rho}{\rho_{th}})]100 \quad \text{in percent} \tag{4.4}$$

The density was determined at least two times per sample. Between each of the measurements, the samples were dried in an oven.

The theoretical density of a composite material depends on the amount of the phases present in a particular material. In this work, the amount of aluminium added to the boron nitride ranged between 15 and 50 vol. %. The densities associated with these different mixtures are presented in Table 4.3. The densities of Al (2.701 g/cm^3) and cBN (3.48 g/cm^3) were used for the calculation shown in column 4 of Table 4.3.

Table 4.3: Some of the theoretical densities of the Al-cBN powder mixtures

Vol. % of Al	**m % of Al**	**m % of cBN**	$\rho = \frac{100}{\sum \frac{m_i}{\rho_i}}$ **(g/cm^3)**
15	12.0	88.0	3.36
20	16.3	83.7	3.32
30	25.0	75.0	3.25
35	29.5	70.5	3.21
40	34.1	65.9	3.17
45	38.8	61.2	3.13
50	43.7	56.3	3.09

The theoretical densities are a first approximation because they do not take into account the presence of some Al_2O_3 on the surface of the Al.

4.5.2 X-ray diffraction phase analysis: qualitative and quantitative

X-ray diffraction (XRD) analysis was performed to describe qualitatively the phase development and to determine quantitatively the evolution of aluminium nitride (AlN) in the study of the reaction kinetics (see Appendix A). The samples were examined using a PW 1710 Philips powder diffractometer, using monochromatic Cu Kα radiation produced at 40 KV and 20 mA. Diffractograms were collected over a range of 2θ between 20 and 80°, with a step size of 0.02° 2θ, together with a scan step time of 4.0 s. In other diffractograms, a range of 10 – 120° was used. In some cases an MoKα tube was used. If the radiation tube was not indicated for a particular XRD pattern, then CuKα was used.

The XRD analysis results were used to estimate the amount of hBN phase formed from the cBN powder during the hexagonalization experiments. The estimation was obtained by comparison with the five prepared secondary standards with volume ratios of cBN to hBN of 50, 65, 80, 90 and 95%. These two BN phases were thoroughly mixed for 60 min using the turbular mixer. Figure 4.12 below shows the ratio of the peak heights (hBN to cBN (Ih/Ic)) as a function of the vol. % ratio of cBN/hBN. These peak height ratios were calculated using the hBN peak, which was around 26.7° (2θ), and the cBN peak, which was around 43.3° (2θ) when the Cu tube was used and around 13° to 20° when the Mo tube was used.

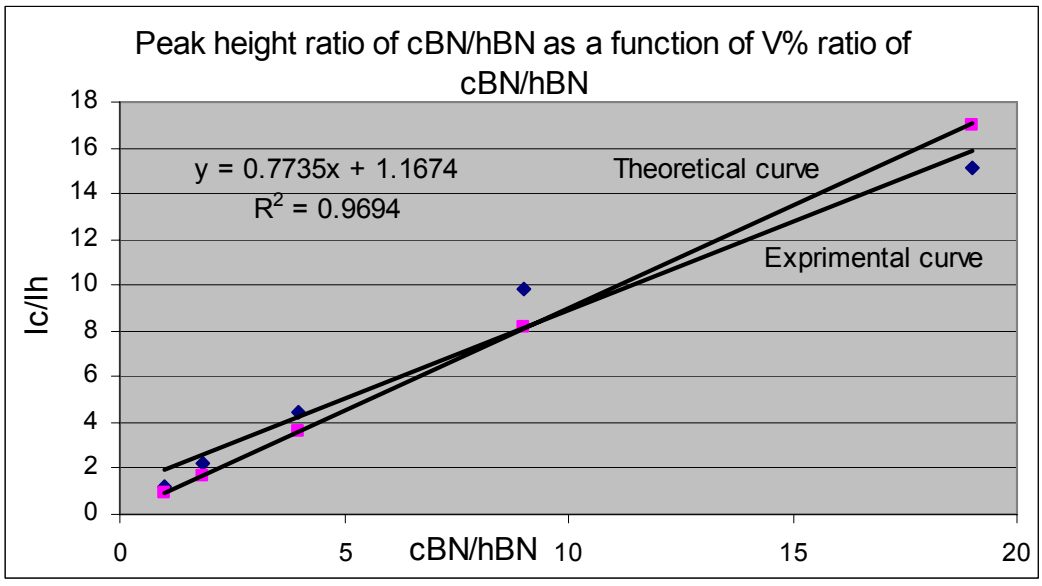

Figure 4.12: Results obtained from the standards that were used to estimate the cBN/hBN ratio during the hexagonalization experiments

The above graph shows that there is, as a first approximation, a linear relationship between the peak height ratio and the volume per cent ratio. This relationship can be defined by the following equation:

$$\frac{I_c}{I_h} = 0.7735 \times \frac{cBN}{hBN} + 1.17 \quad \text{.....(4.5)}$$

XRD analysis was also used to study the phase composition of the cermets that were produced by the infiltration of the ceramic cBN with the metal Al. A detailed XRD study at room temperature of the ceramic phases produced by the reaction between cBN and Al as a function of temperature in the range 1 000 to 1 600 ^{o}C was performed. The phases were clearly identified by comparing the resultant patterns with the International Centre for Diffraction Data (ICDD) database cards. Table 4.4 below summarizes the structural data for the phases involved. Table 4.6 shows the calculated absolute intensities obtained using the program Powder cell and the data from the ICDD database shown in Table 4.5. The data are normalized with regard to the volume of the three most intense peaks for the phases presented in Table 4.5.

Table 4.4: Structural data for phases involved

Phases	**Lattice parameters (nm)**	**Crystal structure**	**ICDD database**
hBN	a=b=0.2504, c= 0.6661	hexagonal	34-421
cBN	a=0.3615	cubic	25-1033
Al	a=b=c= 0.4049	cubic	4-787
AlN	a=b=0.3082, c=0.4945	hexagonal	25-1133
AlB_2	a=b=0.3009, c=0.3262	hexagonal	39-1483
AlB_{12}	a=b=1.016, c= 1.427	tetragonal	12-639
Al_2O_3	a=b=0.4759, c=1.299	rhombohedral/trigonal	10-173

XRD phase quantification calculations were done for the mixture of phases present in the material. The intensity of a peak of a phase can be calculated from equation 4.6 (Krawirz, 2001).

$$I(hkl) = I_o A_o \frac{e^4}{m^2 c^4} \frac{\lambda^3 phw}{32 \pi R^2 w_s V_{uc}^2 \mu_l} F_{hkl}^2 \frac{1 + \cos^2 2\theta}{2 \sin 2\theta \sin \theta} \qquad (4.6)$$

where

I_o = the intensity

A_o = the cross-sectional area of the beam

e = the electron charge

m = the mass of an electron

c = the speed of light

λ = the wavelength

p = the multiplicity of diffractometer parameters

h = the slit height

w = the slit width

ω_s = the sample speed

R = the radius of the diffractometer

V_{uc} = the unit cell volume

μ_l = the linear absorption

F_{hkl} = the structure factor

The trigonometric term is known as the Lorentz-Polarization (L-P) factor:

$$I(hkl) = k_m k_p \tag{4.7}$$

where

k_m = the physical constant and measurements factors

k_p = represents the phase-related factors:

$$k_{pAlN}(100) = \frac{p(100)}{V_{uc}^{\ 2}} F^2_{(100)} \frac{1+\cos^2 2\theta_{(100)}}{2\sin 2\theta_{(100)} \sin \theta_{(111)}} = 3.84 \tag{4.8}$$

Table 4.5: Values required for the material phase analysis

Quantity	**AlN 100)**	**cBN (111)**	**AlB_2(101)**	**AlB_{12}(202)**	**hBN(002)**	**Al(111)**
Cell volume	40.68	47.25	25.58	1472.42	36.17	66.4
Diffraction angle (2θ)	33.548	43.313	44.5	21.5	26.7	38.5
Structure factor (F)	14.12	18.20	10.82	66.15	17.40	35.82
Multiplicity Mu (P)	6	8	12	8	2	8
k_p	3.84	3.6	6.93	0.221	4.01	9.15

The volume content of the AlN phase can be calculated using the following equation:

$$V_{AlN} = \frac{\frac{I_{AlN}}{k_{pAlN}}}{\frac{I_{AlN}}{k_{pAlN}} + \frac{I_{cBN}}{k_{pcBN}} + \frac{I_{AlB_2}}{k_{pAlB_2}} + \frac{I_{AlB_{12}}}{k_{pAlB_{12}}} + \frac{I_{Al}}{k_{pAl}}} \times 100 \qquad (4.9)$$

For the other phases it could be calculated in a similar way.

In this equation the intensity, I, is the peak area of a particular phase. Program Origin 6.1 was used to calculate the integral intensities from the XRD data. All the values are shown in Appendix A.

Table 4.6: Absolute intensities normalized with regard to unit cell volume

Phases (ICS Database No.)	**2θ (°)**	**hkl**	**$I_{theoretical}$**
hBN (24644)	26.7	002	399.57
	41.6	100	64.1
	50.2	102	62.4
cBN (40914)	43.3	111	358.58
	74.1	220	128.8
	89.9	311	76.96
Al	38.5	111	916.0
	44.7	200	443.1
	78.2	311	325.5
AlN (82790)	33.5	100	384.2
	38.3	101	361.3
	36.3	002	240.2
AlB_2 (43851)	44.5	101	611.8
	34.4	100	195.3
	61.6	110	156.9
AlB_{12} (1091)	21.5	202	22.1
	23.2	212	16.8
	20.6	103	8.4
Al_2O_3 (88027)	37.8	110	442.5
	35.2	104	383.8
	57.5	116	144.8

4.5.3 Microstructural SEM-EDS analysis

A Scanning Electron Microscope (SEM), equipped with a Field Emission Gun (FEG), was used in this work. The SEM was used to study the microstructure, i.e. particle size, particle size distribution and porosity. SEM and EDX (energy dispersive X-ray) analyses were used to identify the elemental compositions of various phases to support the XRD results. The results from the SEM and EDX analyses were used to identify the amount of free aluminium present in the sample and the borides that were not easily detected with XRD analysis.

The SEM was normally set at a low accelerating voltage of 5 KeV. Since the samples were non-conductive (like most ceramic materials), a special mounting resin was used to provide electrical conductivity. In the case of the samples removed from the resin, carbon tape was used. Therefore the polished samples were not coated. The samples were polished as described in Section 4.2.6. The powder samples were embedded in a double-sided carbon tape which was mounted on an aluminium stub. Both aluminium and tape provided the electrical conductivity required.

4.5.4 Vicker's hardness determination

The hardness of the polished samples was tested using Vickers indentation. The Vickers hardness method that was used in this work measures the size of the impression left by an indenter of prescribed geometry under a known load (Martin, 1998). The macrohardness was determined for constant loads which were varied between 10 and 30 kg. The hardness reported in the next chapters will be reported as $H_v x$, where x is the load at which the hardness was determined.

The Vickers test machine used in this work uses a diamond square-based pyramid of 136° angle as the indenter, which gives geometrically similar impressions under differing loads. A square indent was produced and the average diagonal length was measured and the hardness number (H_v) was obtained using the formula given in equation 4.10.

$$H_v = 1.85437 \times \frac{\mathrm{P}}{d^2} \tag{4.10}$$

where

P = applied load in kg

d = diagonal of indentation in mm

4.5.5 Thermal analysis

Thermogravimetric analysis (TGA) and Differential Thermal Analysis (DTA) are analytical techniques used to study the changes occurring in a material as its temperature is raised or lowered. TGA relies on the accurate monitoring of the sample's weight as the temperature is increased or decreased. Any reactions entailing loss or gain of mass are recorded and appear as steps in the weight versus temperature graph that the instrument produces. DTA relies on the accurate monitoring of the sample's temperature as the latter is raised or lowered. An inert sample, positioned in the same furnace, next to the sample being studied is used as a means of comparison. The temperatures of the two samples are monitored as the furnace temperature is increased at a constant rate. The instrument's output in this case is the difference between the temperature of the two samples. Any reactions occurring in the sample under study causes a temporary drop or rise in sample temperature, depending on whether this reaction is endothermic or exothermic. Since no such disturbance occurs in the temperature of the inert sample, the curve of the difference between the two temperatures, when plotted versus time or average temperature will show a peak, the direction of which (upward or downward) will indicate whether the reaction observed was endothermic or exothermic.

Thermogravimetric analysis (TGA) was done on a Perkin Elmer TGA 1. The TGA apparatus consists of a vertical aluminium oxide tube furnace that operates up to a maximum temperature of 1 600 ^{o}C, and gas-cleaning and flow-regulating apparatus. The samples were loaded into platinum sample holders and heated at a rate of 10 ^{o}C/min under a constant flow of ultra high purity argon gas and the mass was continuously monitored during the heating cycle. The TGA apparatus was used primarily to determine the temperature at which the organics (polybutylene succinimide) present in the green compacts can be volatilised out of the sample. TGA experiments in UHP argon show that it is possible to sublimate this substance off the green body. The onset of the reaction is determined as per the international convention, as the point of inflection of the weight vs temperature graph away from the baseline.

Differential thermal analysis (DTA) was used to study the phase transformation from cBN to hBN and the formation of AlN from Al. This was performed with a Perkin Elmer DTA 7 apparatus. In the DTA apparatus, two small platinum crucibles, one containing an inert reference substance (aluminium oxide) and the other containing the test sample of no more than 10 mg, were placed close together in a furnace and heated at a rate of 10 ^{o}C/min. During heating, two thermocouples were used to record the temperature of the test sample, as well as the temperature

difference between the sample and the reference substance (T_S-T_R). Some of the results obtained from this technique are shown in Figure 7.1 section 7.1.

Thermal conductivity can be defined as the quantity of heat that passes per unit time through a plate of unit area and unit thickness when its opposite faces differ in temperature by one degree centigrade. The thermal conductivity of a particular sample was calculated from the measured thermal diffusivity. Thermal diffusivity was measured using a laser flash technique. A laser pulse of typical 400 mJ and 8 ns duration is used to heat the front surface of the sample. A detector on the reverse side measures the temperature rise on the back surface. The time taken for the temperature to reach half maximum value is chosen as a measure of the thermal diffusivity of the sample, given by the relationship:

$$\alpha = \frac{0.139 d^2}{t_{\frac{1}{2}}} \qquad (4.11)$$

where d =sample thickness (cm)

and $t_{1/2}$ = time taken to reach half maximum value (second)

Hence, from the thermal diffusivity, thermal conductivity can be calculated if the density and specific heat capacity is known:

$$\lambda = \alpha \times \rho \times C_p \qquad (4.12)$$

where λ = the thermal conductivity

α = the thermal diffusivity

ρ = the density

C_p = the specific heat capacity under constant pressure

4.5.6 Pore channel distribution measurement

Pore size distribution measurement relies on the principle of Mercury porosimetry analyzer acquired from Quantrachrome Instrument. The Quantachrome Autoscan 60 Mercury Porosimetry is used to measure the open pore size distribution in consolidated samples. In this system, mercury is forced into evacuated surface pores by applying pressure to the specimen. The pore radius at a given applied pressure can be calculated from the Washburn equation (see equation 2.3 section 2.8.1), which shows an inverse relationship between the intruded pore radius and the applied pressure. The instrument can measure pore radii varying from about 100 μm to 1.8 nm.

In this work the Quantachrome Autoscan 60 Mercury Porosimetry was used to analyze the pore channel distribution of the cBN green compact containing about 10 vol% Al binder. The pore size distributions were determined in a low pressure station at pressures of up to 350 kPa using a PoreMaster-60 with PoreMaster software for data collection and interpretation . For the interpretation of the data the volume distribution functions (($D_v(R)$ and $D_v(D)$) as a function of radius and diameter can be plotted. These show the change in volume of mercury intruded/extruded per unit of interval pore radius (diameter). D_v (r)is calculated as follows:

$$d_v(r) = \frac{P}{r}\frac{dV}{dP} \qquad .(4.13)$$

Substituting $$r = \left|\frac{2\gamma\cos\theta}{p}\right| \qquad (4.14)$$

D_v (r) can be written as: $$d_v(r) = \frac{dV}{dP}\left|\frac{p^2}{2\gamma\cos\theta}\right| \qquad (4.15)$$

At high pressures, the D_v (r) data are extremely sensitive to any slight fluctuation in the dV/dP term due to the multiplication by the p^2 term in the above equation. D_v (d) is found by dividing D_v (r) by 2 (Smith and Stermer, 1987).

CHAPTER 5 REACTION KINETICS OF AL AND CBN

Understanding the reaction kinetics in the Al-cBN system is very important. A basic understanding of the product to be formed over certain temperatures and times provides information that can be used to optimize the infiltration and hot pressing of the cBN with Al. Section 4.4.4 described the experiments, together with the heat treatments conducted in the study of the reaction kinetics.

The reaction of Al and cBN was studied using samples containing 50 vol. % of Al and 50 vol. % of cBN (12 μm), hot pressed at 800 ^{o}C. It must be stated that the amount of Al after hot pressing decreased to about 35 vol. % (see Figure 5.1). Quantitative analysis of the powder before hot pressing shows that about 45 vol. % Al was recovered after mixing (before hot pressing). The loss of Al during mixing can be attributed to its ductility. Aluminium metal tends to adhere to the ball of milling medium (this portion of Al would be discarded when the balls were removed from the mixed powder), and this behaviour is not expected in the case of hard ceramic cBN particles. It is possible that some of the fine Al powder oxidizes during the mixing, resulting in amorphous Al_2O_3 or $Al(OH)_3$ layers. The results show that after hot pressing, the Al phase was further reduced to about 35 vol. %. Some Al was found on the side of the punch after hot pressing. The force applied during hot pressing forced the liquid Al to escape from the pot. This analysis shows that when the heat treatment was done, only 35 vol.% of Al was available, with about 65 vol. % of cBN.

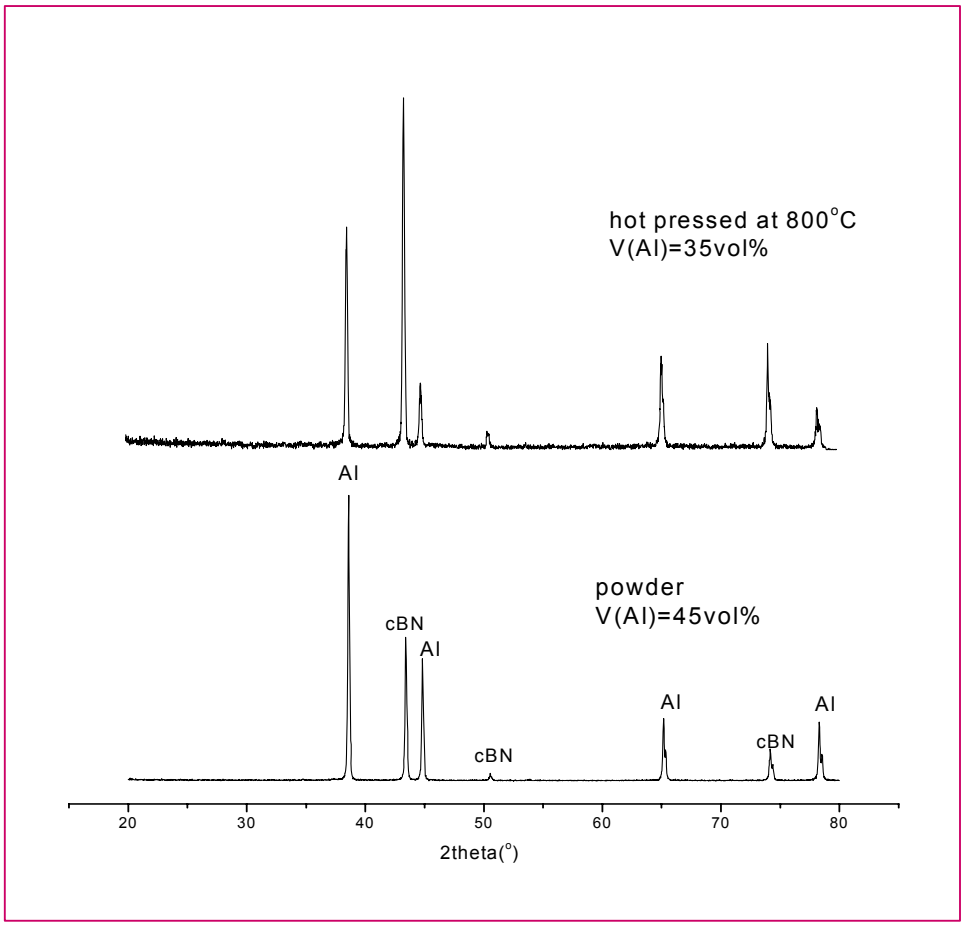

Figure 5.1: XRD results of the sample before and after hot pressing

(The volume content was determined using method described in Section 4.5.2.)

The investigations were carried out under nitrogen and argon atmospheres. Firstly, the phase formation in nitrogen will be outlined.

5.1 Reaction kinetics in a nitrogen atmosphere

Table 5.1 below lists all the samples prepared for the reaction kinetics studies conducted in a nitrogen atmosphere. Included in the table are the densities and open porosities of the samples before and after heat treatment. A qualitative XRD analysis of the samples listed in Table 5.1 was also done. A typical XRD scan is shown in Figure 5.2. There are three distinguishable phases after heat treatment of the samples at 1 400 ^{o}C for 2 h. These phases are labelled as AlB_{12}, AlN and cBN. The peaks of Al and AlB_2 are present at 1 100 ^{o}C. The rest of the phases present at different temperatures and times are shown in the last column of Table 5.1. The formation of AlB_{12} takes place at temperatures > 1 200 ^{o}C and the amount increases with increasing temperature. The amount of Al decreases as the temperature increases, as expected. However,

some weak Al peaks were identified at high temperatures, e.g. at 1 400 ^{o}C. The peak at this temperature is very weak and the amount of Al is estimated to be below 2 vol. %. The amount of AlB_2 increases from 1 000 ^{o}C to 1 100 ^{o}C, but it is weaker at 1 200 ^{o}C. This is expected since at temperatures ≥1 100 ^{o}C, aluminium diboride phase AlB_2 decomposes in Al and aluminium dodecaboride (AlB_{12}) is formed. The Al in the sample is able to form aluminium nitride by reacting with nitrogen from the atmosphere due to the open porosity present in the composite.

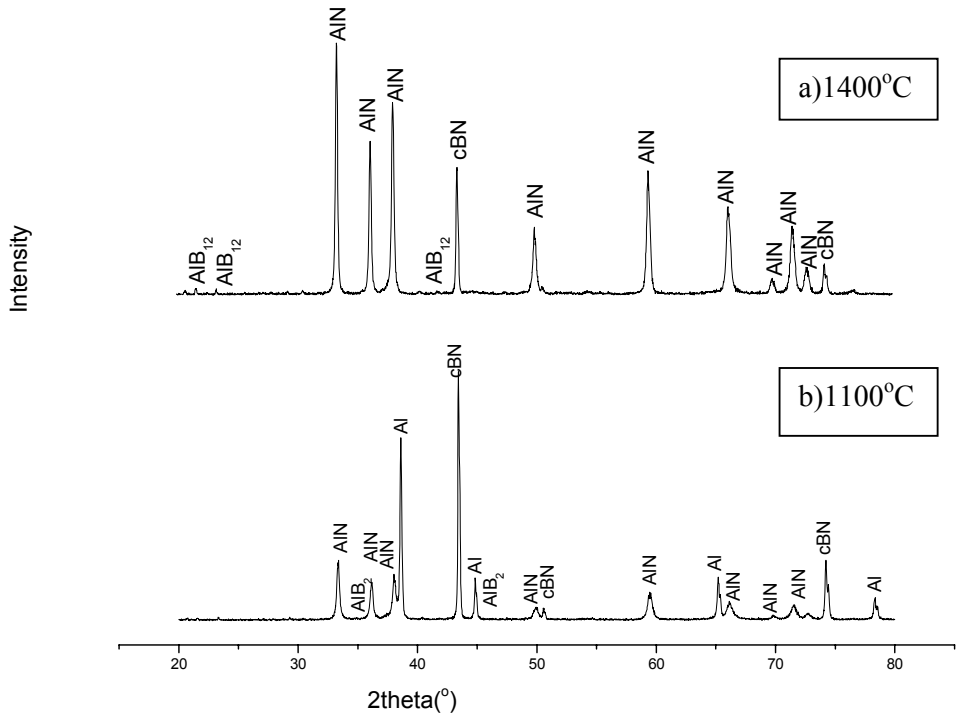

Figure 5.2: Typical XRD results of the samples prepared to study the reaction kinetics of 50 vol. % Al with 50 vol. % cBN (12 µm) after 2 h at (a) 1 400 ^{o}C and (b) 1 100°C

Table 5.1: Results of the samples prepared to study the reaction kinetics of 50 vol. % Al with 50 vol. % cBN (12 µm) in a nitrogen atmosphere

Temperature (^oC)	Time (min)	Density after 800 ^oC (g/cm^3)	Open porosity (%)	Density after heat treatment (g/cm^3)	Open porosity (%)	Increase in mass (%)	Phase content by XRD
1 100	30	2.95	2.0	2.94	2.1	-	AlN, Al, AlB_2, cBN
	60	2.95	2.0	-	-	-	AlN, Al, AlB_2, cBN
	120	2.92	2.0	2.96	0.8	-	AlN, Al, AlB_2, cBN
	180	2.93	2.2	2.91	1.8	-	AlN, Al, AlB_2, cBN, AlB_{12}
1 200	30	2.92	2.0	2.91	2.1	1.8	AlN, Al, AlB_2, cBN, AlB_{12}
	60	2.93	2.2	2.89	1.9	2.6	AlN, Al, AlB_2, cBN, AlB_{12}
	120	2.92	2.0	2.93	2.0	2.9	AlN, Al, AlB_2, cBN, AlB_{12}
	180	2.95	2.2	2.93	1.4	2.9	AlN, Al, AlB_2, cBN, AlB_{12}
1 300	30	2.96	1.8	-	-	-	AlN, Al, AlB_2, cBN, AlB_{12}
	60	2.95	2.2	2.96	1.5	-	AlN, Al, AlB_2, cBN, AlB_{12}
	120	2.95	2.0	-	-	-	AlN, Al, AlB_2, cBN, AlB_{12}
	180	2.96	1.8	2.95	1.9	-	AlN, Al, cBN, AlB_{12}
1 400	30	2.97	2.4	2.93	1.8	2.1	AlN, Al, AlB_2, cBN, AlB_{12}
	60	2.93	2.2	2.88	2.2	2.6	AlN, Al,, cBN, AlB_{12}
	120	2.93	2.2	2.91	1.7	2.6	AlN, cBN, AlB_{12}
	180	2.93	2.2	2.94	1.9	2.9	AlN, cBN, AlB_{12}

The XRD technique was used to calculate the volume percentages of the phases in the samples. The relevant equations, together with some important theoretical calculations, are provided in Section 4.5.2. The results are presented graphically in Figures 5.3 to 5.7. The results were obtained using five different peaks for AlN, four for Al, three for AlB_2 and one each for AlB_{12} and cBN. The results for similar experiments conducted in an argon atmosphere are presented in Figures 5.8 to 5.11. The data used to plot these graphs are presented in Appendix A.

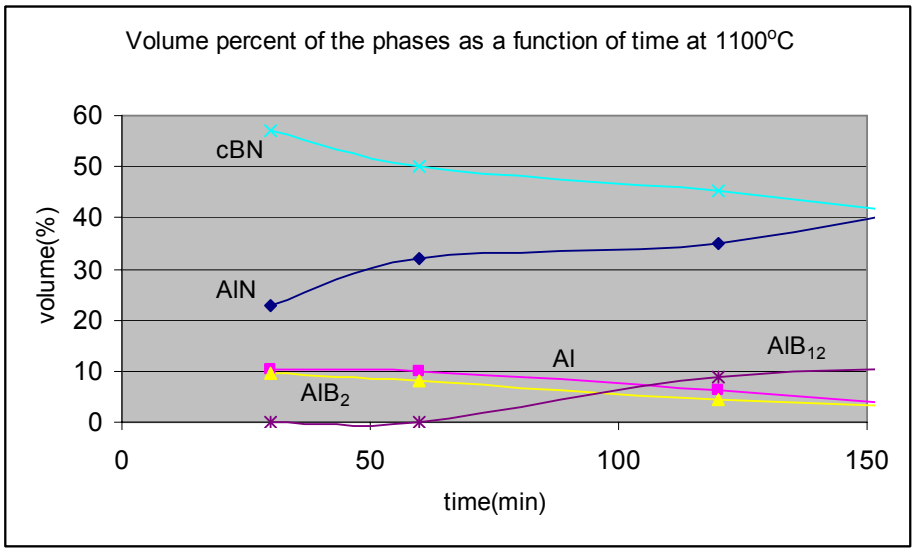

Figure 5.3: Effect of holding time at a temperature of 1 100 °C in a N_2 atmosphere

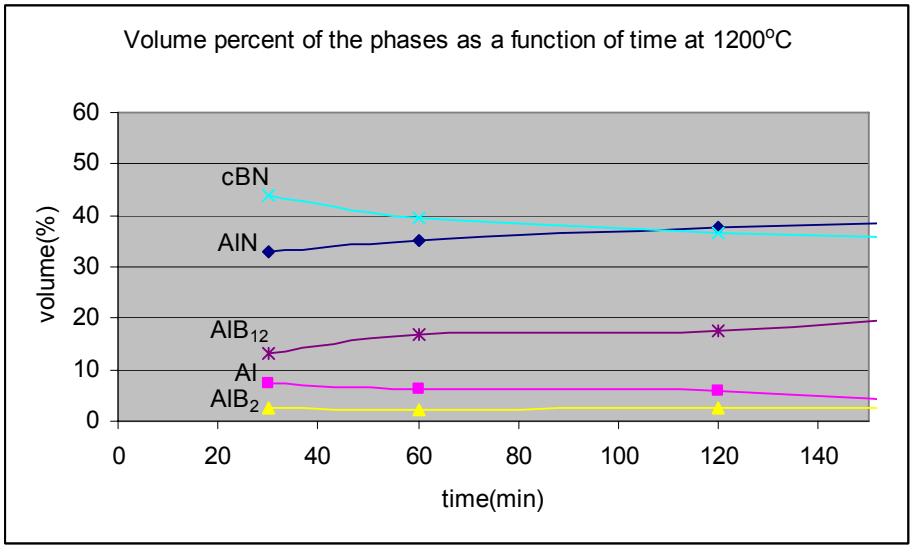

Figure 5.4: Effect of holding time at a temperature of 1 200 °C in a N_2 atmosphere

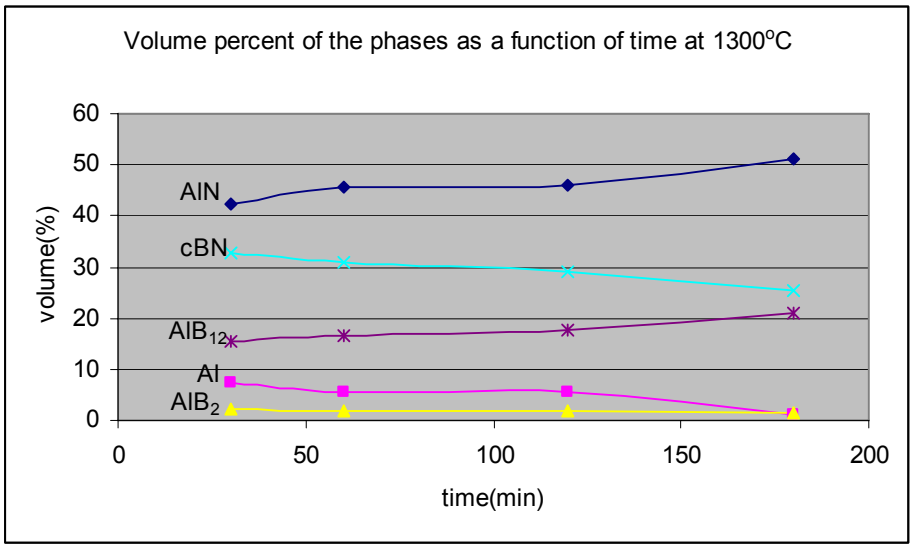

Figure 5.5: Effect of holding time at a temperature of 1 300 °C in a N_2 atmosphere

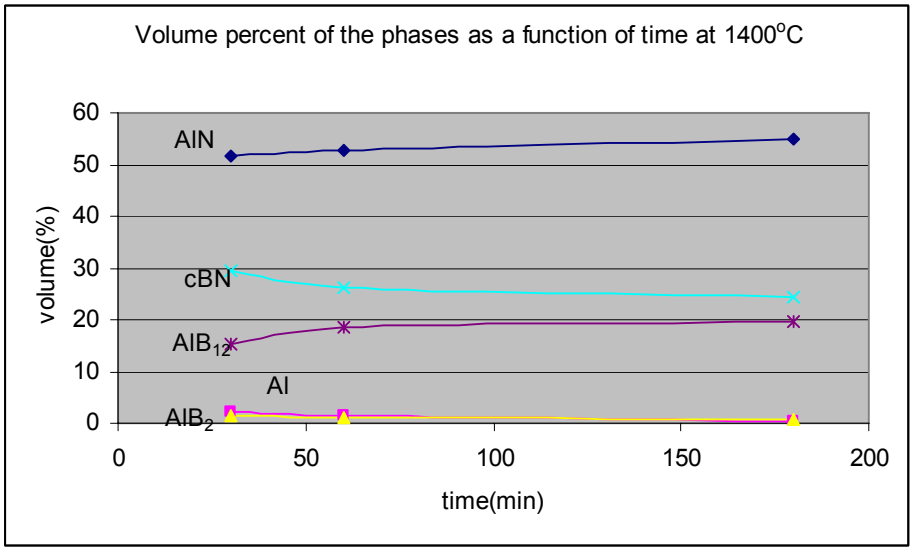

Figure 5.6: Effect of holding time at a temperature of 1 400 °C in a N_2 atmosphere

Figure 5.3 shows that the increase in the holding time results in an increase of boride phases. Comparison of the graphs in Figures 5.3 and 5.4 shows that increasing temperature results in an increase of AlN and a decrease of AlB_2. At the higher temperature (Figure 5.5), the AlN phase increases to above 50% and AlB_2 almost disappears. It was at this temperature that the AlB_{12} peak was seen to be stronger than at previous temperatures. The amount was found to be more than 20%. It can be seen that the amount of the Al phase is below 10% from Figures 5.4 to 5.6. This leads one to the conclusion that AlB_2 decomposes to form AlN and AlB_{12}, which is stable at higher temperatures.

Samples that had been heat treated for 3 h at different temperatures were scanned three times on the X-ray machine to confirm the reproducibility of the results. Figure 5.7 shows the relationship between the phase content and the temperature after 3 hours heat treatment. The standard deviation in each of the five phases present is reasonably low. The phases that experience the greatest change in volume as the temperature increases are cBN, AlN and AlB_{12}. Both AlN and AlB_{12} increased by more than 10%, while the decrease in cBN was just above 15%. The results in Figure 5.7 show that after heating for 3 h at 1 300 ^{o}C, there is a negligible amount of both Al and AlB_2. This is to be expected since at heating at high temperatures for a longer time will lead to all the Al reacting to form both AlN and AlB_{12}. Two mechanisms are responsible for the formation of aluminium dodecaboride (AlB_{12}). Firstly, it is formed from the reaction of Al and cBN, and secondly, by the decomposition at high temperatures of AlB_2.

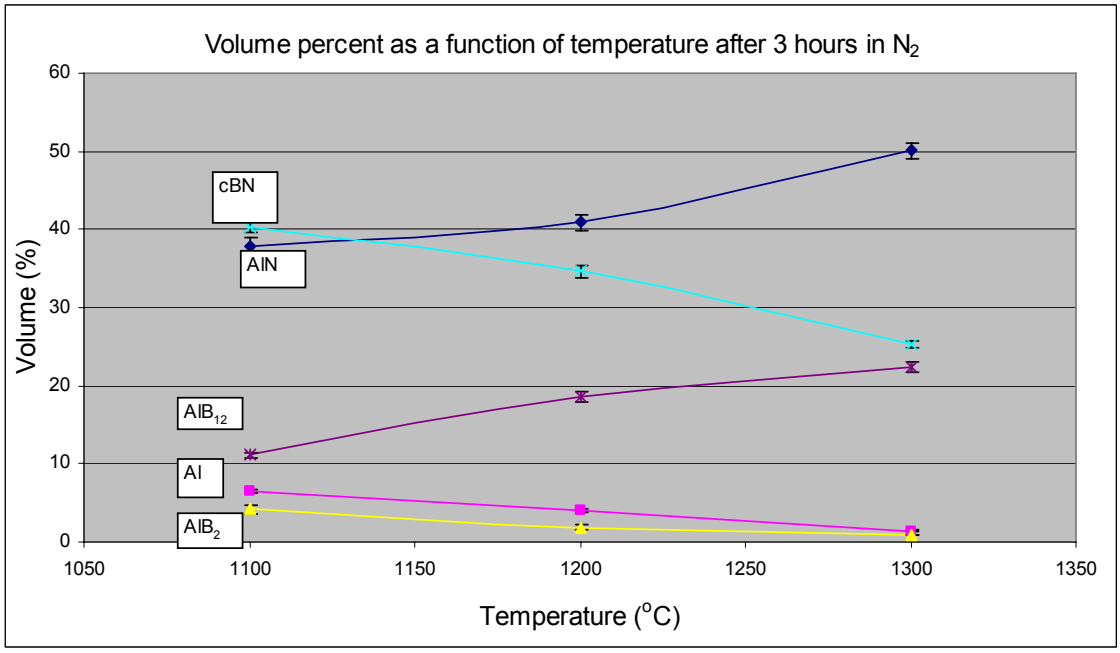

Figure 5.7: Effect of varying temperature at constant time in a N_2 atmosphere

5.2 Reaction kinetics in an argon atmosphere

Table 5.2 presents the results obtained by heat treating the samples in argon. The heat treatments in an argon atmosphere resulted in a different behaviour from those conducted in a nitrogen atmosphere. The heat treatment results in an argon atmosphere are presented in Figures 5.8 to 5.11.

Table 5.2: Results of the reaction kinetics study in an argon atmosphere of samples containing 50 vol. % Al with 50 vol. % cBN (12 µm)

Temperature (^{o}C)	Time (min)	Density after 800 ^{o}C (g/cm^3)	Open porosity (%)	Density after heat treatment (g/cm^3)	Open porosity (%)	Decrease in mass (%)	Phase content by XRD
1 100	30	2.98	1.4	2.91	1.8	0.9	AlN, Al, AlB_2, cBN
	60	2.98	1.4	2.95	1.7	1.3	AlN, Al, AlB_2, cBN
	120	2.98	1.4	2.96	1.5	1.5	AlN, Al, AlB_2, cBN
	180	2.98	1.4	2.92	1.8	1.4	AlN, Al, AlB_2, cBN, AlB_{12}
1 200	30	2.95	1.9	2.95	1.9	1.3	AlN, Al, AlB_2, cBN, AlB_{12}
	60	2.95	1.9	-	-	1.5	AlN, Al, AlB_2, cBN, AlB_{12}
	120	2.95	1.9	-	-	1.5	AlN, Al, AlB_2, cBN, AlB_{12}
	180	2.95	1.9	2.94	2.0	0.9	AlN, Al, AlB_2, cBN, AlB_{12}
1 300	30	2.96	1.8	-	-	0.7	AlN, Al, AlB_2, cBN, AlB_{12}
	60	2.96	1.8	-	-	0.8	AlN, Al, AlB_2, cBN, AlB_{12}
	120	2.96	1.8	2.97	1.6	0.6	AlN, Al, AlB_2, cBN, AlB_{12}
	180	2.96	1.8	2.95	1.9	0.7	AlN, Al, cBN, AlB_{12}
1 400	30	2.97	1.7	2.94	2.1	1.5	AlN, Al, AlB_2, cBN, AlB_{12}
	60	2.97	1.7	2.96	1.7	0.6	AlN, Al, cBN, AlB_{12}
	120	2.97	1.7	2.94	1.7	0.9	AlN, cBN, AlB_{12}
	180	2.97	1.7	2.97	1.5	0.9	AlN, cBN, AlB_{12}

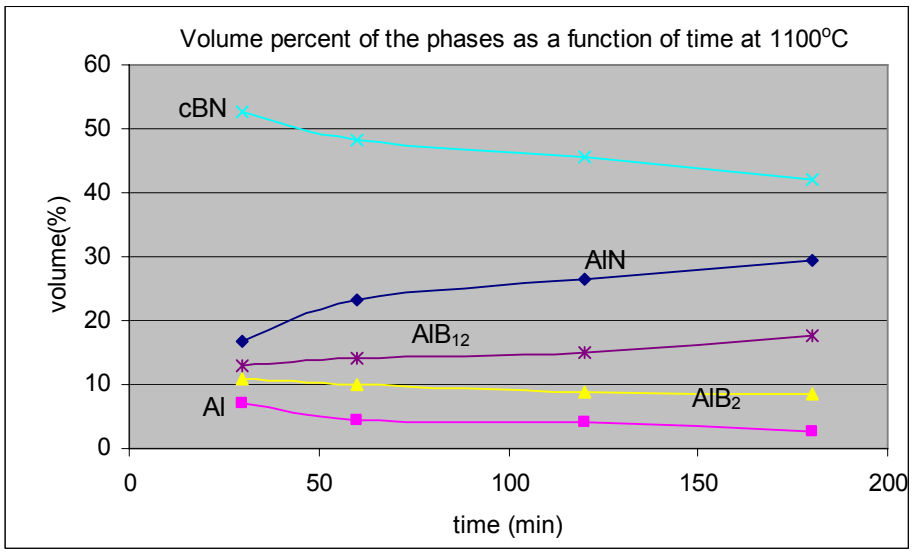

Figure 5.8: Effect of holding time at a temperature of 1 100 °C in an Ar atmosphere

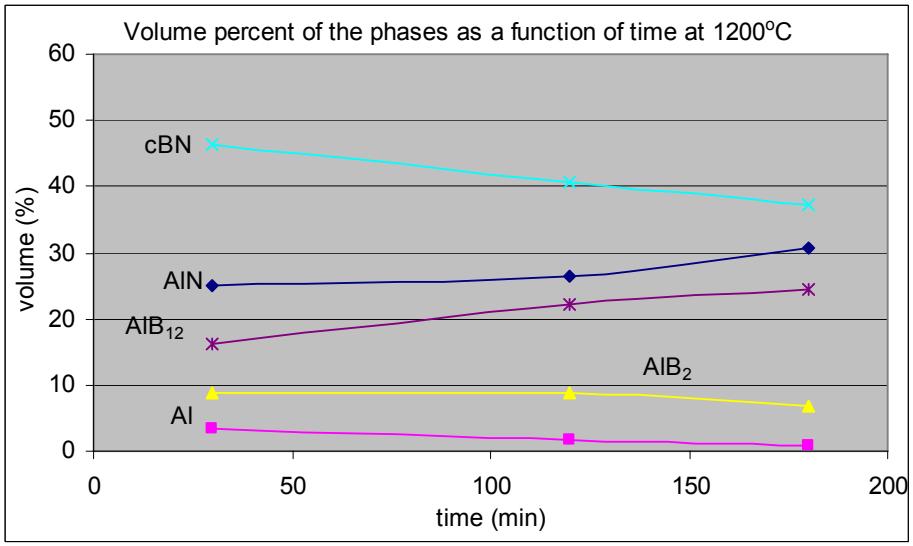

Figure 5.9: Effect of holding time at a temperature of 1 200 °C in an Ar atmosphere

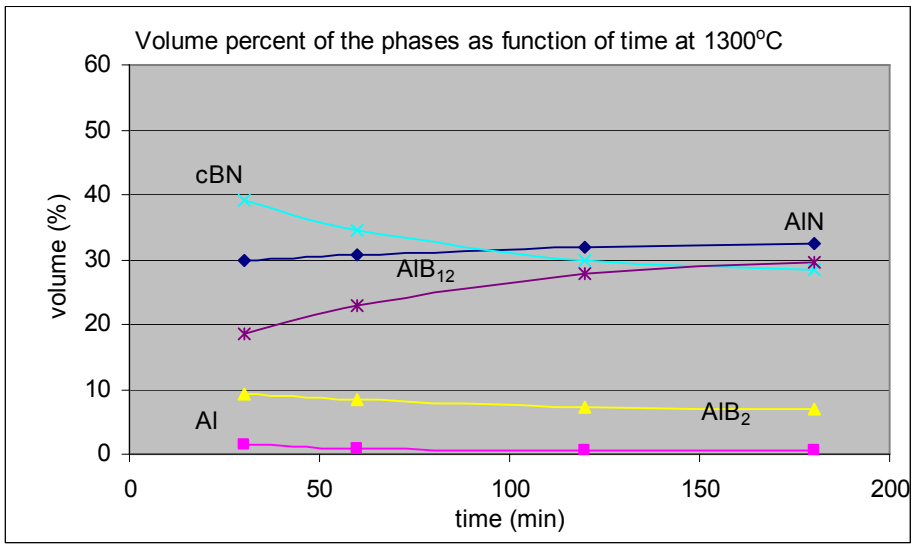

Figure 5.10: Effect of holding time at a temperature of 1 300 °C in an Ar atmosphere

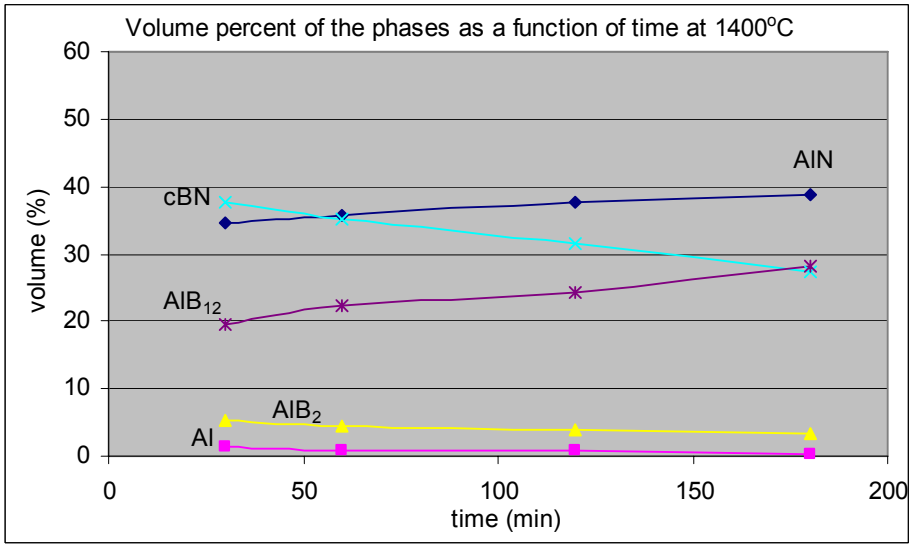

Figure 5.11: Effect of holding time at a temperature of 1 400°C in an Ar atmosphere

Figures 5.8 to 5.11 show that there was an increase in the amount of AlN with increasing time and temperature. However, the volume percentage of AlN remains below 40, whereas when heat treatments were done in a nitrogen atmosphere, the amount of AlN formed was above 50 vol. % (as shown in Figures 5.5 and 5.6 above). A higher volume of AlN is always formed in a nitrogen atmosphere compared with the heat treatments in an argon atmosphere. An increase in the mass of the sample of about 3% was reported in Table 5.1. This increase can be attributed to the additional nitrogen coming from the atmosphere which reacts with Al to form AlN. Contrary to this, Table 5.2 shows a decrease in the mass of the sample (of about 1%). The overall change in mass resulted in an increase in the AlN content in comparison with the heat treatment in argon.

Figure 5.9 shows that there is an appreciable increase in the amount of AlB_{12} between 120 and 180 min simultaneously with the decomposition of AlB_2. A similar trend is observed at higher temperatures (see Figures 5.10 and 5.11). This leads one to the conclusion that AlB_2 decomposes to form AlB_{12} which is a more stable phase at high temperatures. The increase in the AlB_{12} phase is accompanied by a decrease of about 5 vol. % in the cBN phase. There is no obvious change in the amount of AlN, AlB_{12} and cBN between 120 and 180 min at a temperature of 1 300 ^{o}C (Figure 5.10). The graphs in Figure 5.11 show that the reaction has gone almost to its completion since there is no Al left to react and there is almost no AlB_2 that can decompose to form Al and AlB_{12}. The amount of AlN formed remains below 40 vol. %, 30 vol. % AlB_{12} was formed and about 30 vol. % cBN was left unreacted.

5.3 Calculating the initial amount of Al

As described in the beginning of this chapter. the samples were infiltrated with Al at 800°C. The samples thus produced were analysed by XRD (see Figure 5.1) and the amount of Al present in them was determined. In order to fully understand the processes occurring during reaction sitering, it is necessary to account for the entire Al initially present in the samples prior to the onset of these reactions. This amount of aluminium should be equal to the amount detected in the corresponding samples infiltrated at 800°C. Because it was the 12μm saples that were fully infiltrated, almost fully dense and analysed (See Section 6), this comparison will be done for those samples only, as shown below.

The volume fraction of Al in the 12μm samples after they were infiltrated with Al at 800°C was 35 vol% (see Figure 5.1 and paragraph 2 of chapter 5).

After heat treatment at 1 400 ^{o}C for 180 min (Figure 5.11), there are only three phases left, i.e. AlN, AlB_{12} and cBN. Reaction of the starting compounds can be described by the equation:

$$13Al+12cBN \longrightarrow 12AlN+\alpha\text{-}AlB_{12} \qquad (5.1)$$

A small fraction of the Al initialy present in the sample reacted with cBN according to the reaction

$$3Al + 2cBN \longrightarrow AlB_2 + 2AlN \qquad (5.2)$$

These equations can be used to calculate the amount of Al that took part in the reaction. Knowledge of the volume of the reaction products allows the volume change of the phases during the reaction to be calculated. The data in Table 5.3 were used to calculate the amount of Al that was present before the reaction at 1 400 ^{o}C for 3 h.

Table 5.3: Data used to calculate Al before the reaction at 1 400 ^{o}C for 3 h

Phases present in reaction products	Density (g/cm^3)	Volume (%) in reaction products	Mass (g) in 100 cm^3	Amount of Al (%)	Mass of Al(g) in 100 cm^3 of reaction product sample.
AlN	3.25	40	130	65	84.5
AlB_{12}	2.55	29	74.0	16	11.8
cBN	3.48	28	97.4	-	-
AlB_2	3.19	3	9.57	55	5.25

Total mass of 100 cm^3 of sample = 130 + 74.0 + 97.4 + 9.57 = 310.97 g

Total mass of Al = 0.65 x 130 + 0.16 x 74.0 + 0.55 x 9.57 = 101.55 g

Density of the bulk as reported in Table 5.2 = 2.973 g/cm^3

$$\text{Volume of the bulk} = \frac{m}{\rho} \qquad (5.2)$$

$$= \frac{301.4}{2.973}$$

$$= 104.6 \text{ cm}^3$$

$$\text{Volume of Al} = \frac{101.55}{2.701}$$

(where 2.701 g/cm^3 is the density of Al)

$$= 37.6 \text{ cm}^3$$

$$\text{Initial volume content of Al} = \frac{37.6}{104.6} \times 100 = 35.9\%$$

Thus the starting materials contained 35.9 vol. % Al and 65 vol. % cBN.

The recalculated values are very near to those determined directly for the starting composition. These indicate the correctness of the determined phase contents. To further illustrate this, similar calculation were done for the reaction taking place at 1 300 ^{o}C for 3 hours. The data in Table 5.4

based on the result in Figure 5.10 were used to calculate the amount of Al that was present before the reaction at 1 300 ^{o}C for 3 h.

Table 5.4: Data used to calculate Al before the reaction at 1 300 ^{o}C for 3 h

Phases present in reaction products	**Density (g/cm^3)**	**Volume (%) in reaction products**	**Mass (g) in 100 cm^3**	**Amount of Al (%)**	**Mass of Al(g) in 100 cm^3 of reaction product sample.**
AlN	3.25	33	107.3	65	69.7
AlB_{12}	2.55	30	76.5	16	12.2
cBN	3.48	29	100.9	-	-
AlB_2	3.19	7	22.3	55	12.3

Total mass of 100 cm^3 of sample = 307 g

Total mass of Al = 94.2 g

Density of the bulk as reported in Table 5.2 = 2.95 g/cm^3

$$\text{Volume of the bulk} = \frac{m}{\rho} \qquad (5.2)$$

$$= \frac{307}{2.95}$$

$$= 104.1 \text{ cm}^3$$

$$\text{Volume of Al} = \frac{94.2}{2.701}$$

(where 2.701 g/cm^3 is the density of Al)

$$= 35.3 \text{ cm}^3$$

$$\text{Initial volume content of Al} = \frac{35.3}{104.1} \times 100 = 33.9\%$$

Thus the starting materials contained 33.9 vol. % Al and 66.1 vol. % cBN. This is close to expected values of 35 vol% Al and 65 vol% cBN.

5.4 Reaction kinetics of Al and single-crystal cBN

Layers of an Al sheet (cleaned by acetone in an ultrasonic bath for 30 min) were put in a graphite pot with ABN800 crystals (particle size of ~200 μm) placed on top. The ABN800 crystals were then infiltrated with 50 vol. % Al by heating the furnace, using a heating rate of 10 ^{o}C/min up to 800 ^{o}C without applying pressure. The temperature was kept at 800 ^{o}C for 30 min. The resulting sample was cut into four pieces using a diamond wheel.

The pieces were heat treated to 1 300 ^{o}C for 30, 60 and 300 min under nitrogen and argon. The volume percent (thickness) of AlN formed was measured and the results are presented in Figure 5.12. The volume percent of AlN formed during the reaction was also calculated using the UTHSCSA Image Tool (Dove, 2001) which is an image processing and analysis program for Microsoft Windows (see appendix B); six micrographs were used per point plotted in Figure 5.12. The heat treatment was carried out under argon and the results are included in Figure 5.12.

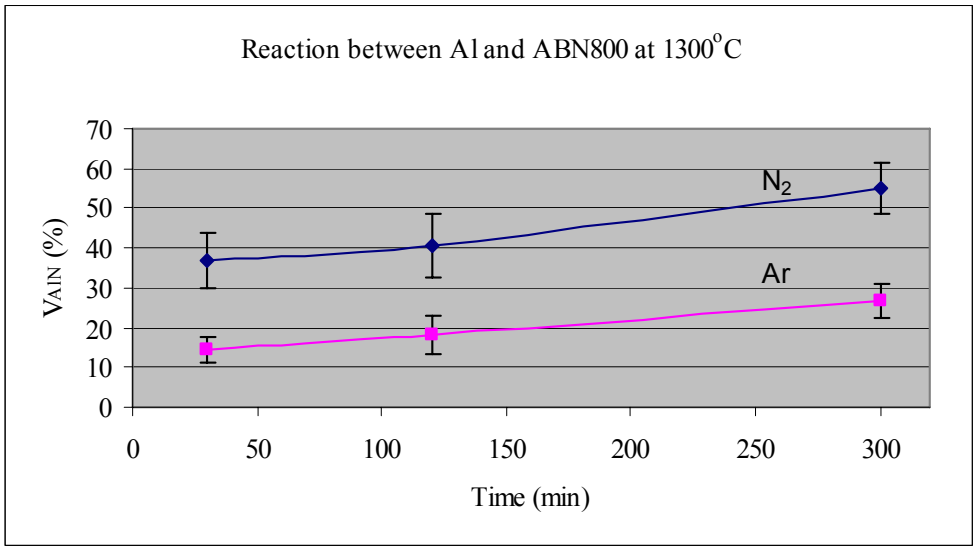

Figure 5.12: Volume percent of AlN formed as a function of time at a temperature of 1 300 ^{o}C in both N_2 and Ar atmospheres

The volume of AlN in argon was found to be less than that found for the heat treatment in a nitrogen atmosphere. SEM images of the polished microstructure of the infiltrated sample are shown in Figures 5.13 to 5.16. Clearly visible are the dark phase of the ABN800 crystal, the grey phase of AlN and the light phase of Al. The EDX analyses did not reveal the boride phases and they were not detected by XRD analysis. Since there is still a lot of free Al present, the boron might have dissolved in the Al, prohibiting any boride formation.

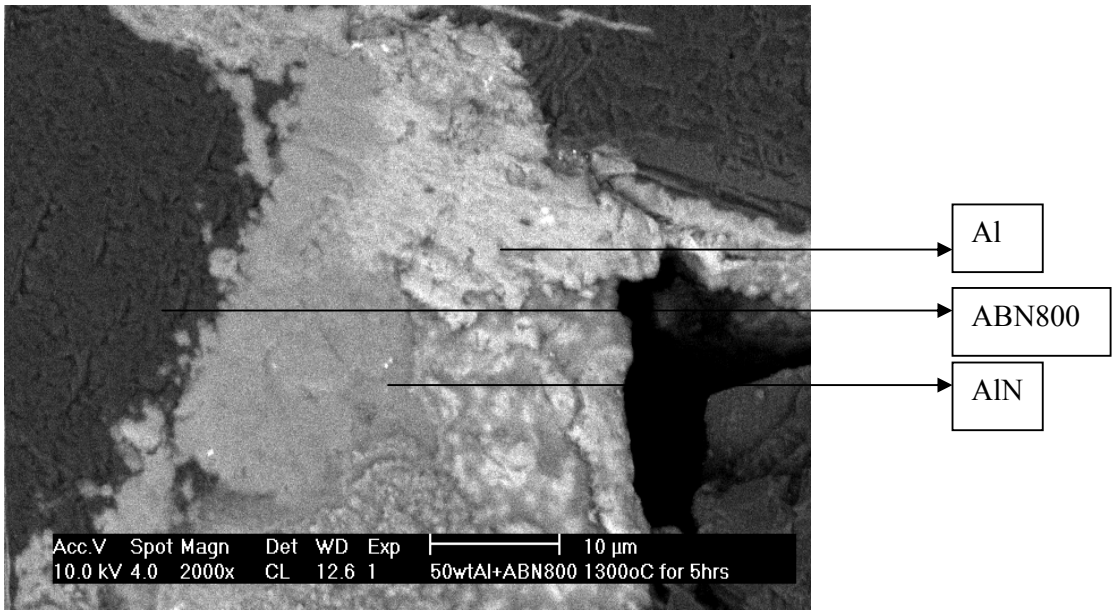

Figure 5.13: SEM image of the sample after 5 h in a N_2 atmosphere

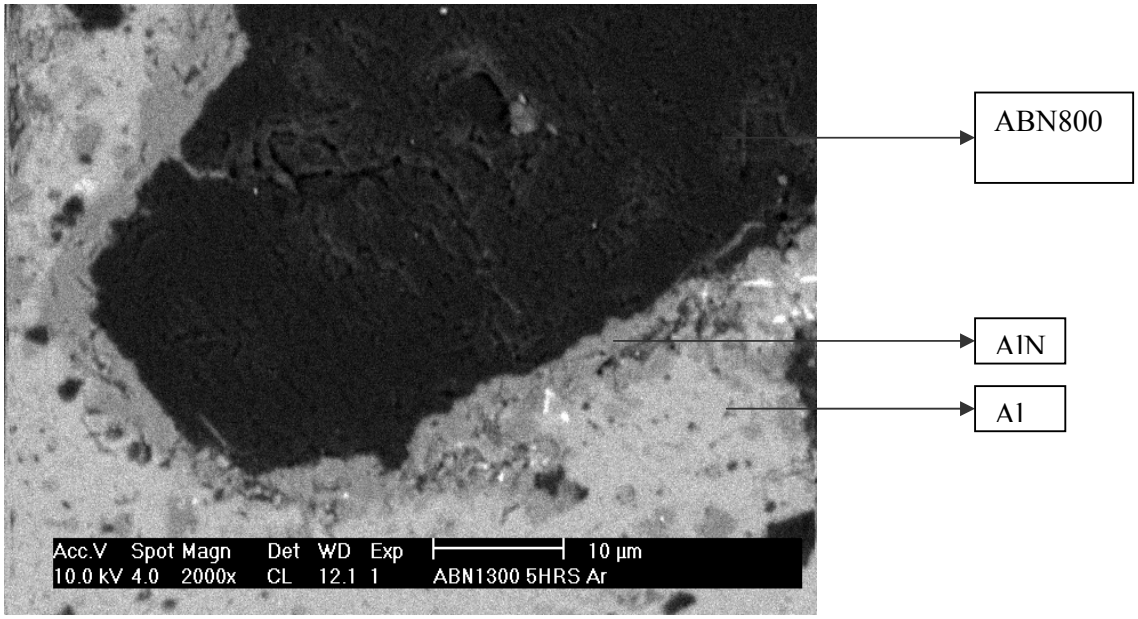

Figure 5.14: SEM image of the sample after 5 h in an Ar atmosphere

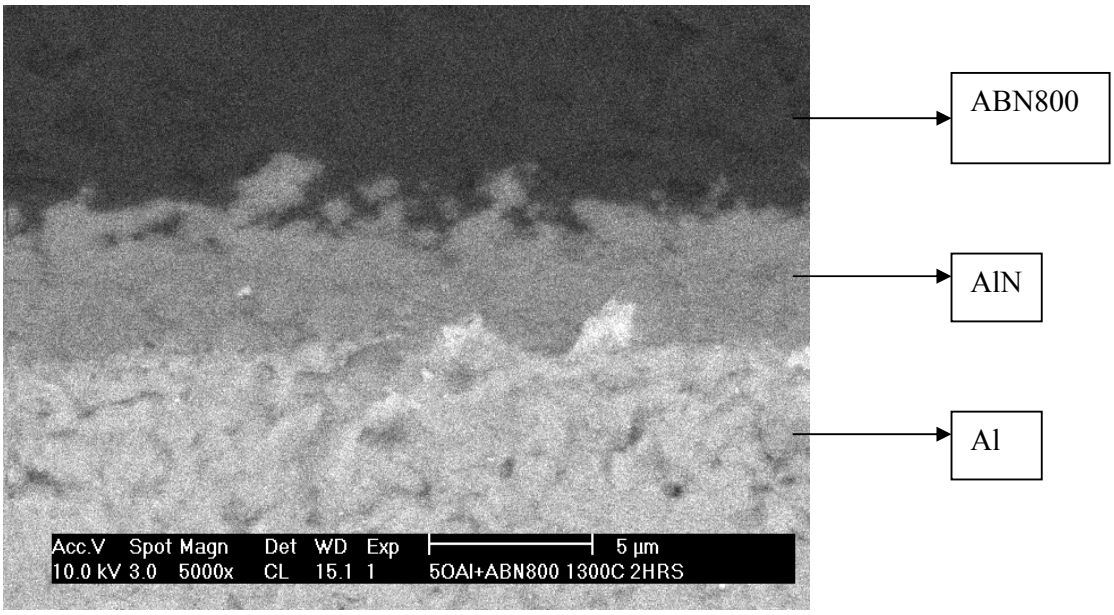

Figure 5.15: SEM image of the sample after 2 h in a N_2 atmosphere

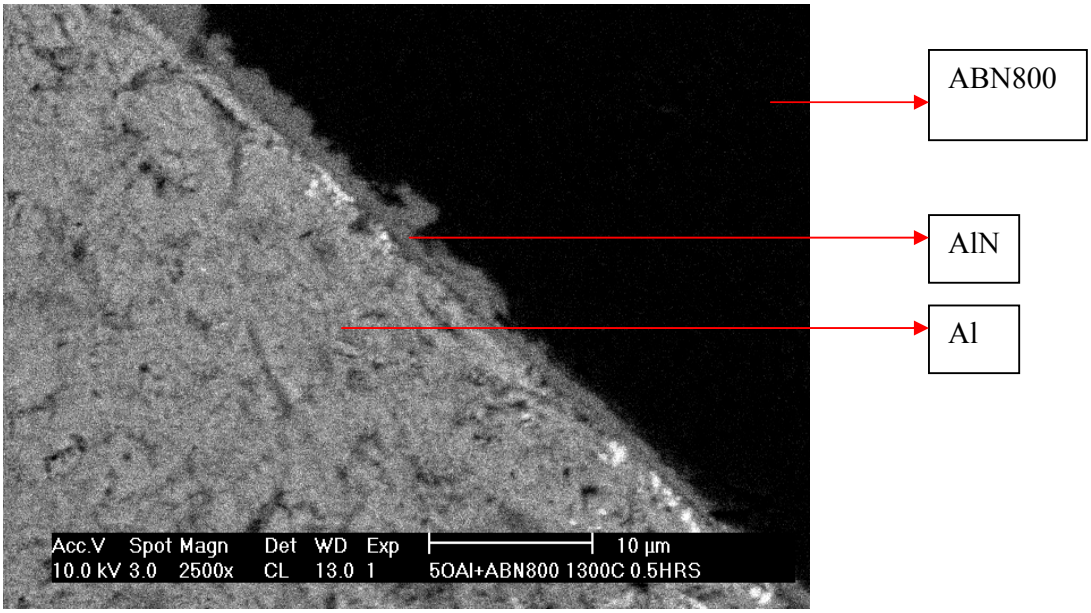

Figure 5.16: The very thin layer of AlN present after 30 min under N_2

Figure 5.14 shows a very thin layer of AlN forming. This image was taken after the sample had been heated for 5 h at 1 300 ^{o}C in an argon atmosphere. The layer of AlN shown in Figure 5.13 is much thicker than this layer. This further supports the findings of the XRD quantitative analysis, namely that AlN is more pronounced when formed in a nitrogen atmosphere rather than in an argon atmosphere.

CHAPTER 6 RESULTS OF THE INFILTRATION OF THE BN SAMPLES

This chapter describes the results obtained from infiltration of both hBN and cBN by Al. The first part deals with the infiltration of hBN. This is followed by a study of the hexagonalization of cBN powder. The hexagonalized powder was infiltrated with Al. Lastly, cBN powder without prior hexagonaliztion was also infiltrated with Al. All the infiltration results are discussed in this chapter.

6.1 Infiltration of the hexagonal BN (hBN) samples

Details of the samples prepared as described in Section 4.2.3, and some of their properties, are given in Table 6.1. All these samples were infiltrated in vacuum with Al at 800 ^{o}C. Table 6.2 shows the results after heat treatment for 1 h at 1 300 ^{o}C under argon. The procedure in naming the samples was as follows: hBN-26 means a sample containing hBN and 26% Al; hBN-18HT13 contains hBN with 18% Al and heat treated to 1 300 ^{o}C, etc. The amount of Al added was determined by comparing the green density of the hBN pellet with the density of hBN powder (2.25 g/cm^3), i.e. the porosity of the green pellet is equivalent to the amount of Al added.

Table 6.1: Al-infiltrated hBN samples after heat treatment at 800 ^{o}C for 30 min

Sample name	Green density[1] (g/cm^3)	Al content (%)	Density after treatment at 800 ^{o}C (g/cm^3)	Porosity (%)	Phases present
hBN-18	1.84	18	2.17[1]	3.0	Al, hBN
hBN-19	1.85	19	2.19	2.6	Al, hBN
hBN-24	1.72	24	2.20	2.2	Al, hBN
hBN-26	1.67	26	2.21	1.7	Al, hBN

[1] Density after removing non-infiltrated parts of the sample.

The densities of the samples were measured using Archimedes' principle described in Section 4.5.1 of this thesis. The measured densities are presented in Table 6.1 for samples after infiltration and in Table 6.2 for samples after heat treatment. All the composite materials

prepared were found to be more than 97% dense. The densities measured after heat treatment are slightly lower than those measured after infiltration.

Table 6.2: Al-infiltrated hBN samples after heat treatment at 1 300 ^{o}C for 60 min

Sample name	Density after treatment at 1 300 ^{o}C (g/cm^{3})	Open porosity (%)	Phases present
hBN-18HT13	2.15	0.52	AlN, hBN, AlCu
hBN-19HT13	2.17	0.34	AlN, hBN
hBN-24HT13	2.19	0.23	AlN, hBN, AlCu
hBN-26HT13	2.18	0.23	AlN, hBN, AlCu

The hBN matrix with 26% porosity (referred to as hBN-26 in Table 6.1) was infiltrated with molten aluminium. The hBN powder used had an average particle size of 40 μm, while the aluminium was in the form of a sheet. The infiltration was done at a temperature of 800 ^{o}C under a pressure of 12 MPa, as described in Section 4.4.1. The sample was kept under these conditions for 30 min. Most of the infiltration was expected to take place during this phase. Eight pieces were cut from one 26 mm diameter sample. These pieces were then separately heat treated at different temperatures for 60 min. The temperatures used were 1 100 ^{o}C, 1 200 ^{o}C, 1 250 ^{o}C, 1 300 ^{o}C and 1 350 ^{o}C. The pieces were characterized using XRD to identify the phases present and with the SEM to study the microstructure.

6.1.2 Phase composition of both infiltrated and reacted samples

Figure 6.1 shows the results for the hBN-26 sample. The (002) diffraction peak of hBN was observed at 2θ = 26.7^{o} (d = 0.3331 nm). Other diffraction maxima were observed at 2θ = 41.6^{o} (d = 0.2169 nm), 43.8^{o} (d = 0.2064 nm), 50.1^{o} (d = 0.1818 nm) and 75.9^{o} (d = 0.1253nm), corresponding to the (100), (101), (102) and (110) reflections of the hBN. Due to the change of orientation after pressing (affecting the texture), the (110) diffraction peak is stronger than the (002) diffraction peak. In the case of the original hBN powder, the (002) diffraction peak is the strongest. At 800 ^{o}C, the diffraction maxima observed at 2θ = 38.4^{o} (d = 0.2340 nm), 44.7^{o} (d = 0.2026 nm) and 65.0^{o} (d = 0.1434 nm), corresponding to the (111), (200) and (220) reflections of the Al. At higher temperatures these peaks disappeared, confirming the reaction between Al and hBN, where Al acts as a limiting reagent. At 1 200 ^{o}C, the diffraction maxima observed at 2θ = 33.3^{o} (d = 0.2670nm), 36.1^{o} (d= 0.2487nm) and 37.9^{o} (d= 0.2370nm) correspond to the (100),

(002) and (101) reflections of the AlN. These peaks increased with temperature, but not much change was observed from 1 300 ^{o}C to 1 350 ^{o}C.

There was an overlap between the (103) line of hBN and the (110) reflections of AlN at an angle of $2\theta = 59.4^{o}$ (d = 0.1558 nm). The formation of AlB_2 and/or AlB_{12} could not be detected. Thus only two phases, AlN and hBN, were detected by XRD technique.

Figure 6.2 presents the results for the hBN-18 sample. These results are similar to those in Figure 6.1, with the only obvious difference being that the aluminium peaks were weak compared with the 26% porosity sample. The AlN peaks can be clearly observed at higher temperatures, which confirmed the reaction between Al and hBN. Again, here no AlB_2 and/or AlB_{12} could be detected, as in Figure 6.1. The hBN peak detected at 43.8^{o} overlaps with the AlB_2 peak at 44.5^{o}. The possibility of this peak belonging to AlB_2 was ruled out since it was also present at 800 ^{o}C (where no/minimum reaction takes place).

Figure 6.3 shows the ratio of V_{AlN}/V_{hBN} (where the (100) peak of hBN was used with both (100) and (002) AlN peaks) as a function of temperature; this was constructed using information from Figure 6.2. The graph shows that after 1 300 ^{o}C, the reaction is nearly saturated, i.e. not much changes in the ratio after 1 300 ^{o}C. These results confirm that 1 300 ^{o}C is the lowest temperature at which the reaction between Al and hBN can proceed to completion.

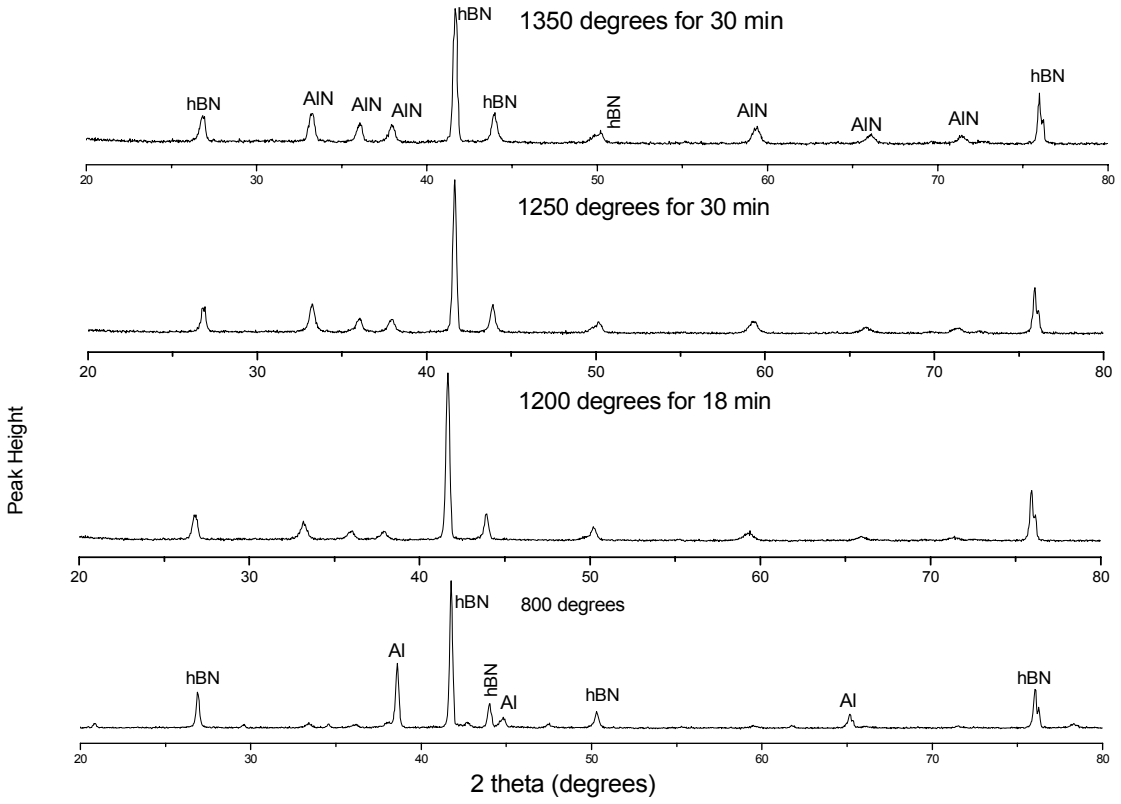

Figure 6.1: Some of the XRD results for the hBN-26 sample

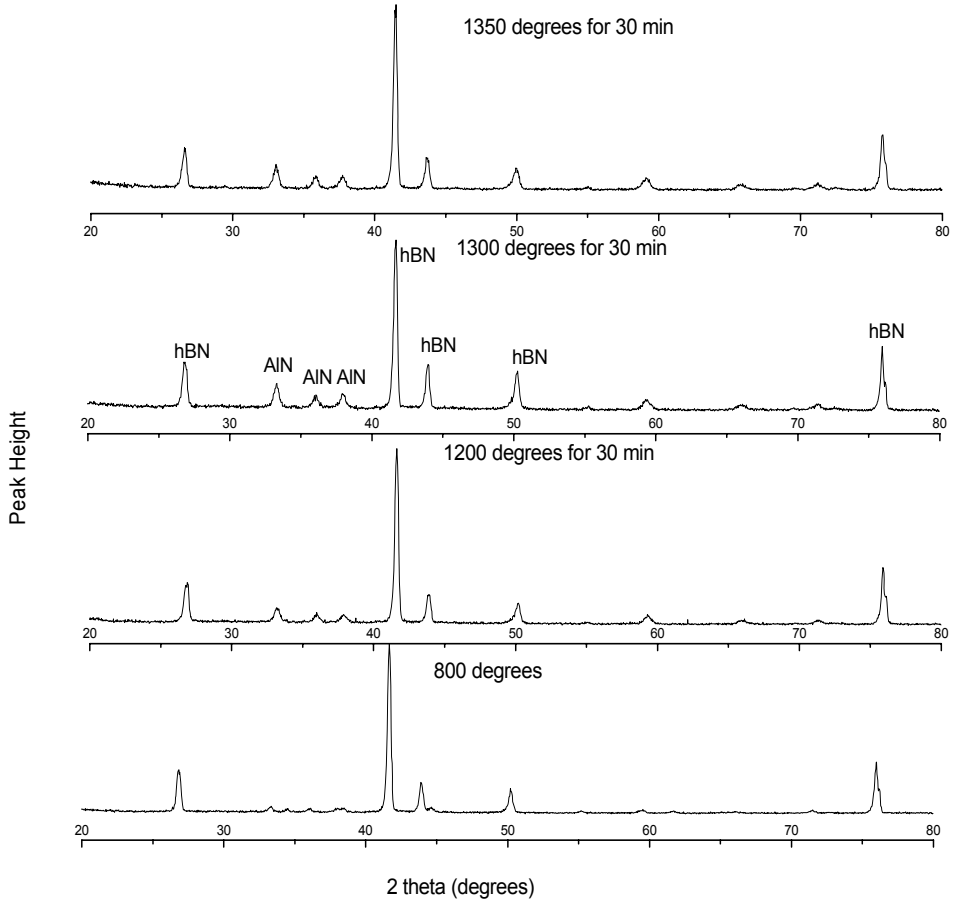

Figure 6.2: Some of the XRD results for the hBN-18 sample

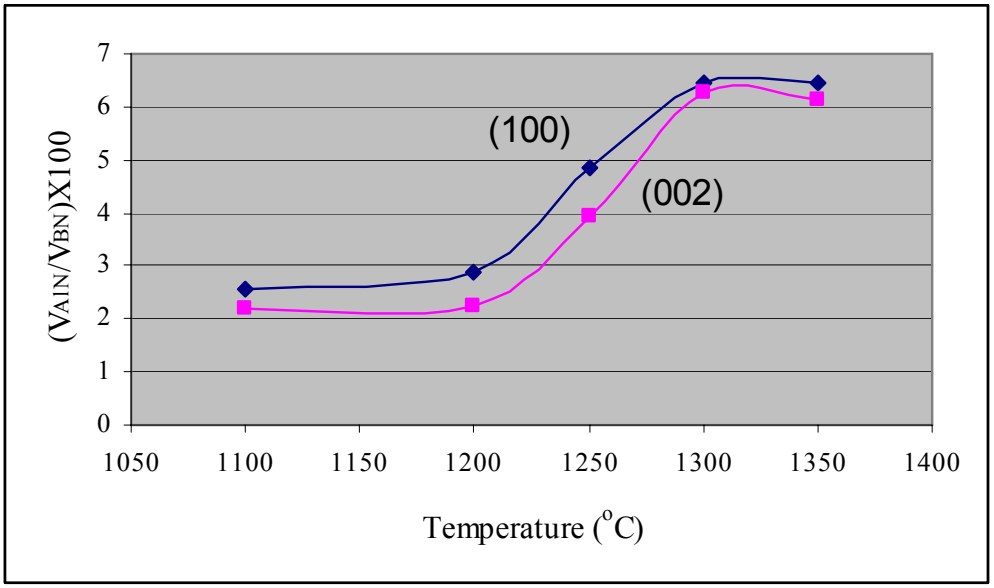

Figure 6.3: Ratio of V_{AlN}/V_{hBN} (where the (100) peak of hBN was used) as a function of temperature for the hBN-18 sample

6.1.3 Microstructure analysis of both infiltrated and reacted samples

The fracture surfaces of the hBN-26 and hBN-26HT13 samples are shown in Figures 6.4a to 6.4c. Figure 6.4a shows some Al to be present, which implies that infiltration did take place. The image shows a large number of pores – much higher than the 2% measured. This is evidence that most of the Al fell off when the sample was broken, leaving voids in the hBN matrix. This was expected since the bond between Al and hBN at 800 °C is not strong because there is very little reaction at this temperature. After heating at 1 300 °C, the hBN particles show more plate-like forms which are not clear at 800 °C (Figures 6.4b and 6.4c). The structure of the white particles after treatment at 800 °C is different from that after treatment at 1 300 °C. This is due to the reaction between Al and BN. The EDX analysis showed that the white needle-like particles after 1 300 °C are composed mainly of AlN.

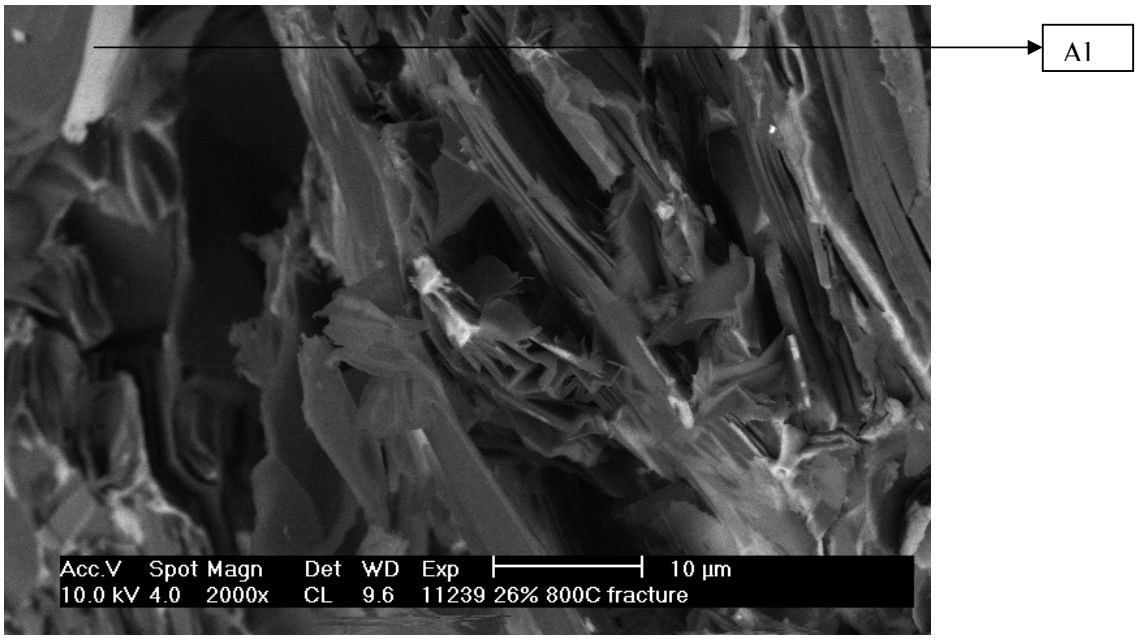

Figure 6.4a: Fracture surface SEM micrograph of the hBN-26 sample

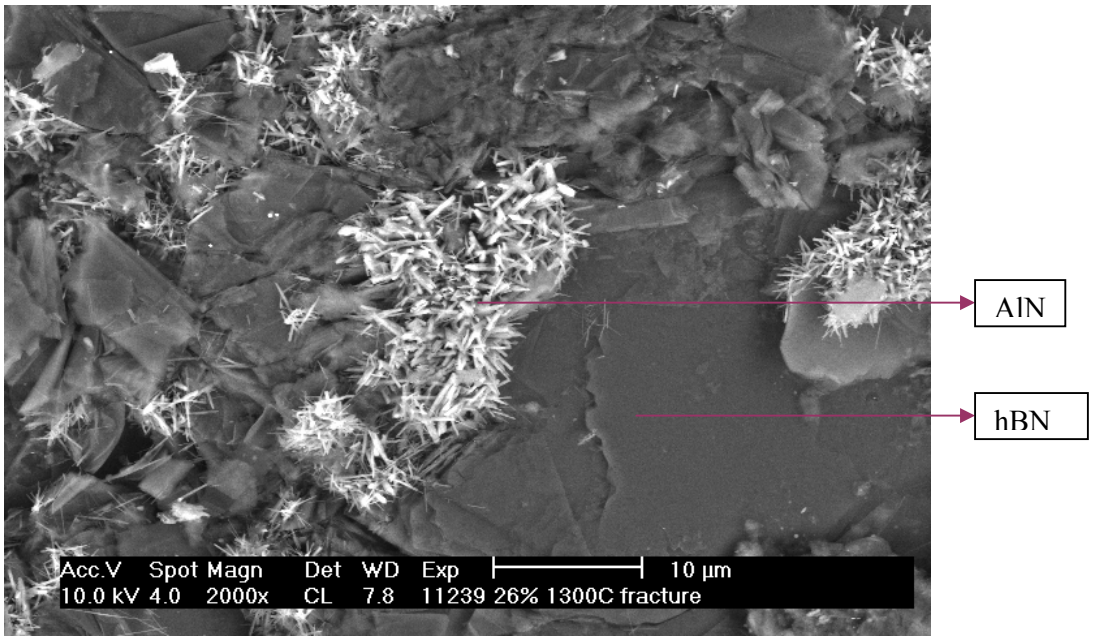

Figure 6.4b: Fracture surface SEM micrograph of the hBN-26HT13 sample

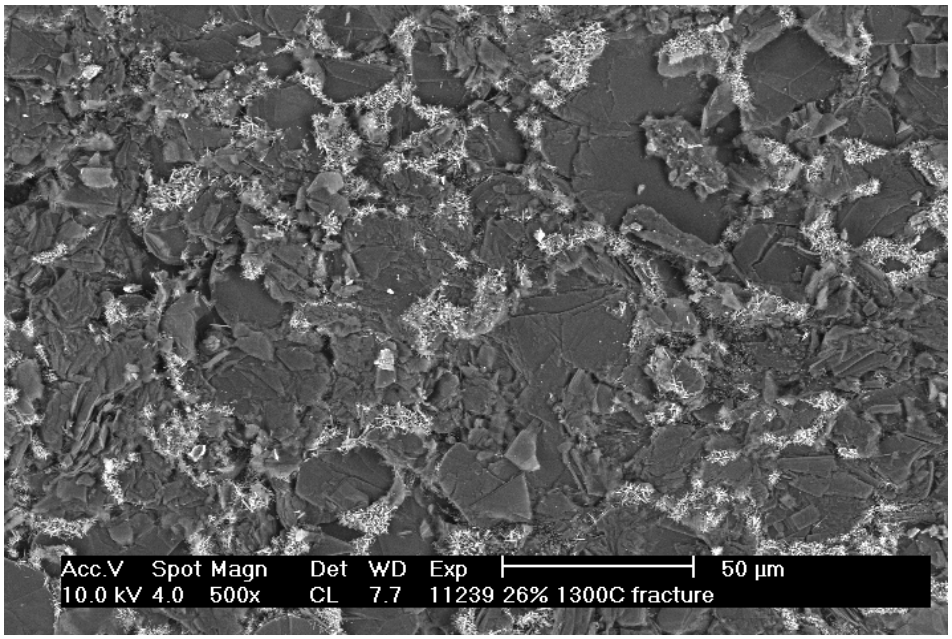

Figure 6.4c: Fracture surface SEM micrograph of the hBN-26HT13 sample

Another sample with 18% porosity (referred to as hBN-18 in Table 6.1) was also infiltrated and was subjected to the same treatment as the 26% porosity sample. By examining this sample it was clear that not enough aluminium had been added, since near the top of the sample the boron nitride could be distinguished from the composite (hBN + Al). The density was measured after removal (by polishing on SiC paper) of this non-infiltrated section.

The results from the polished SEM micrographs show the presence of copper (identified using EDX) in the material. A washer made up of copper metal had been placed on top of the hBN pellet (see experimental procedure in Section 4.4.1). Some copper from the washer may have dissolved in the Al and then been forced into the hBN pellets.

Figures 6.5a and 6.5b show SEM micrographs of the polished surface of samples heat treated at different temperatures. Figure 6.5a shows the micrograph for the hBN-18 sample, while Figure 6.5b shows the hBN-26 sample after it had been heated for 60 min at 1 300 ^{o}C (referred to as hBN-26HT13 in Table 6.1). The dark regions correspond to hBN grains and the light regions correspond to Al-containing particles. Three different phases are clear in Figure 6.5a; they are: hBN, Al (grey particles) and the whiter particles are Al with Cu. After heating at 1 300 ^{o}C, the AlN and AlB_x phases appeared, while the Al phase disappeared. Since the borides could not be detected by means of XRD, it was not easy to distinguish between AlB_2 and AlB_{12} using EDX. Some oxide was detected at the surface. In Figure 6.5b it can be seen that the hBN particles are

uniformly distributed in the AlN/AlB_x matrix, with elongated hBN particles favouring a certain direction, probably due to the manner in which the pellet was pressed. The sample has some pores, which may mean that insufficient Al was added to fill all the pores present before infiltration. There are more pores in Figure 6.5a compared with the micrograph in Figure 6.5b. The reason for this may be the amount of Al added to fill up the pores. The micrograph in Figure 6.5b was taken from the sample containing 26% Al, while the sample shown in Figure 6.5a had only 18% Al added to fill the pores.

To eliminate the copper observed in the previous infiltrated samples, a graphite foil (thickness 0.5 mm) was placed between the hBN pellet and the copper washer. To reduce oxides in the sample, a purer Al sheet (99.999% purity) was used instead of a commercial aluminium foil. The SEM micrograph of the hBN-24 sample in Figure 6.6 shows that Cu is still present in the material. The next infiltration experiment was done using tantalum foil (thickness 0.12 mm) instead of a copper washer. A sample with 19% porosity filled with Al (referred as hBN-19 in Table 6.1) was prepared. The SEM micrograph for this sample is shown in Figure 6.7. The micrograph shows three phases: the dark region is hBN, the white region is AlN and the light grey is either AlB_2 and/or AlB_{12}, confirmed by EDX. The oxide was also much reduced compared with the hBN-26 sample with which commercial aluminium foil was used. Neither copper nor tantalum was found in this sample.

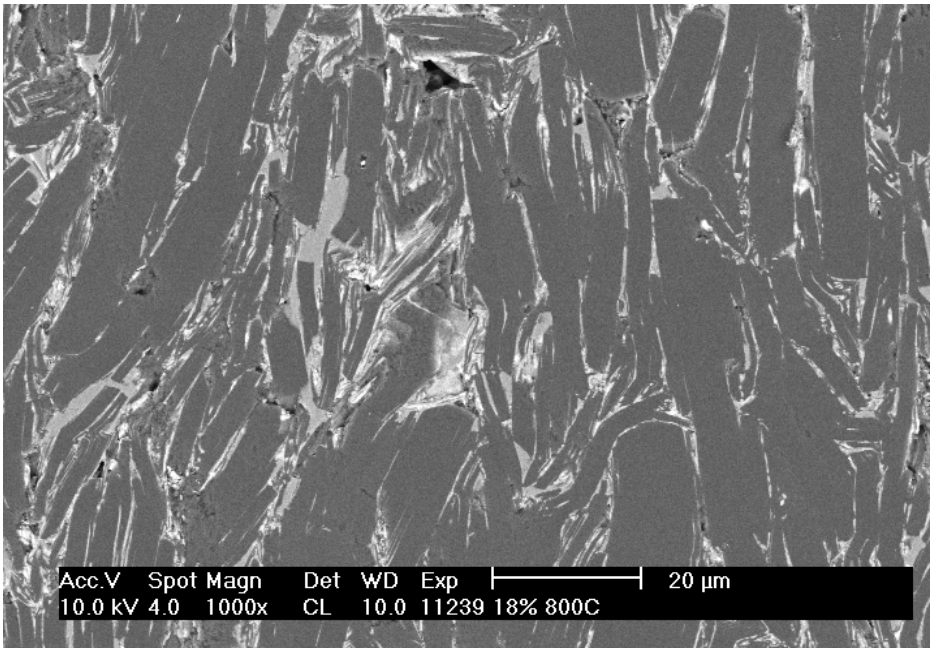

Figure 6.5a: SEM micrograph of the hBN-18 sample

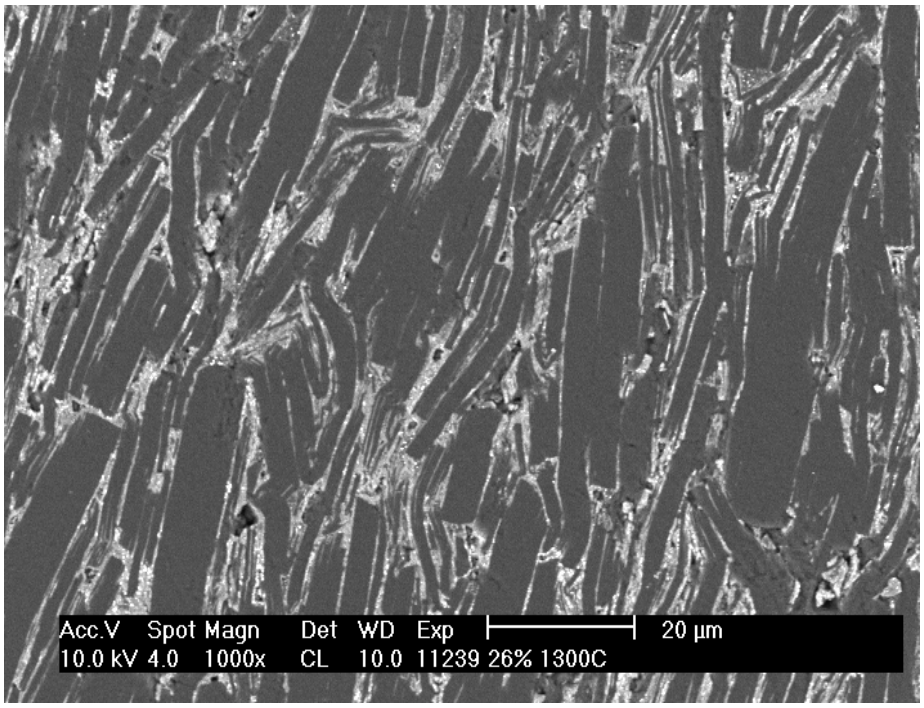

Figure 6.5b: SEM micrograph of the hBN-26HT13 sample

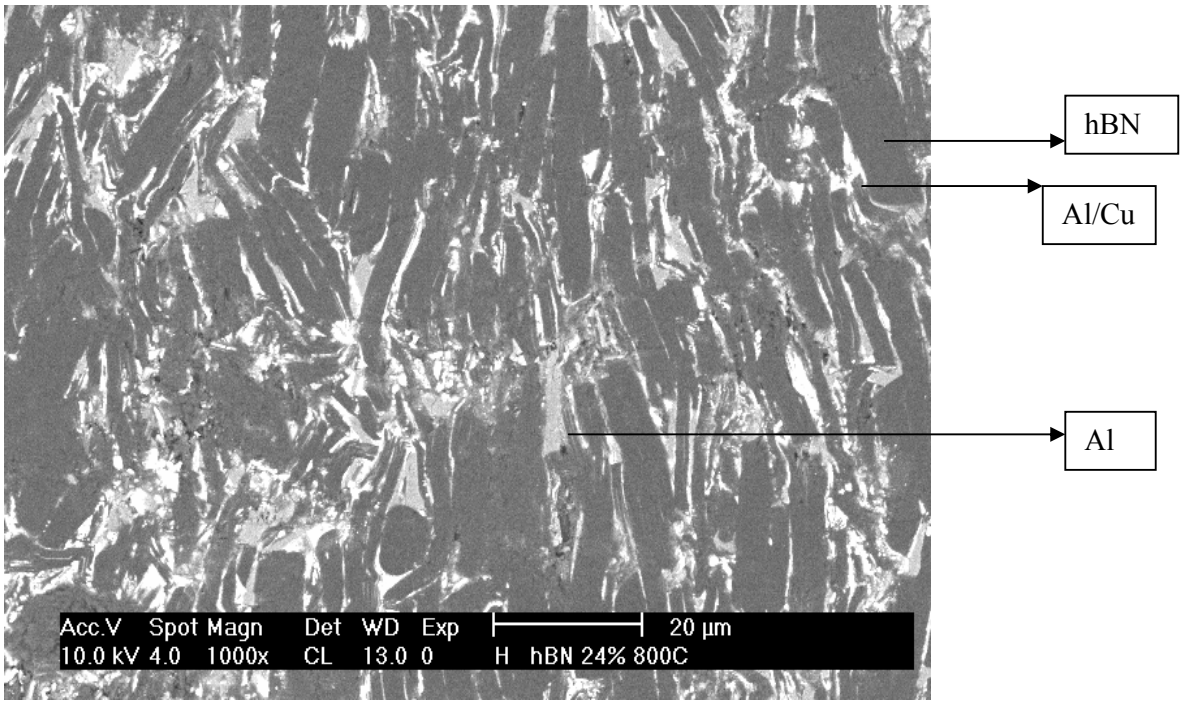

Figure 6.6: SEM micrograph of the hBN-24 sample

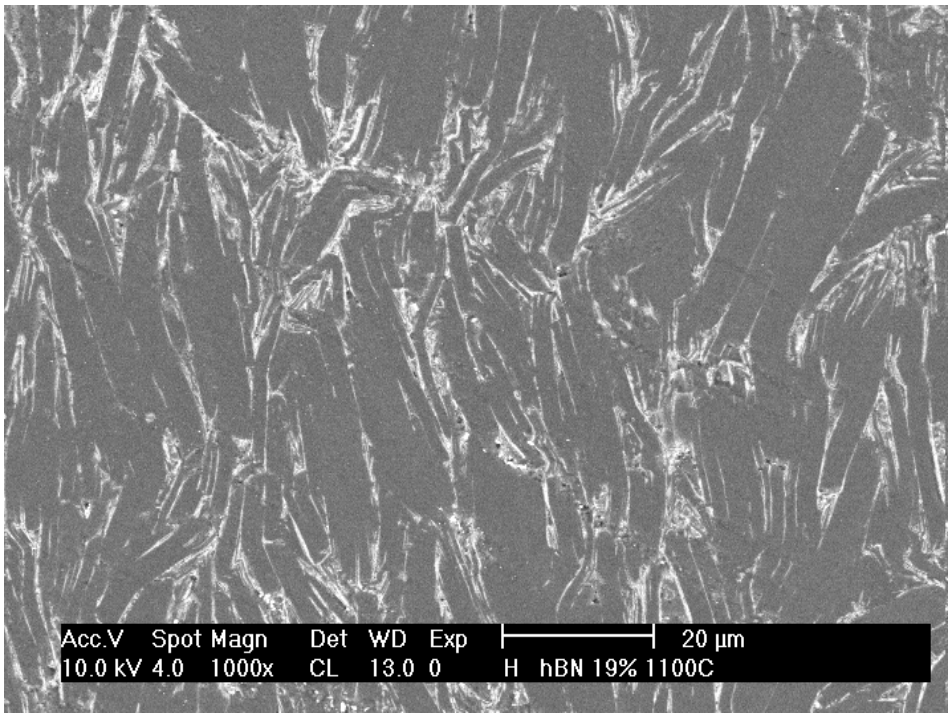

Figure 6.7: SEM micrograph of the hBN-19HT13 sample

6.2 Infiltration of the cubic BN (cBN) samples

6.2.1 Hexagonalization of the cBN particles

The hexagonalization of coarse cBN (12 µm) and fine cBN (3 µm) powder in a nitrogen atmosphere at ambient pressure was examined. This was tried at different temperatures and times. Table 6.3 shows all the samples, together with the conditions and final ratios of cBN to hBN. The procedure in naming the samples was as follows: cBN12HT12.5-48 means a 12µm cBN powder heat treated to 1 250 ^{o}C for 48 hours. The ratios were calculated based on equation 4.4 of Section 4.5.2. The ratios of the peak heights (cBN to hBN (Ic/Ih)) are also included in the table.

Table 6.3: Samples heat treated during the hexagonalization experiments

Sample	BN particles	T (^{o}C)	Time (min)	Ic/Ih	cBN/hBN
cBN12HT12.5-48	12	1 250	2880	No hBN	-
cBN12HT13-4	12	1 300	240	59	75
cBN12HT13-12	12	1 300	720	12	14
cBN12HT13-36	12	1 300	2160	7.7	8.5
cBN12HT13.5-12	12	1 350	720	1.4	0.3
cBN12HT14-12	12	1 400	720	0.26	-
cBN3HT13-36	3	1 300	2160	127	163
cBN3HT13.5-12	3	1355	720	10	11.5
cBN3HT13.7-12	3	1 375	720	6.3	6.7
cBN3HT14-12	3	1 400	720	28	34.8

No hBN peaks were observed in the XRD spectrum of the run at 1 250 ^{o}C after heating for 2880 min. The temperature was increased to 1 300 ^{o}C. At this temperature the 12μm powder was heated for 240, 720 and 2160 min. The hBN peak was found to be higher after a longer heating time, as shown in Figure 6.8a. At a temperature of 1 350 ^{o}C, the hBN can be estimated to be about 40% after heating for 720 min. The hBN peak was found to be higher than the cBN peak at 1 400 ^{o}C after heating for 720 min. Figure 6.8b below shows the results of the experiments at different temperatures.

The SEM micrograph of a single grain taken from cBN3HT13.5-12 is presented in Figure 6.9a while Figure 6.9b shows a cBN grain from the same batch before annealing. The conversion from cBN to hBN takes place on the grain surface. The calculations show that about 40% of hBN was formed at this temperature. From the image shown in Figure 6 9a there is no evidence of such an amount of hBN. It is possible that some hBN peeled off the surface and fell away during hexagonalization.

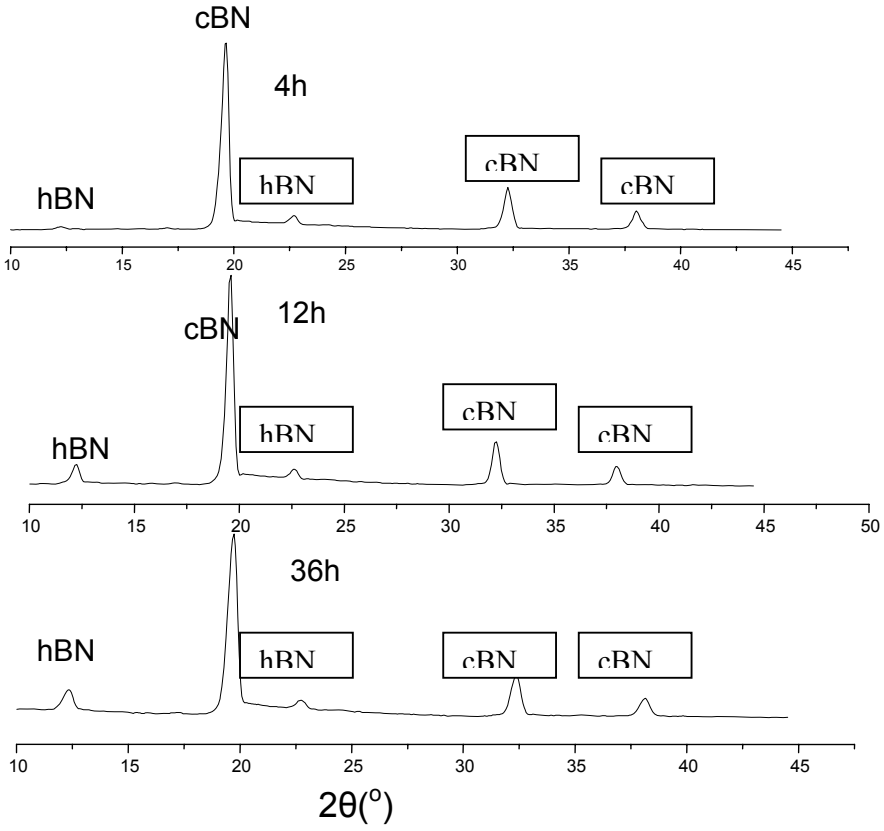

Figure 6.8a: Results of the XRD measurements for the 12 µm cBN powder heated at 1 300 °C for different times using the Mo tube

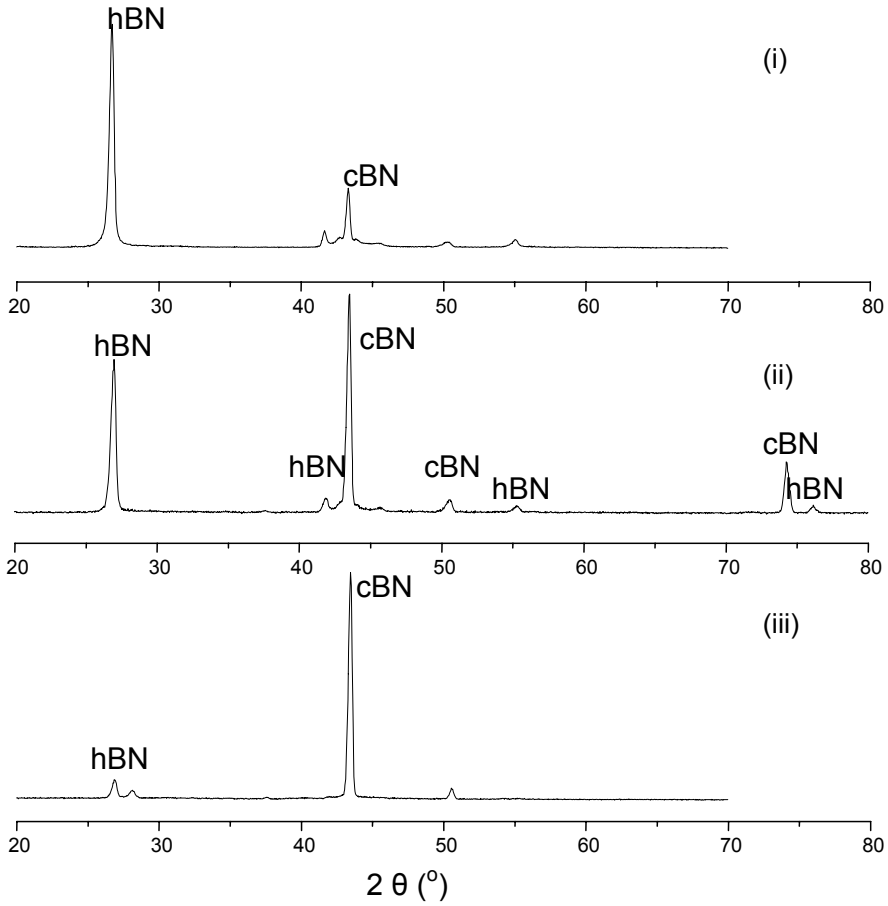

Figure 6.8b: Results of the XRD measurements for the samples (i) cBN12HT14-12, (ii) cBN12HT13.5-12 and (iii) cBN12HT13-36

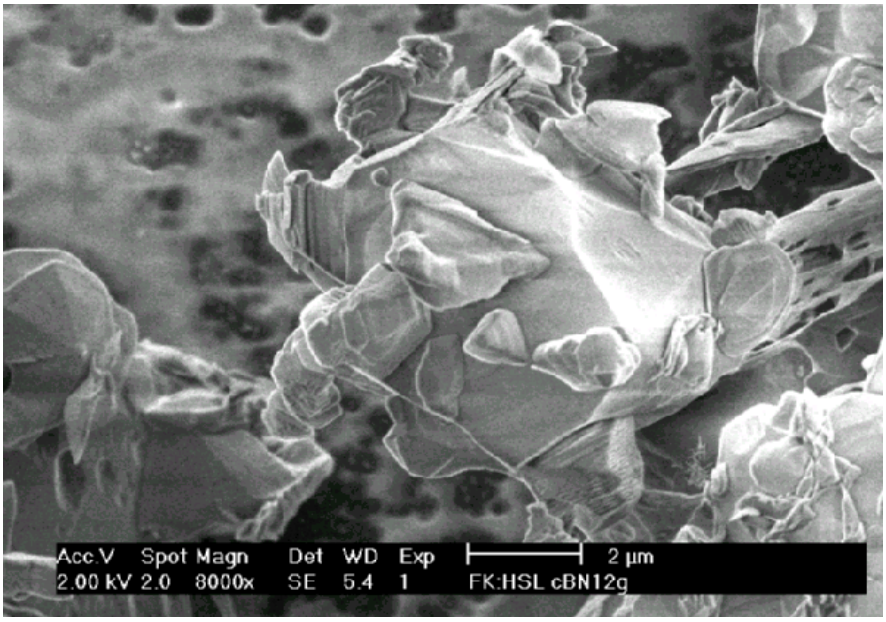

Figure 6.9a: SEM micrograph of sample cBN12HT14-12

The hexagonalization takes place on the surface of the crystal.

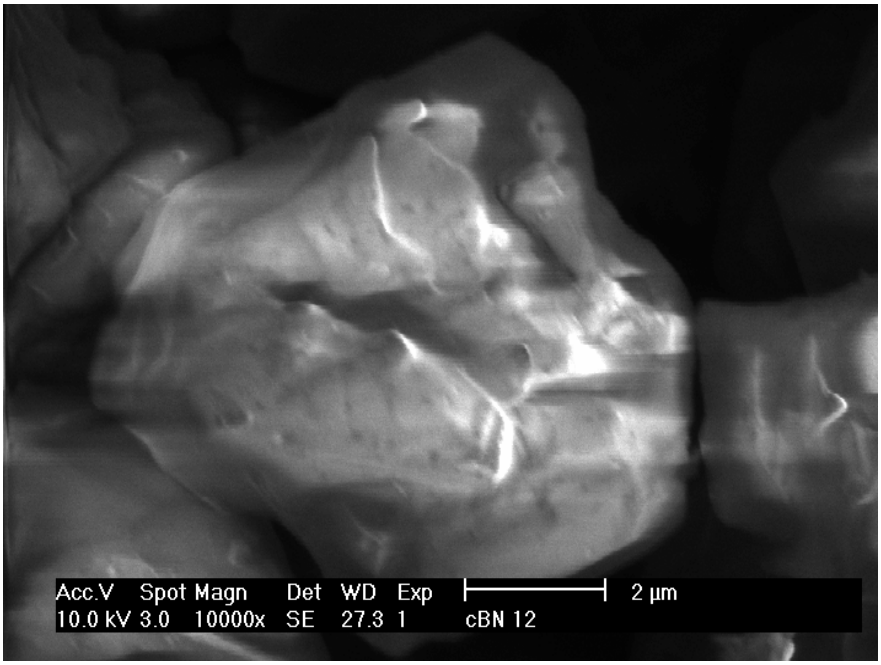

Figure 6.9b: SEM micrograph of sample cBN12HT14-12 before annealing

No hBN flakes are present as in Figure 6.9a.

The hexagonalization experiments of the 3 µm cBN powder were done for 12 h at different temperatures. The hBN peaks are hardly visible from the XRD results measured after the powder had been heated at 1 300 ^{o}C. However, after heating for 12 h at 1 355 ^{o}C, a peak at around 26.7^{o},

which is known to be a 002-hBN line, can be observed. This hBN peak is slightly higher at 1 375 ^{o}C for the equivalent amount of time, but hardly recognizable after heat treatment at 1 400 ^{o}C. This was an unexpected result. Therefore, the heat treatment was repeated at 1 400 ^{o}C and the hBN peak was not significantly different to that observed for the heat treatment done at 1 375 ^{o}C.Thus the 1400°C measurement shown in figure 6.10 below was discarded. Figure 6.10 shows the results for the experiments done at these temperatures. The ratio of the peak heights (Ih/Ic) is included in Table 6.3.

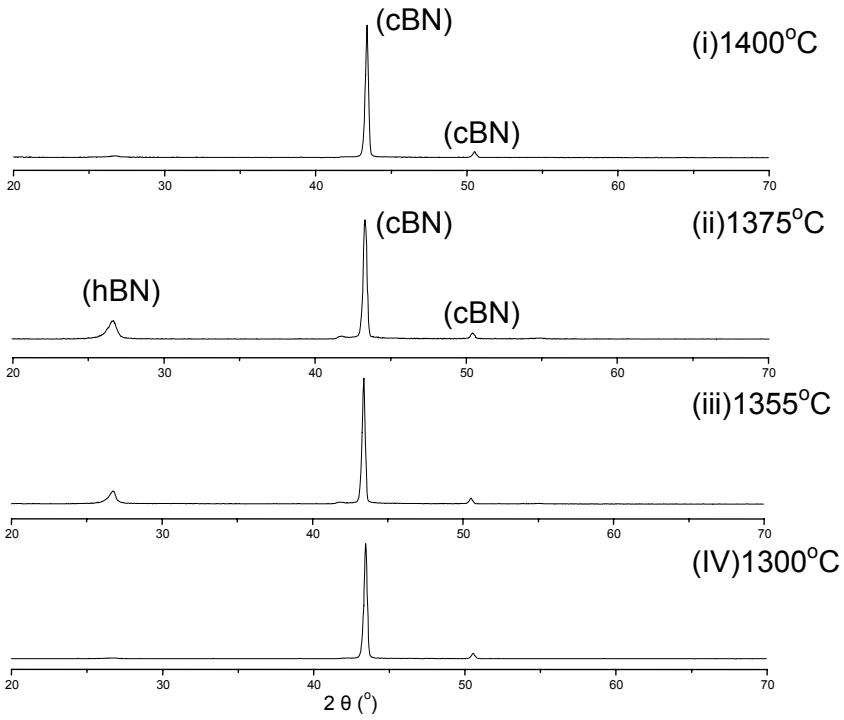

Figure 6.10: Diffractograms of the samples (i) cBN3HT14-12, (ii) cBN3HT13.7-12, (iii) cBN3HT13.5-12 and (iv) cBN3HT13-12 at different temperatures for 12 hours

The XRD result for this powder was quite astonishing – unlike for the 12 μm cBN powder (where ~40% hBN formed at 1 350 ^{o}C), the hBN peak for the 3 μm was hardly visible at 1 355 ^{o}C. These results were unexpected since the 3 μm powder should have a much larger surface area than that of the 12 μm powder. The powder heated at 1 400 ^{o}C for 720 min (cBN3HT14-12) was viewed under the scanning electron microscope (Figure 6.11a). The micrographs show that there is very little hBN on the grain surface. This is evident from a comparison of the

micrographs in Figure 6.9a with those in Figure 6.11a. There is also no difference between the grains before and after heat treatment Figures 6.11b and 6.9a respectively.

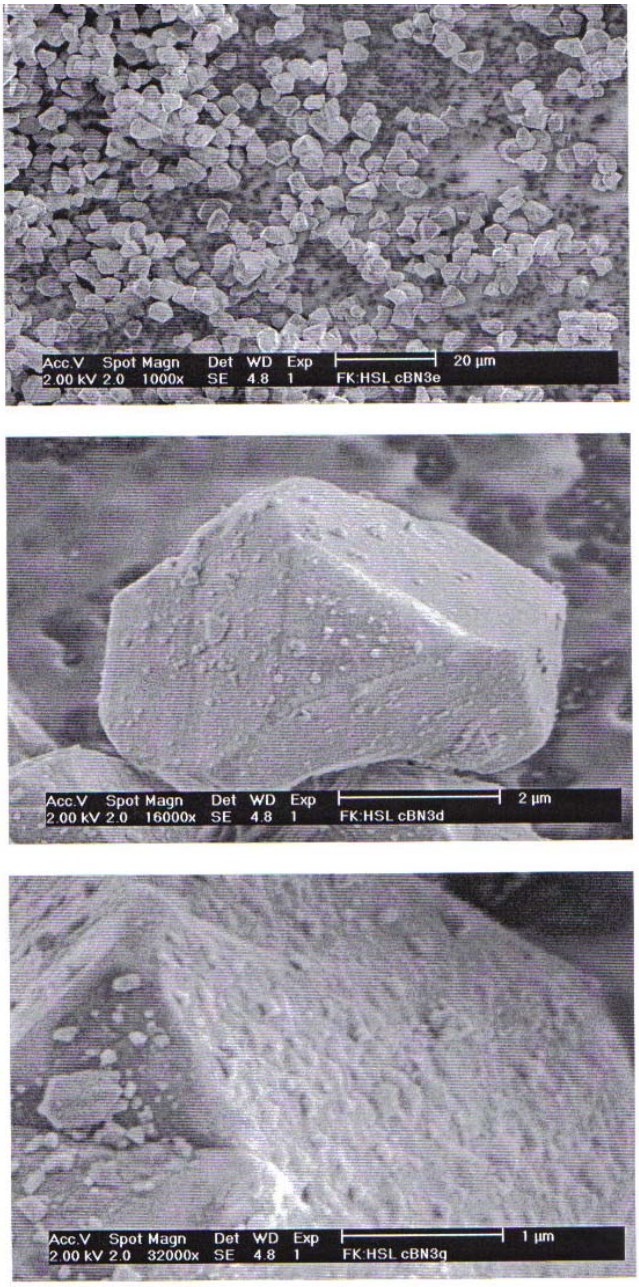

Figure 6.11a: Images of the cBN3HT14-12 samples taken at different magnification

Evidence of hexagonalization is not clear in these images taken at 1 000x, 16 000x and 32 000x.

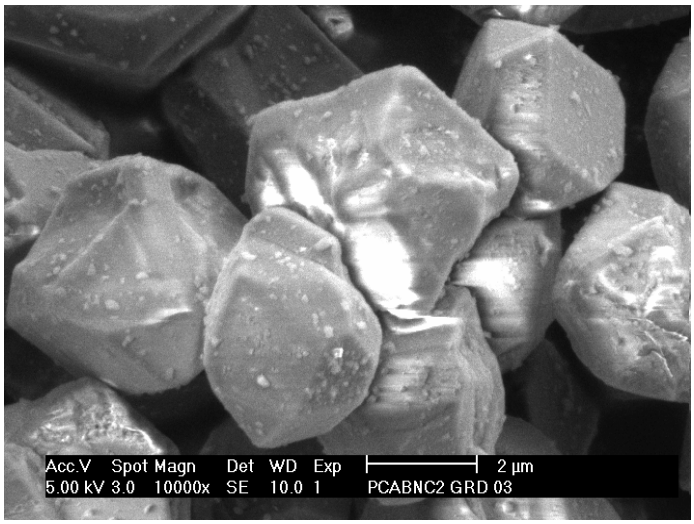

Figure 6.11b: SEM micrograph of sample cBN3-4 before annealing

The grain of grade 12 µm cBN shown in Figure 6.9b shows a nodular particle shape with clearly no defined planes. These grains were produced from the crushing of the larger grains, while grade 3 particles, shown in Figure 6.11a are seen to be made up from well faceted crystals. The 3 µm particles (Figure 6.11) were not produced through crushing process of larger ones, but were crystal grown to that dimension. This explains the good crystallinity observed. This would be the possible explanation for this strange behaviour as such particles would have smooth surfaces with fewer nucleation sites. Indeed this difference can be clearly explained by heterogenous nucleation theory (Porter and Easterling, 1992). According to that theory, the free energy associated with the nucleation of a new phase is given by $\Delta G = 0.5V^{*}\Delta G_V$, where V^{*} is the volume of a critical nucleus and ΔG_V is the free energy difference per unit volume. The critical volume is constrained by the "wetting" angle between the new phase being formed and the substrate on which the new phase is being generated. Smaller "wetting" angles result in drastically smaller critical volumes, and therefore in drastically smaller activation energies for nucleation of the new phase. For a given "wetting" angle, surface irregularities serve to decrease the volume of the critical nucleus, as shown in Figure 6.11c below. As the 12 µm cBN is produced by crushing, it is seen from Figure 6.9b above to have on its surface many irregularities, which serve to decrease the activation energy for the nucleation of the hBN phase. Therefore the hBN phase is generated on the surface of the particles of this grade at temperatures lower than on the surfaces of the well faceted grade three particles, despite the fact that the latter grade has a larger specific surface area.

N.B! In the context of the discussion above, by "wetting angle" we mean the angle formed by the free surface of the nucleus and its interface with the substrate, at their point of peripheral contact. That angle is determined by the balance of the surface energy forces at the periphery of the nucleus, and therefore it has a clearly defined value.

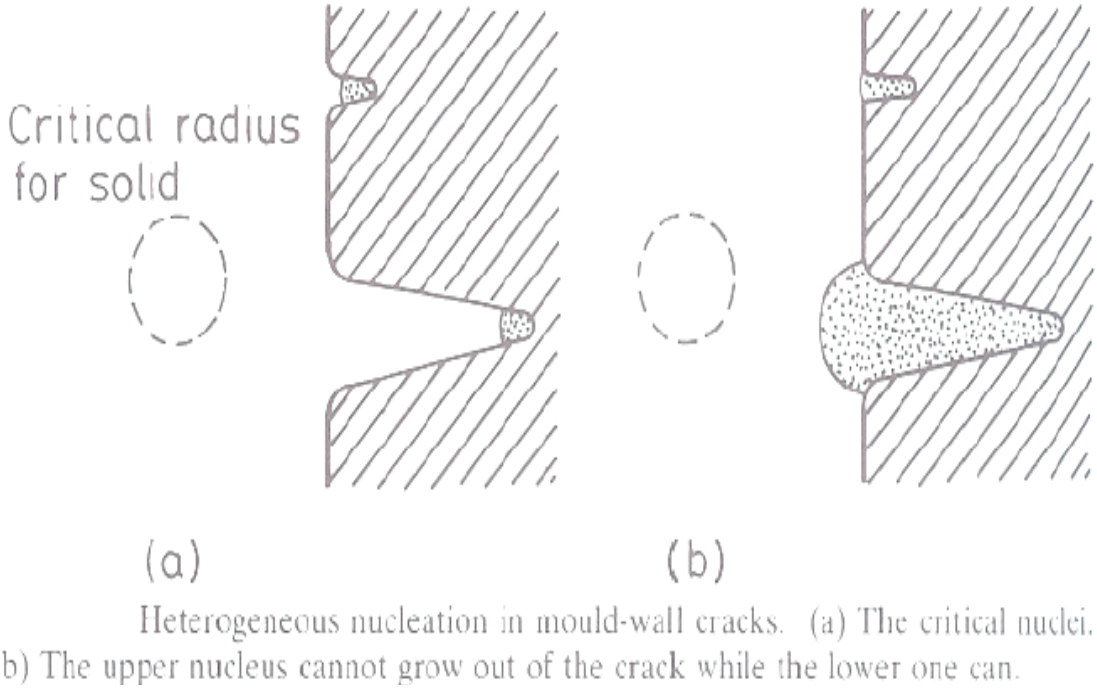

Heterogeneous nucleation in mould-wall cracks. (a) The critical nuclei. (b) The upper nucleus cannot grow out of the crack while the lower one can.

Figure 6.11c: Heterogeneous nucleation in mould-wall cracks (Easter and Porterling,1992)

6.2.2 Infiltration of the hexagonalized cBN samples

Two samples with different porosities were prepared from partially hexagonalized BN powders. Their properties are summarized in Table 6.4. The properties of the annealed samples are shown in Table 6.5. The procedure in naming the samples was as follows: 40cBN12-36 means a sample containing partially hexagonalized 12 μm cBN powder with approximately 40 vol. % hBN and 36% Al, and 40cBN12-36HT13-1 is the same sample heat treated at 1 300 ^{o}C for 60 min.

Table 6.4: The partially hexagonalized cBN containing samples prepared by infiltration at 800 ^{o}C for 30 min

Sample name	Original powder sample	Green density (g/cm^3)	Porosity (%)	Density after heat treatment at 800 ^{o}C (g/cm^3)	Phases present
40cBN12-36	cBN12HT13.5-12	1.91	36	2.82	Al, hBN, cBN
10cBN12-40	cBN12HT13-36	1.87	40	2.69	Al, hBN, cBN

Table 6.5: The hBN containing samples containing Al after 60 min of heat treatment

Sample name	Density after heat treatment (g/cm^3)	Open porosity (%)	Phases present
40cBN12-36HT12-1	2.83	0.11	Al, AlN, hBN, AlCu, cBN
40cBN12-36HT13-1	2.85	0.14	AlN, hBN, AlCu, cBN
40cBN12-36HT14-1	2.77	0.10	AlN, hBN, AlCu, cBN
10cBN12-40HT13-1	2.72	1.2	AlN, hBN, cBN, Al

It was important to calculate the change in volume during the reaction before starting the sintering experiments. As discussed previously, the reaction between Al and BN was expected to produce AlN, AlB_2 and AlB_{12} as products. The aim was to use up all the Al metal in reacting with hBN and have the cBN phase left unreacted.

The samples in table 6.5 show a respectable density after the heat treatment with all the samples containing an open porosity of about 0.1% except for the sample 10cBN12-40HT13-1. Comparing the measured densities in table 6.5 with the calculated theoretical densities, all the samples were found to be more than 98% of the theoretical densities. The densities measured on these materials shows that the infiltration was successful.

6.2.3 Phase composition and microstructure of infiltrated samples

Figure 6.12 shows the XRD results for the 40cBN12-36 sample. After infiltration, the sample contained hBN, cBN and Al. The AlN peaks, present at both 1 100 ^{o}C and 1 250 ^{o}C, confirm the reaction between Al and BN. At 1 100 ^{o}C, there are peaks that are no longer present above 1 250

^{o}C. These peaks are observed at 47.4^{o} (d = 0.1918 nm), 2θ = 42.6^{o} (d = 0.2119 nm) and 2θ = 20.8^{o} (d = 0.4261 nm). They are found to correspond to the (310), (112) and (110) reflections of Al_2Cu. These peaks are not present at 1 250 ^{o}C, which may mean that the aluminium from these alloys has reacted with the boron nitride. No formation of AlB_2 and/or AlB_{12} could be detected.

The presence of the hBN peak in the final product is a problem. This is a soft phase of boron nitride and it led to poor hardness. It was observed that the hBN peak decreased from 1 100 ^{o}C to 1 250 ^{o}C. This was expected since hBN reacts with Al. However, above 1 300 ^{o}C , the hBN peak increased and it was found to be even higher at 1 350 ^{o}C and 1 400 ^{o}C. This may suggest that some of the cBN grains suffered hexagonalization at higher temperatures or that the difference in the reaction rate between cBN and hBN has been reduced.

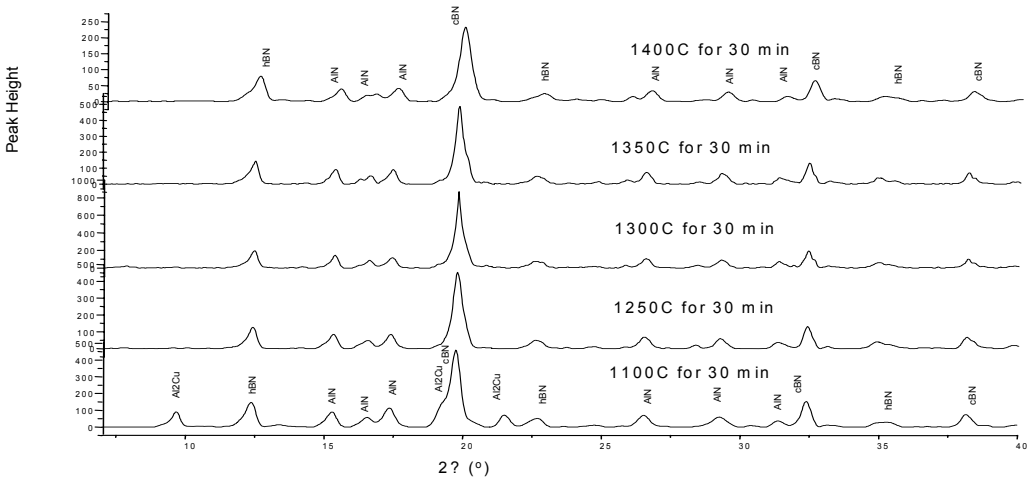

Figure 6.12: Diffractograms of the 40cBN12-36 sample heat treated at different temperatures. Mo-Kα radiation was used.

Another sample was prepared from the partially hexagonalized cBN 12 μm powder containing about 10% hBN and it was infiltrated with 42% Al (10cBN12-42). This sample was prepared with less hBN phase on the hypothesis that all the hBN would be used up during the reaction at higher temperatures. The pieces of this sample were heat treated at 1 100 ^{o}C, 1 200 ^{o}C, 1 300 ^{o}C and 1 350 ^{o}C. The AlN peaks were observed from the XRD results, and cBN and hBN peaks were found at all temperatures.

The polished surface of the 40cBN12-36HT13-1 sample was observed by SEM and is shown in Figure 6.13 below. There are three clear phases: cBN, AlN and AlCu alloy. The AlCu alloy, represented by the white regions, was in quantities sufficient to be detected by XRD and was found to be Al_2Cu. Although this alloy was present in the hBN samples, it was not detectable by XRD. This may mean that more copper was present in the 40cBN12-36HT13-1 sample. The cBN particles are uniformly distributed in the AlN/Al_2Cu matrix.

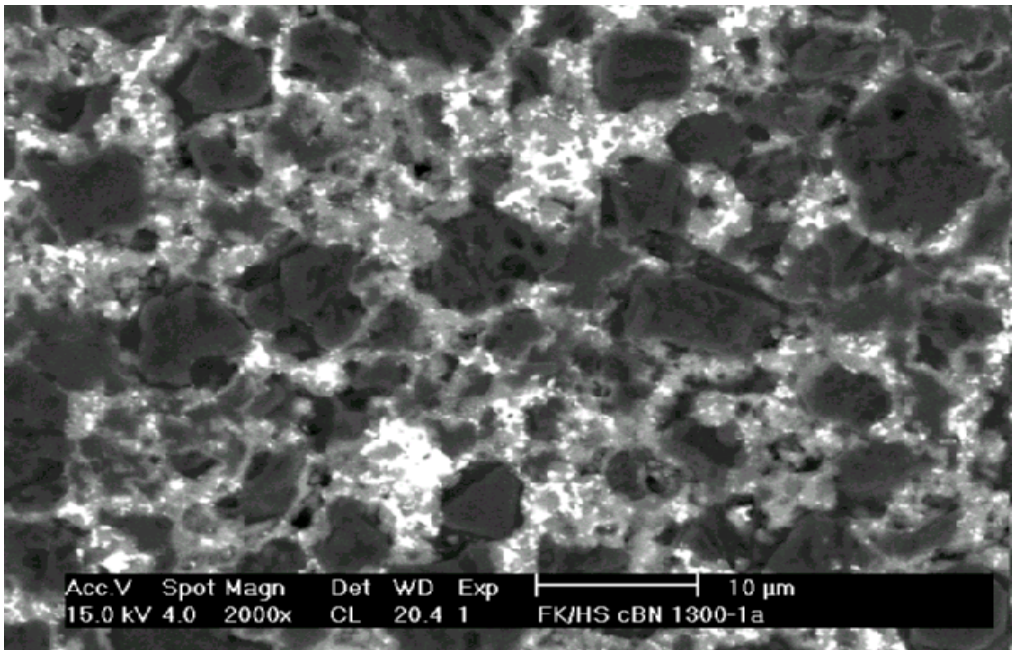

Figure 6.13: SEM micrograph of the 40cBN12-36HT13-1 sample

6.2.4 Hardness of the sample

The Vickers hardness Hv(30) was measured on the 40cBN12-36HT13-1 sample and was found to be 6.5 ± 4.8 GPa. This hardness result proved that the sample is very soft compared with the 31 GPa of AMB 90 (Amborite). It is suggested that the low hardness and the high standard deviation is connected with the high hBN content, which differs locally.

The reduction of the initial hBN phase did not help to use up all hBN present during the reaction with Al. The conclusion from this work was that the presence of the initial hBN phase provided nucleation sites for further hexagonalization at higher temperatures. The results also showed that differences in the reactivity of hBN and cBN with aluminum are small, therefore higher amount of hBN in the starting preform will not be consumed preferentially during the reaction with the

aluminum. Therefore metallic binder phases for the shaping are more suitable than the use of the hBN-binder.

On the basis of the above findings, it was decided to attempt reaction sintering of cBN with Al without any previous hexagonalization of the cBN particles.

6.3 Infiltration of the 12 μm cBN particles without previous hexagonalization

Infiltration of the pure cBN pellet (without hexagonalization) was done. Some aluminium was added initially to facilitate the formation of the pellet. A micronizing mill was used to mix the cBN powder (12 μm), 95 wt %, and the aluminium powder (less than 5 μm), 5 wt %. Agate balls were used as a milling medium for 1 h. The powder was then cold pressed into a pellet of 18.5 mm diameter under 100 MPa. The porosity of the pressed pellet was found to be 42%. Aluminium discs with a mass of 2.45 g were used to fill the calculated porosity. Since the pellet was not very strong, the infiltration was performed under 5 MPa pressure. During the heating, the pressure increased after displacement of peston from 5 MPa until 9.5 MPa at 797°C. At this temperature the pressure was decreased to 5.3 MPa. This indicated that the aluminium had melted and the cBN disc had been pushed through the molten aluminium. The pressure was then increased to 13 MPa and kept there until the temperature had decreased to 380 ^{o}C.

The green density of 2.04 g/cm^3 increased to 2.92 g/cm^3 after infiltration. The sample was found to have 97% of the theoretical density. Heat treatment after infiltration of this sample was carried out at the following temperatures: 1 100 ^{o}C, 1 200 ^{o}C, 1 250 ^{o}C, 1 300 ^{o}C, 1 400 ^{o}C and 1 550 ^{o}C. The heat treatments done on this sample are summarized, together with some properties, in Table 6.6. The procedure in naming the samples was as follows: cBN12-42HT15.5-1 means a sample containing 12μm cBN powder was infiltrated with 42vol.% Al and heat treated at 1 550 ^{o}C for 1 hour.

Table 6.6: Some of the cBN samples prepared

Sample name	Density after heat treatment (g/cm^3)	Open porosity (%)	Phases present
cBN12-42HT11-1	2.87	0.35	Al, AlN, cBN, AlB_x
cBN12-42HT12-1	2.90	0.24	Al, AlN, Al_2O_3, cBN, AlB_x
cBN12-42HT13-1	2.85	0.24	AlN, Al_2O_3, cBN, AlB_x
cBN12-42HT155-1	-	-	AlN, hBN, cBN, AlB_{12}
cBN12-42HT14-1 HT700-3*	2.89	0.21	AlN, hBN, cBN, AlB_2

*cBN-42 sample heat treated for 60 min at 1 400 ^oC and for a further 3 h at 700 ^oC.

AlB_x refer to either AlB_2 and/ or AlB_{12}

The density of the cBN12-42HT12-1 sample, obtained using Archimedes' principle, was found to be 2.90 g/cm^3, with a standard deviation of 0.05 g/cm^3, which is 97.4% of theoretical density. The open porosity was measured to be 0.24 ± 0.03%. The density of this material shows that the infiltration was successful. From the previous experiments, it was found that at 1 300 ^oC the formation of aluminium nitride is almost complete and thus there was no need to use higher temperatures. However, heat treatment at a temperature of 1 400 ^oC was done to see whether hexagonalization would take place at a higher temperature. Hexagonalization was not expected to take place below 1 300 ^oC. The temperatures were normally kept constant for 60 min, except for one sample (cBN12-42HT14-1HT700-3) where the temperature was kept constant for 60 min at 1 400 ^oC and for a further 3 h at 700 ^oC. The purpose of this experiment was to try to enhance the formation of AlB_2 and to confirm that the hBN phase does not form if it was not present in the initial stage. An extreme temperature of 1 550 ^oC was also used to test hexagonalization.

6.3.1 Phase composition and microstructure of the heat-treated samples

The phase compositions of the heat-treated samples are also shown in Table 6.6 The XRD result of the sample heat treated at 1 550 ^oC for 60 min is presented in Figure 6.14. It can be seen that the hBN phase *is* formed at this temperature. This is to be expected since the heat treatment was done under no pressure. Additional experiments at 1 450 ^oC and 1 550 ^oC were done to determine the temperature at which hexagonalization takes place and it was concluded that the use of temperatures above 1 400 ^oC would result in the hBN phase forming from cBN, which

would be detrimental to the mechanical properties of the resulting material. No hBN formed after heat treatments at 1 400 ^{o}C for 60 min; however, when the temperatures were kept constant for longer periods, e.g. 3 h, some hBN peaks were observed in the XRD traces.

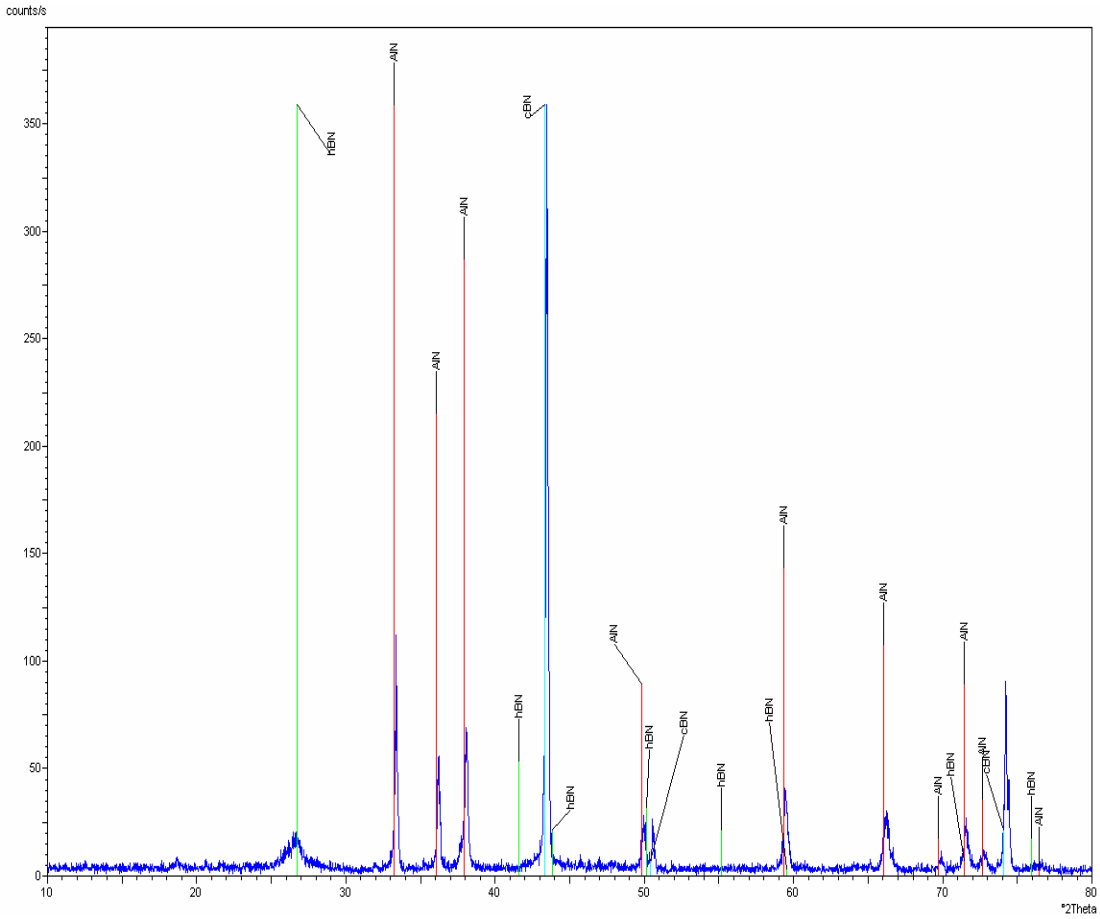

Figure 6.14: Diffractogram of the cBN12-42HT155-1 sample

The polished surface of the cBN12-42HT14-1HT700-3 sample was observed by SEM and is shown in Figure 6.15. The micrograph has two major phases: the dark cBN phase and a light AlN phase present in the boundary of the cBN grains. The light phase is composed mainly of aluminium nitride. However, the borides and alumina also form part of this phase. EDX was used to identify the phases.

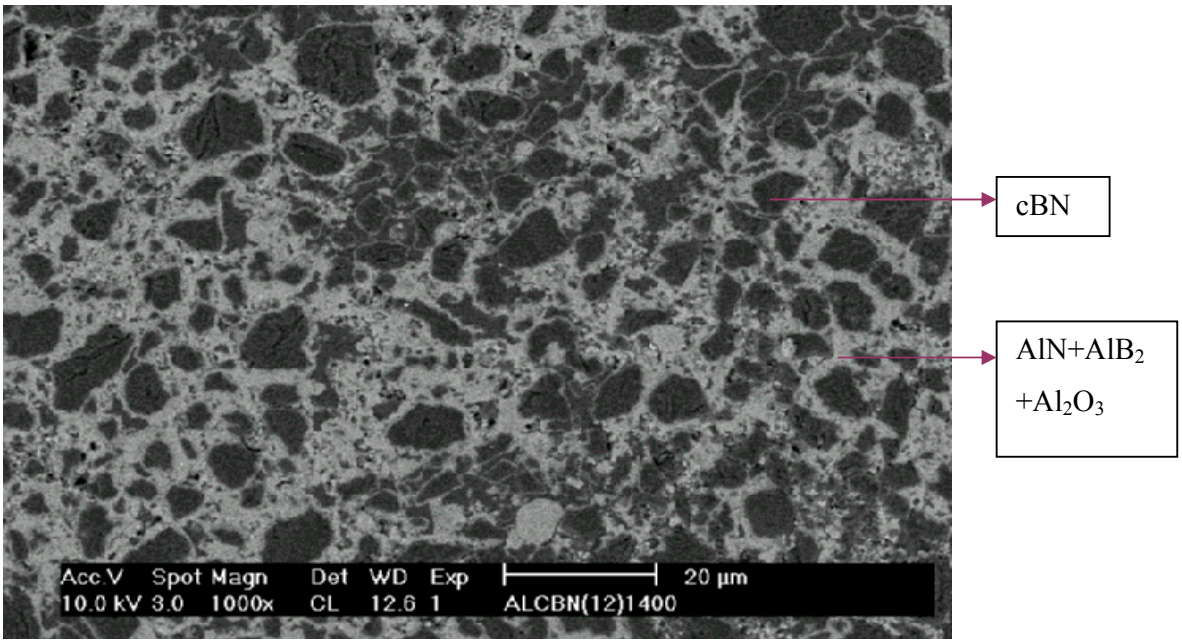

Figure 6.15: SEM micrograph of the cBN12-42HT14-1HT700-3 sample

6.3.2 Vickers hardness of the sample

The Vickers hardness Hv(10) was measured on the cBN12-42HT13-1 sample and was found to be 12.0 ± 2.0 GPa and Hv(30) was found to be 10.8 ± 1.1 GPa. The hardness of the cBN12-42HT13-1 sample was found to be better than that obtained for the 40cBN12-36HT13-1 sample which was heat treated at the same time and temperature but contained hBN in the starting material.

The Vickers hardness of the cBN12-42HT14-1HT700-3 sample was measured to be Hv(10) = 14.8 ± 1.2 GPa and Hv(30) was 14.4 ± 1.6 GPa. The increase of about 13% in the hardness compared with the cBN12-42HT13-1 sample can be attributed to the formation of AlB_2. There may be some aluminium that could not be detected by XRD; this free aluminium should have reacted with boron to form aluminium diboride. The presence of Al metal is expected to have a negative effect on the hardness of the material.

To improve the hardness of the resulting material, fine cBN powder with an average particle size of 3 µm was used, instead of 12 µm.

6.4 Infiltration of the 3 µm cBN particles

Several experiments were conducted in the quest to infiltrate fine cBN (average grain size 3 µm) particles. A small amount of Al powder (maximum of 10 vol. %) was mixed with the cBN powder to assist in the formation of the green pellets. The pellets formed from the mixed powders crumbled when handled, and hence their green densities could not be measured.

For infiltration of the fine cBN particles, Al discs were placed inside the graphite pot and the cBN powder was added on top of the Al discs. Pressure of 5 MPa was applied and kept constant during ramping up. This was done to keep the loose powder together and to increase the capillary forces responsible for infiltration. The amount of Al to be added was estimated on the basis of the experiments previously done with the 12 µm cBN powder. The infiltration of fine cBN particles proved to be difficult and an infiltration depth of only about 0.6 mm was obtained. The Vickers hardness measured from a thin sample obtained from the infiltration was Hv(30) = 22.0 ± 0.6 GPa. This encouraging hardness led to more experiments being done to increase the height of infiltration. An increase of the applied pressure up to 50 MPa, however, did not improve infiltration of the preform prepared from the fine grained cBN-powder.

The infiltration of the preforms prepared from the 12 µm cBN powder was successfully achieved under the same conditions as those used for the infiltration of hBN (see section 6.1). The results obtained were independent of whether the preform was prepared with the partially hexagonalized cBN powder or with pure cBN with a maximum of 10 vol.% Al binder. Figure 6.16 below shows the pore size distribution for the 12µm and 3µM cBN powders. The pressure required to infiltrate a porous preform is given by the Washburn equation, see Section 2.8.1, equation 2.3. From that equation, and using the data in Figure 6.16 it can be calculated that the pressure required to infiltrate 90% of the pores of the 12µm cBN preforms was 4.22MPa. The wetting angle for molten aluminium was obtained from Figure 2.9. From a similar calculation it can be found that the pressure required to infiltrate 90% of the pores of the 3µm cBN preforms was 23.3MPa. However, the pressure we applied in practice ranged up to 50MPa. Although that pressure was well in excess of the pressures required according to Wasburn's equation, it has not been possible to completely infiltrate the 3µm preforms. Preforms of up to 3mm thickness of the 12µm cBN were infiltrated. On the other hand, it has only been possible to infiltrate 3µm cBN preforms up to a maximum thickness of 1mm.

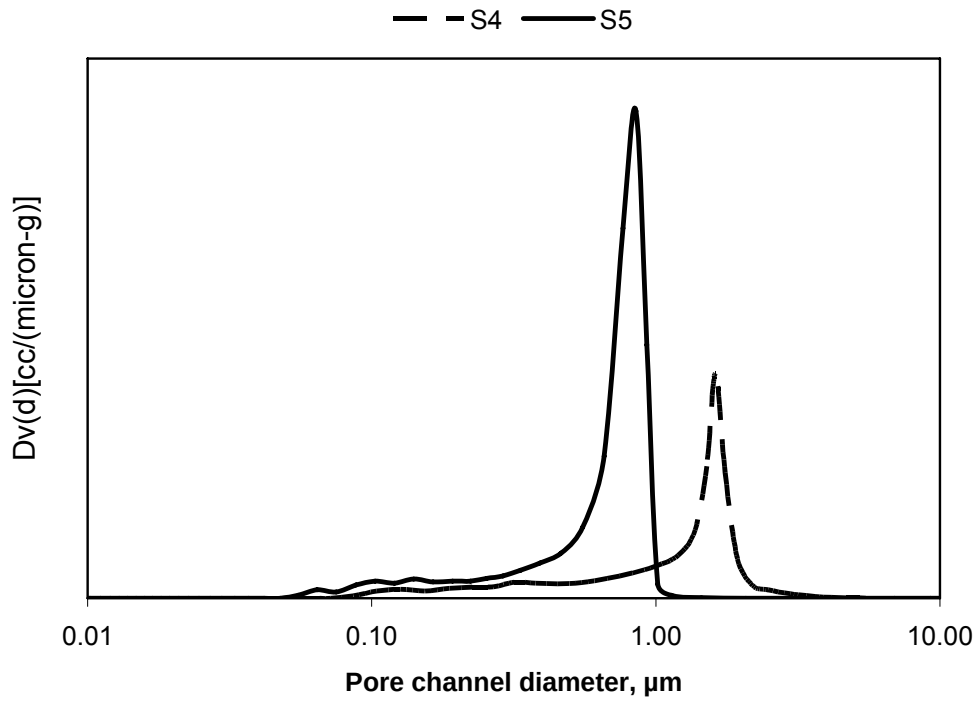

Figure 6.16: Spore diameter distribution in green samples made of 3 µm (S5) and 12 µm cBN (S4).

6.5 Discussion of the infiltration experiments

The infiltration of an hBN matrix with molten aluminium was successful. This was done at a temperature of 800 ^{o}C and a pressure of 12 MPa. The SEM microstructure of the sample shows that the Al phase is homogeneously distributed in the hBN matrix. The optimum temperature for the reaction between Al and hBN was found to be 1 300 ^{o}C after 1 h. The amount of the AlN phase increases with increasing temperature; however, very little increase was observed above 1 300 ^{o}C. This must be due to the depletion of the free aluminium present above 1 300 ^{o}C. All the composite materials prepared were found to be more than 97% dense.

The infiltration of the partially hexagonalized cBN matrix with molten aluminium was equally successful under the same conditions used for the hBN matrix. The sample that initially contained 40 vol. % hBN and 60 vol. % cBN was found to exhibit a density of 98% of the theoretical density. During heat treatment at temperatures between 1 000 ^{o}C and 1 300 ^{o}C, the amount of the hBN phase decreases due to its reaction with aluminium. However, at a

temperature of 1 400 °C the volume of the hBN phase increases again, probably due to the further hexagonalization of cBN.

It was possible to infiltrate cBN with an average particle size of 12 μm, containing no hBN, completely with Al. The Al reacted with the cBN and no hBN was observed at temperatures below 1 400 °C. However, sample cBN12-42HT155-1 showed that at higher temperatures, hexagonalization of the cBN particles did take place. Figure 6.17 shows the Vickers hardness measured for three different samples prepared with 12 μm cBN powder and for one sample prepared with 3 μm cBN powder.

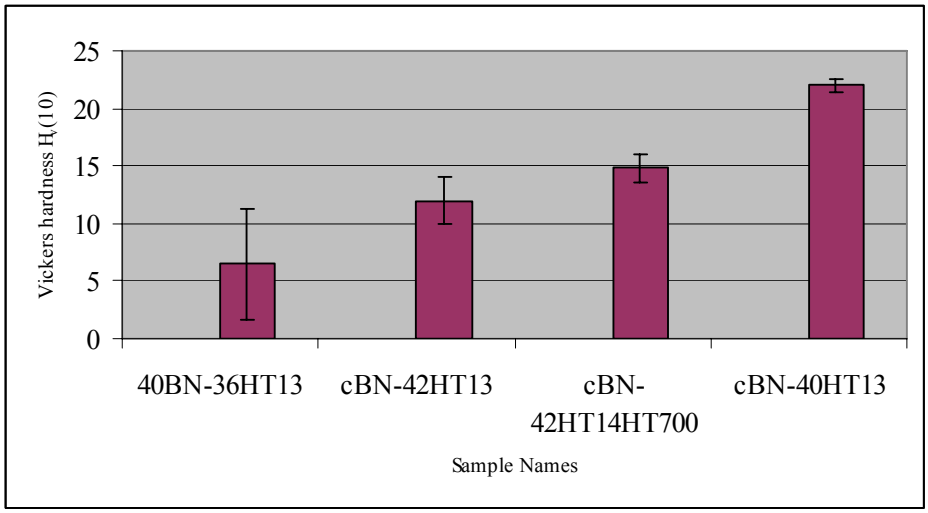

Figure 6.17: Vickers hardness measured on the Al-infiltrated cBN samples
Sample cBN-40HT13 contains 3 μm of cBN instead of 12 μm.

The Vickers hardness measured on the 40BN-36HT13 sample was found to be low. The possible reason is that the final material (after heat treatment) contained an undesirable amount of the hBN phase. This phase was created before infiltration so that it could react with Al. It was expected that the Al would react better with hBN than with cBN (it has been observed that Si reacts more easily with graphite than with diamond) (Skeleton Technologies, 2000).

Another sample with a reduced initial hBN phase (10 vol. %) was prepared. However, even in this sample the hBN phase was not substantially reduced during the reaction with Al. The Vickers hardness of this sample could not be measured due to the poor surface finish obtained, even after extensive metallographical polishing. The conclusion reached is that it is not possible

to use up all the hBN phase when it was present prior to the infiltration, i.e. the differences in the reaction rates of cBN and hBN with Al have to be small.

The hardness of the cBN12-42HT13-1 sample (12.0 ± 2.0 GPa) that was infiltrated without prior hexagonalization was found to be higher than that obtained for the hexagonalized 40cBN12-36HT13-1 sample (6.5 ± 4.8 GPa). The hardness of the 40cBN12-36HT13-1 sample is not only low, but it also has a very high standard deviation, whereas the standard deviation of the sample with no hBN phase is low.

The Vickers hardness for the cBN12-42HT14-1HT700-3 sample increased compared with both the sample with partial hexagonalization and the cBN12-42HT13-1 sample. However, the Vickers hardness of 14.4 ± 1.6 GPa is far below that for Amborite AMB 90, which is 31 GPa. The micrograph of the sample shown in Figure 6.15 shows a homogeneous microstructure. This means that the problem that leads to poor properties is not the inhomogeneity of the microstructure.

Infiltration of the 3 μm cBN powder proved to be difficult. The low infiltration could be connected with some surface reaction of the BN with Al reducing pore channels; however by XRD such reactions were not observed. On the other side, on the surface of the BN there exists some B_2O_3, which amount for the low grained material is larger than that of the course grained material. Only a thin layer of cBN was infiltrated with Al. However, the Vickers hardness measured on the thin cBN3-40HT13-1 sample was found to be 22.0 ± 0.6 GPa.

The difficulty associated with infiltration led to the exploration of other methods i.e admixing of the powders. The powders were admixed and the hot press was used. The following chapter gives results obtained followed by the discussion.

CHAPTER 7 RESULTS FOR THE HOT-PRESSED SINTERED AND HEAT-TREATED SAMPLES

7.1 Densification by hot pressing of 3 µm cBN

The infiltration of fine cBN was unsuccessful, as discussed in Section 6.4. This was a problem because finer cBN powder would result in better mechanical properties. The failure of the infiltration method led to the use of the hot-press densification method because of Al-cBN mixtures. It was hoped that the Al could be squeezed between the cBN grains before an intensive reaction took place. The apparatus used during hot pressing is described in Section 4.2.4, which also includes the temperature profile used (Figure 4.9). Most of the runs were carried out at a maximum temperature of 800 ^{o}C. The reason for this choice was that Al melts at a temperature below 700 ^{o}C and the formation of AlN starts at a temperatures just above 900 ^{o}C. This information was extracted from the DTA results presented in Figure 7.1 below and from the XRD experiments. The aim was to separate the densification stage from the reaction of cBN and Al to form AlN and possibly AlB_2. In addition, the temperature and heating rate were varied to achieve full densification before reaction.

Sample preparation for the hot press involved the mixing of different volume percentages of Al and cBN using a turbular mixer, which is described in Section 4.2.1. Samples were prepared by mixing 15 to 50 vol. % Al powder with the 3 µm cBN powder. The pellets obtained were hot pressed under 50 MPa in an argon atmosphere. These samples were prepared using different temperature profiles. In the case of higher temperatures a step was made at 800°C before further heating to the required temperature. After the samples had been removed from the hot press, the densities were measured using Archimedes' principle. The densities and phase compositions achieved are given in Table 7.1. The procedure in naming the samples was as follows: cBN3-15-N1HT13-1 means the first sample containing 3µm cBN powder was infiltrated with 15vol.% Al and heat treated at 1 300 ^{o}C for 1 hour

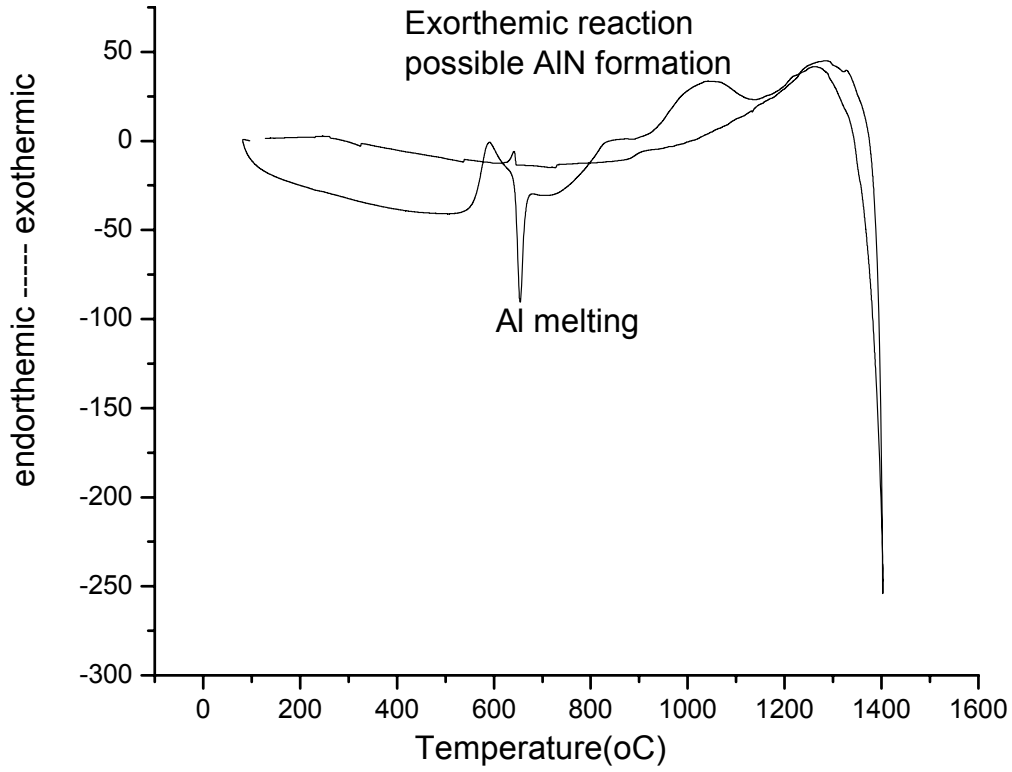

Figure 7.1: DTA measurement for a sample consisting of 40 vol. % of Al and 60 vol. % of cBN

The measurement was done in an argon atmosphere.

Table 7.1: Samples prepared using the hot press under an Ar atmosphere

(Isothermal hot pressing time was 30 min and heating rate was 10 ^{o}C/min)

Sample name	**ρ_g (g/cm^3)**	**Hot pressing condition T_{max}, P_{max}**	**ρ (g/cm^3) after HP**	**Porosity (%)**	**Phases**
cBN3-15-N1	1.79	800 ^{o}C, 50 MPa	2.02	40	Al, cBN
cBN3-20-N1	1.91	1 400 ^{o}C, 50 MPa	2.14	35	AlN, cBN, AlB_{12}
cBN3-30-N1	2.00	800 ^{o}C, 50 MPa	2.35	29	Al, cBN
cBN3-30-N2	2.08	1 100 ^{o}C, 50 MPa	2.43	25	AlN, cBN, Al, AlB_x
cBN3-30-N3	2.03	1 400 ^{o}C, 50 MPa	2.12	34	AlN, cBN, AlB_{12}
cBN3-40-N1	2.09	800 ^{o}C, 50 MPa	2.41	24	Al, cBN
cBN3-40-N2	1.88	1 600 ^{o}C, 50 MPa	1.91	40	AlN, cBN, hBN, AlB_{12}

The measured densities showed that the densification by hot pressing under flowing argon gas was not satisfactory. The experiments revealed that hot pressing at higher temperatures led to less densification. The likely reason is that the liquid Al that was forming reacted with BN to form AlN, which retarded the densification process due to consumption of the liquid Al and by forming strong contacts between the BN particles. In chapter 5 of this thesis it has been shown that above 20vol.% AlN is formed at a temperature of 1100°C. In addition to AlN, there is a total amount of 20vol% borides forming at this temperature. As temperature increases, the reaction products increases which make densification more difficult.

In an attempt to improve the density, hot pressing was done in vacuum instead of argon and in all the samples the temperature was kept at 800 ^{o}C for 30 min.

Another method, known as “sinter forging”, was also employed to improve the density of the cermet. The principle of the sinter-forging process, as applied in the context of this work is shown schematically below in Figure 7.2.
The sample, in the form of a pellet is placed inside a die with an internal diameter significantly bigger than the diameter of the sample. The sample is heated inside the die to a temperature high enough to allow for plastic deformation and flow of the aluminium particles in the pellet, should they be subjected to a moderate deviatoric stress. A force is applied on the piston that closes the open end of the die, causing the pellet to deform and expand until its periphery meets the inner walls of the die. This deformation causes the structure of the pellet to undergo a large amount of shear, enough to destroy the cBN skeleton that has formed.

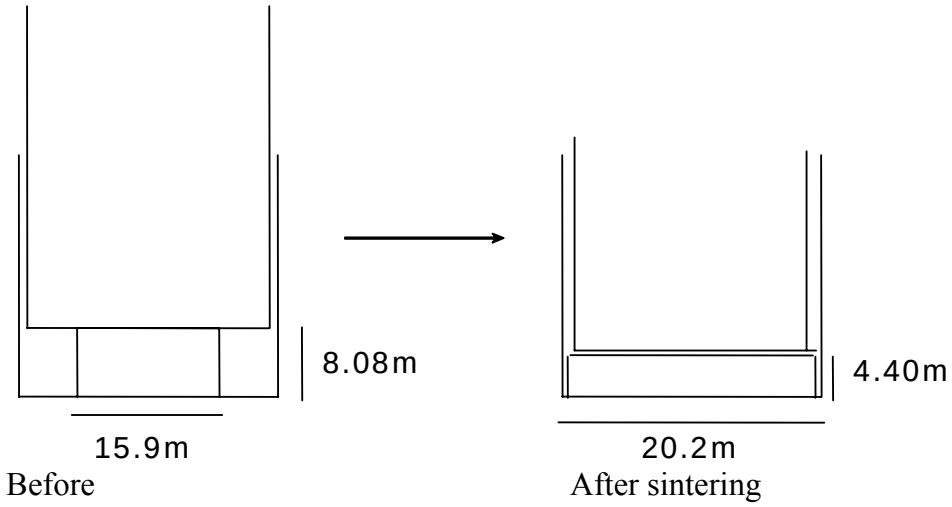

1

Figure 7.2: Schematic diagram showing how sinter forging of the cBN/Al composite pellets was done

The information concerning the prepared samples and some measured results are shown in Table 7.2. The phases obtained after hot pressing under vacuum at 800 ^{o}C were cBN and Al. The following observations were made based on the results in table 7.2:

- Changing from argon atmosphere to vacuum improves the density of the sintered cermet.
- Prepressed samples have better densities than those of the samples hot pressed in powder form (compare cBN3-30-N5 and cBN3-30-N8)
- Increasing the Al content improves the density of the cermet.
- Sinter forging did not improve densification.

Table 7.2: Samples prepared using the hot press at 800 ^{o}C for 30 min under 50 MPa

Sample name	Green density (g/cm^3)	Density (g/cm^3) after treatment at 800 ^{o}C	Porosity (%)	Open porosity (%)
cBN3-20-N2	2.41	2.64	20	-
cBN3-30-N4	2.36	2.70	17	-
cBN3-30-N5	2.35	2.72	16	11.5
[1]cBN3-30-N6	2.10	2.68	18	-
[1]cBN3-30-N7	2.42	2.70	17	7.8
cBN3-30-N8	-	2.61	19	11.9
cBN3-40-N3	-	2.75	13	-
cBN3-50-N1	-	2.80	9	2.3

1) Sinter forged at 800 ^{o}C.

Samples with up to 50 vol. % of Al were prepared. The density of the cBN3-50-N1 sample hot pressed at 800 ^{o}C was 91.0% of theoretical density. This value is higher than that obtained for the samples with only 30 vol. % of Al, but the material still remains quite porous.

The heat treatments to allow the reaction of samples were carried out at temperatures of 1 300 ^{o}C, 1 400 ^{o}C and 1 600 ^{o}C for 60 min. The temperature of 1 300 ^{o}C was used because it is regarded as the optimum temperature for the reaction of Al and cBN. Details of the heat treated samples are shown in Table 7.3. The phases obtained after heat treatment were: cBN, AlN, AlB_2 and AlB_{12}. In some cases small amounts of Al_2O_3 were detected. The other two temperatures (1400 and 1600 ^{o}C) were used to check the hexagonalization of the cBN phase to the hBN phase. The densities of the heat-treated samples were similar to those obtained after hot pressing. The exception is the density of sample cBN3-50-N1HT16-1 unlike the other samples, this sample contained some hBN phase.

Table 7.3: Samples heat treated at different temperatures in N_2 gas

Sample name	Temp-erature (^oC)	Density after heat treatment (g/cm^3)	Porosity (%)	Open porosity (%)	Phase content
cBN3-30-N4HT13-1	1300	2.72	16	10.8	cBN, AlB_{12}, AlN
[1]cBN3-30-N6HT13-1	1300	2.69	17	13.5	cBN, AlB_{12}, AlN
cBN3-50-N1HT13-1	1300	2.82	8	2.2	cBN, AlB_{12}, AlN, Al
cBN3-50-N1HT14-1	1400	2.80	8	2.4	cBN, AlB_{12}, AlN
cBN3-50-N1HT16-1	1600	2.57	17	-	cBN, AlB_{12}, AlN, hBN

7.1.1 Phase composition and microstructure of the reacted samples

The XRD results of the cBN3-50-N1HT13-1 and cBN3-50-N1HT14-1 samples are presented in Figure 7.3. In addition to the expected phases of cBN and AlN present at 1 300 ^oC, Al peaks were detected, which implies that the reaction of Al with BN was incomplete. These Al peaks disappeared at 1 400 ^oC, but AlB_{12} peaks were detected at 1 300 ^oC and 1 400 ^oC. This is in agreement with the phase diagram. There is no hBN phase present after heat treatment at either 1 300 ^oC or 1 400 ^oC.

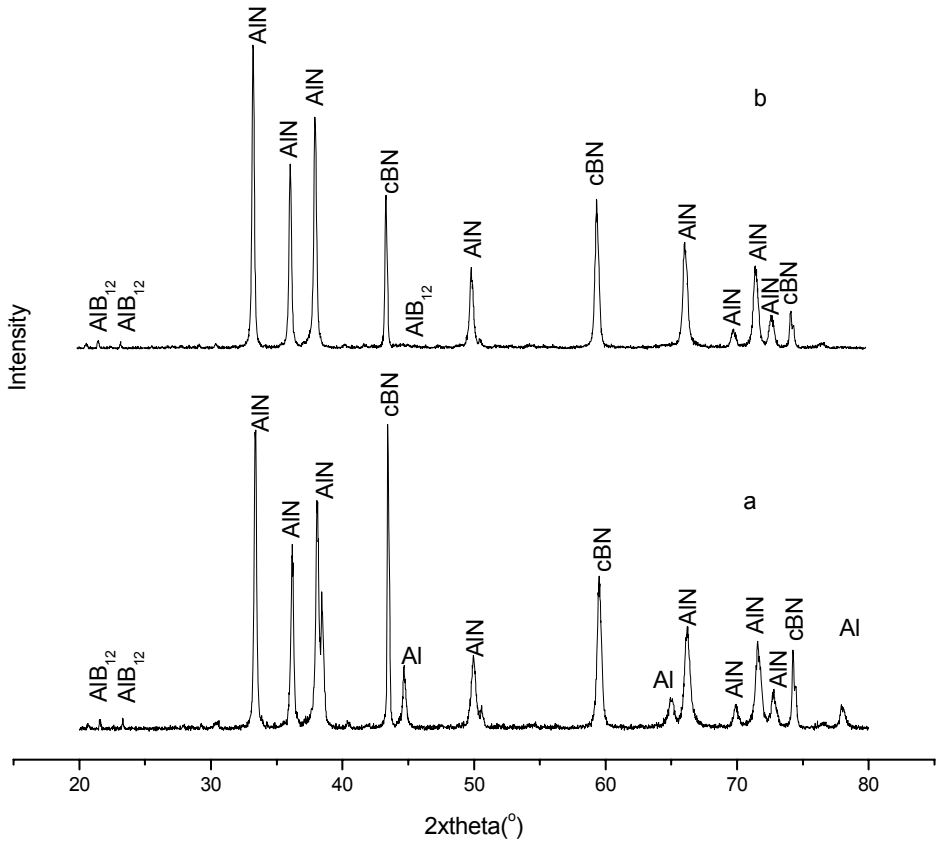

Figure 7.3: XRD results for cBN3-50-N1HT13-1 and cBN3-50-N1HT14-1 samples.

The SEM images of the polished surface of the cBN3-50-N1HT13-1 sample are shown in Figure 7.4. The micrographs reveal two major phases: the dark cBN phase and a light AlN phase present in the boundary. The light phase is composed mainly of AlN. The grey phase found in the boundary between AlN and cBN (higher magnification images) is the boride phase, which was identified as AlB_{12} by XRD. At low magnification, the image shows that the cBN phase is homogeneously distributed in an AlN matrix. It is clear that the AlN phase dominates the cBN phase.

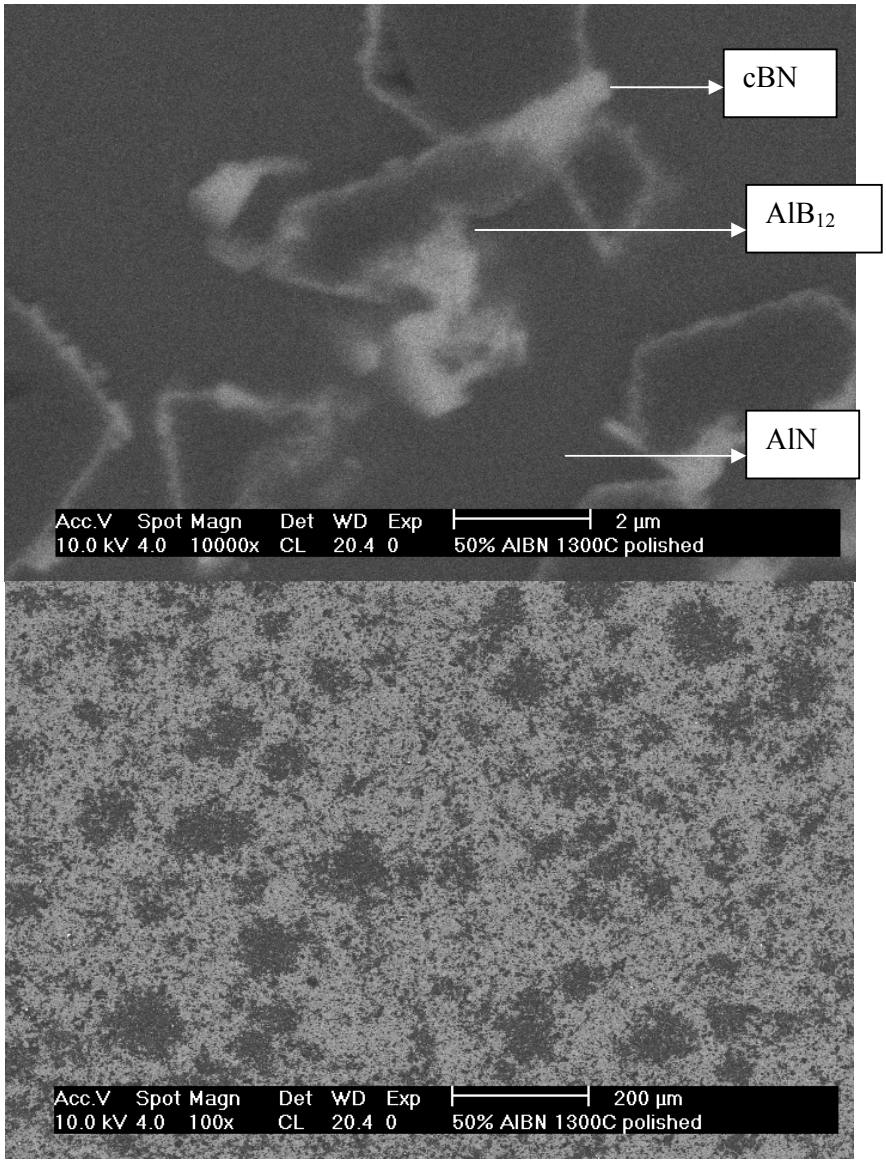

Figure 7.4: SEM micrographs at high and low magnification for the cBN3-50-N1HT13-1 sample. The additional phases indicated were proved by EDX analysis.

7.1.2 Vickers hardness of the sample

The cBN3-50-N1HT13-1 sample was metallographically polished to prepare it for the SEM analysis described above in Section 4.5.3 and to enable the Vickers hardness measurement to be done. The Vickers hardness Hv(10) measured was found to be 19.0 ± 1.2 GPa and Hv(30) was 17.5 GPa. The hardness had therefore increased compared with the hardness measured when 12 µm cBN was infiltrated.

7.2 Densification of multimodal samples by hot pressing

To improve the density of the hot-pressed samples while using minimum Al content, the green density of the cBN powder mixture was optimized. Different grades of cBN crushed powders were mixed together to obtain a reasonable green density. The green density of about 70% meant that a maximum of 30 vol. % Al was required to fill the pores and thus a dense hot-pressed sample could be obtained. The particle size distributions of the cBN powders used are given in Figure 4.4 in Section 4.1. Grade 2 showed a bimodal particle size distribution, while the other grades had a narrow distribution. The volume mean diameters obtained for grades 1, 2, 4 and 9 were 0.52, 0.70, 6.52 and 11.40 μm respectively.

The packing density was modelled using the program based on close-packed balls. This program calculates the packing density of a mixture of powders where each has its own size distribution (see appendix D). In this work, four different grades were used with the size distribution shown in Section 4.1. Table 7.4 shows some of the results obtained from these calculations.

Table 7.4: Calculated possible ratios of the cBN powders to obtain a maximum density

Model	Grade 1	Grade 2	Grade 4	Grade 9	Density (%)
1	0.2	0.36	0.18	0.26	77
2	0.59	0	0.12	0.29	78
3	0.52	0.043	0.29	0.15	78

An attritor mill was used to mix the different grades of cBN powders using the ratios obtained from the packing model program. When mixing, about 1 wt % of polyisobutylene succinimide was added as a dispersant agent and hexane was used as liquid medium. This agent was added to prevent the agglomeration associated with the mixing of fine particles. The green density of the resulting mixture was calculated from the geometry of the sample. The mixed powders were then mixed with aluminium powder. The green densities obtained before and after adding Al are presented in Table 7.5.

Table 7.5: Green densities of cBN/Al mixture (model 1; refer to Table 7.4) as a function of pressure

Pressure (MPa)	Without Al (g/cm^3)	% Density	With Al 30 vol. % (g/cm^3)	% Density
80	2.24	64	2.41	74
110	2.57	74	2.36	73
200	2.69	78	2.48	76

Two methods were employed to densify the samples: firstly, hot pressing as described in Section 4.4.2 which was used in the previous experiments; and secondly, the method known as sinter forging was employed (this is described in section 7.1 and illustration in figure 7.2). After densification, heat treatment was carried out to convert Al to the harder phases of AlN, AlB_2 and/or AlB_{12}. The results of the sintered densities, together with initial green densities, are presented in Table 7.6. In other cases mixed powders were hot pressed in powder form and hence the green densities were not evaluated. The densities obtained using sinter forging are also included in Table 7.6. The procedure in naming the samples was as follows: McBN15-N1HT13-1 means the first sample containing multimodal cBN powder was infiltrated with 15vol.% Al and heat treated at 1 300 ^oC for 1 hour

The hot pressing of the multimodal sample containing 20 vol. % Al (McBN20-N1) was done following the procedure explained in Section 4.2.4 of this thesis. Heat treatment after hot pressing was carried out at 1 300^oC for 60 min. The density of the sample was measured using Archimedes' principle. The porosity calculated for this sample was found to be 20%. This porosity made it difficult to polish the sample. A possible explanation for this was that the amount of Al added was insufficient to fill the pores and hence the porosity remained high.

The multimodal sample containing 30 vol. % Al (McBN30-N1) was then hot pressed using a similar method and, in addition, sinter forging was used. The porosity measured for this sample was 17%. This was not expected since the green density of the sample used was more than 70% of theoretical and hence a completely dense sample was expected.

Table 7.6: Samples prepared using multimodal powder mixtures (based on model 1) with their properties

Sample name	Al content	Hot pressing conditions	Green density (g/cm^3)	Density after hot pressing (g/cm^3)	Porosity (%)	Open porosity (%)	Phase content
McBN20-N1	20	800 ^oC, 50 MPa, 10 ^oC/min	2.41	2.64	20	-	Al, cBN
McBN30-N1	30	800 ^oC, 50 MPa, 10 ^oC/min	2.36	2.71	17	11.5	Al, cBN
[1]McBN30-N2	30	800 ^oC, 50 MPa, 10 ^oC/min	2.35	2.72	16	7.8	Al, cBN
McBN30-N3	30	800 ^oC, 50 MPa, 10 ^oC/min	-	2.63	19	11.9	Al, cBN
McBN40-N1	40	800 ^oC, 50 MPa, 10 ^oC/min	-	2.75	13	3.4	Al, cBN
McBN50-N1	50	800 ^oC, 50 MPa, 10 ^oC/min	-	2.82	9	2.3	Al, cBN

1) Sample prepared by sinter forging method.

Sample McBN30-N2 showed a porosity of 16%. This porosity indicated that sinter forging had not improved the density of the cermet. During sinter forging, a significant amount of shear stress is generated which could be capable of destroying a cBN skeleton. An increase in Al of up to 50 vol. % increased the density to only 91% of the theoretical density (sample McBN50-N1 in Table 7.6). The results showed that the samples which were cold pressed before hot pressing had better densities (compare McBN30-N1 and McBN30-N3).

The XRD results (see Figure 7.5) of the McBN30-N1 sample hot pressed at 800 ^oC showed only the Al and cBN peaks, whereas the samples hot pressed at higher temperature showed the formation of AlN and AlB_2. There are additional peaks in the sample heat treated at 1 300 ^oC and 1 350 ^oC, which were identified as aluminium dodecaboride phase (AlB_{12}). No Al peaks were identified at higher temperatures when a 30 vol. % Al content was used.

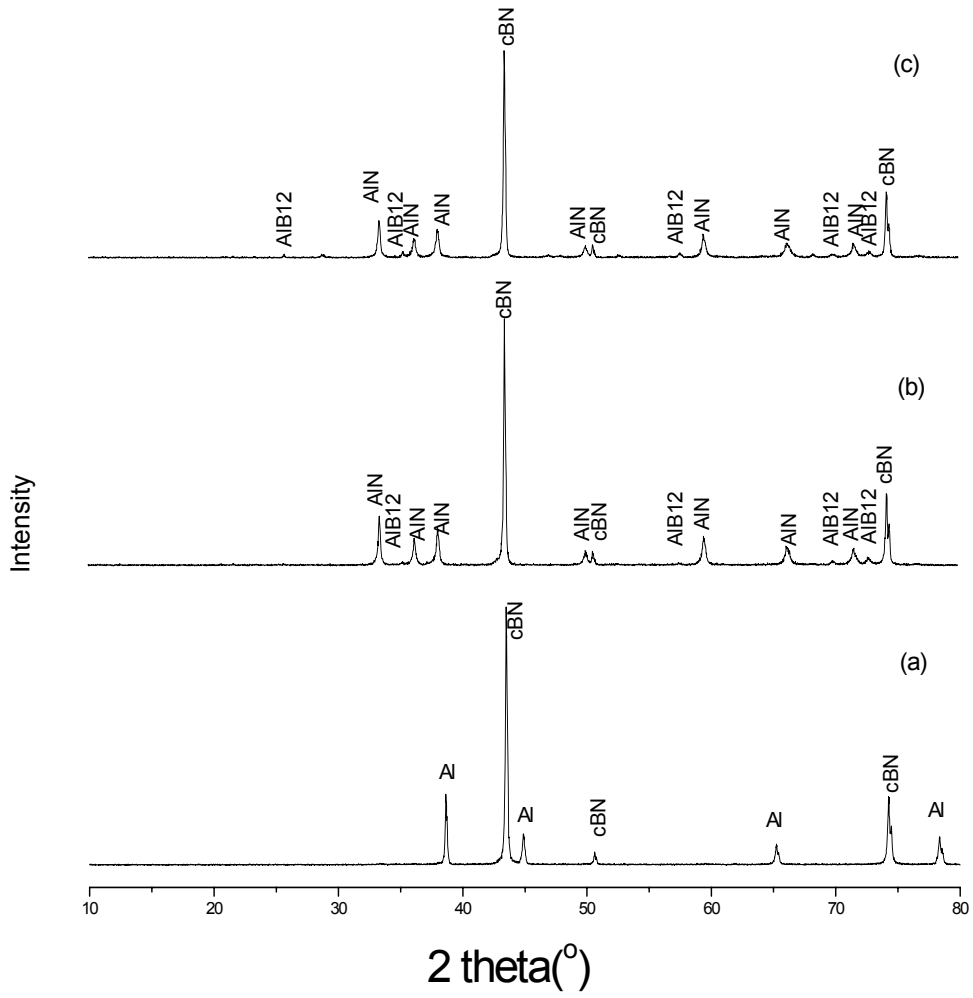

Figure 7.5: XRD results of the McBN30-N1 sample after heat treatment at (a) 800 °C, (b) 1 300 °C and (c) 1 350 °C in an Ar atmosphere

An SEM analysis was done on the McBN30-N1 sample. Figure 7.6 shows the SEM micrographs of the sample after heat treatment at 1 300 °C under flowing argon. This image shows minimum porosity which does not correspond to the 17% calculated from Archimedes' principle. It shows that the sample is almost completely dense and homogeneous, with only a very few large pores visible. This means that 30 vol. % Al could be enough to densify the material as expected. Figure 7.7 shows another image from the same sample. In this image agglomerates of finer cBN grains can be observed. The agglomerates that were not infiltrated could be a source of the high porosity observed. This meant that the process of mixing the powders required some improvement to avoid agglomerates. It was therefore important to improve the mixing technique

in order to achieve a uniform distribution of phases throughout the cBN composite matrix. The mechanical properties could not be measured since the sample could not be properly polished.

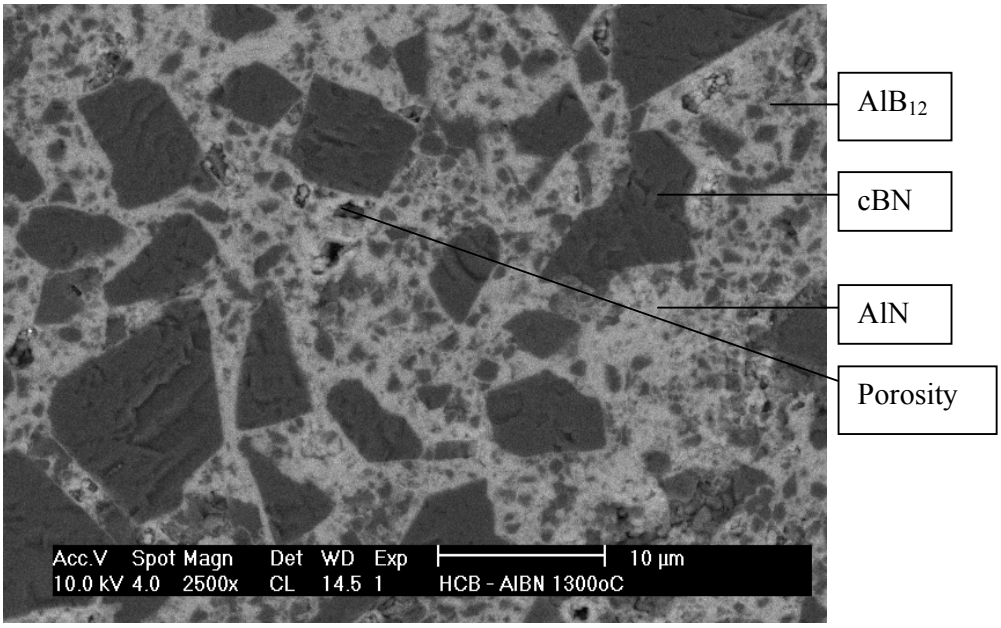

Figure 7.6: SEM micrograph of the McBN30-N1HT13-1 sample.

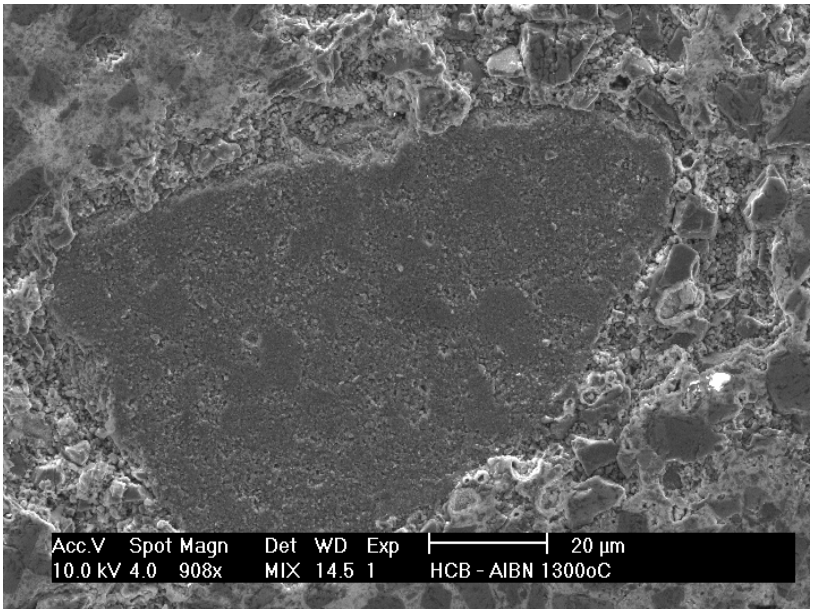

Figure 7.7: SEM micrograph of the McBN30-N1HT13-1 sample

7.3 Optimization of the hot pressing of multimodal cBN

Numerous mixing models were created leading to the number of different powder mixtures mixed in an attempt to improve homogeneity and break agglomerate (such as the one shown in figure 7.7). Optimization of the powder processing seemed to have been achieved using model 2 powder (This multimodal powder contains powders grade 1, grade 4 and grade 9, refer to Table 7.4). The procedure employed when mixing powders is described below, and it did succeed in eliminating agglomerates and in giving good homogeneity, as determined by SEM examination of the powder mixes prepared, as shown in figure 7.9 below. The procedure used was as follows:

Grade 1 (screened with 38 micron sieve, see Figure 7.8) powder was added to the beaker with 25 ml hexane and 1.56 ml of Lubrizol with a concentration of 0.2 g/ml as a dispersant. This was placed in the ultrasonic bath and was stirred vigorously using a spatula.

⇩

After 10 min, the particle size distribution was measured. The solution was then put inside the steel beaker containing an impellor disc and was stirred for further 20 min. The particle size distribution was measured again and the result is shown in Figure 7.8.

⇩

Aluminum was added with 15 ml of hexane and stirring was continued for a further 15 min.

⇩

Grade 4 crushed cBN powder was added, followed after 5 min by the addition of **grade 9** powder with 10 ml of hexane. This was left to mix for 60 min.

The mixture was dried in a rotary evaporator (see section 4.2.2).

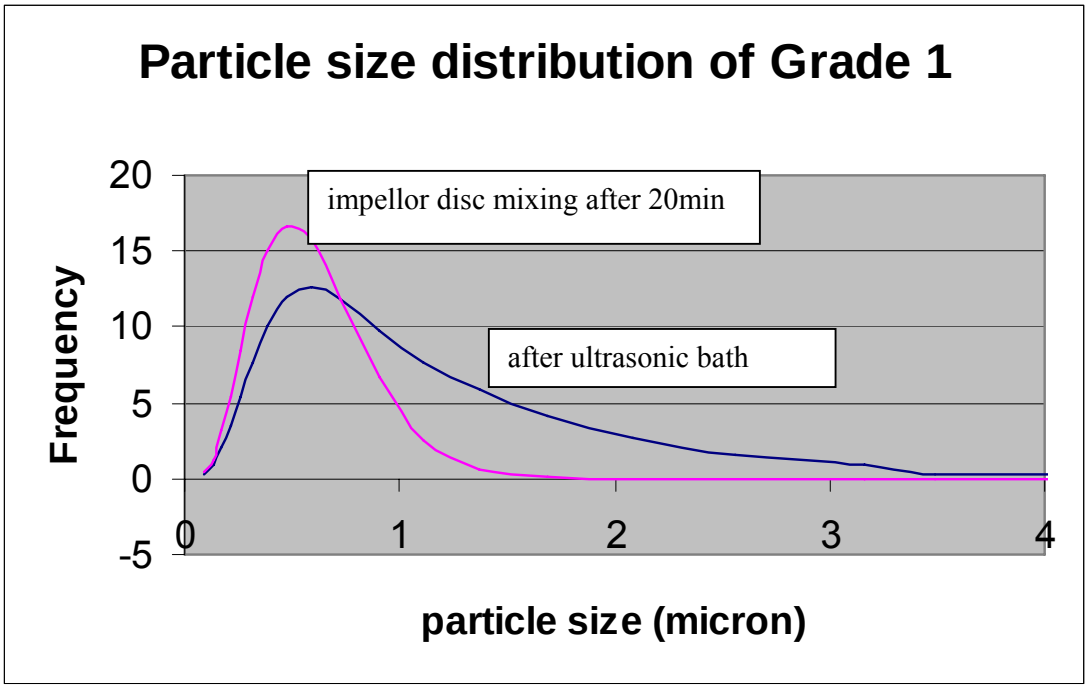

Figure 7.8: Particle size distribution of the grade 1 crushed cBN powder

The powder was then taken to the hot press for densification using the conditions described in Section 4.2.4. The sample was then heat treated at 1 300 ^{o}C for 1 h under nitrogen gas. SEM analysis was used to examine the polished sample. The images in Figure 7.9 show that the large, fine cBN agglomerates are no longer present in the sample. This confirmed that the mixing procedure had been optimized. The images also show minimum porosity. However, the sample still contained a porosity of 17% with an open porosity of 12%.

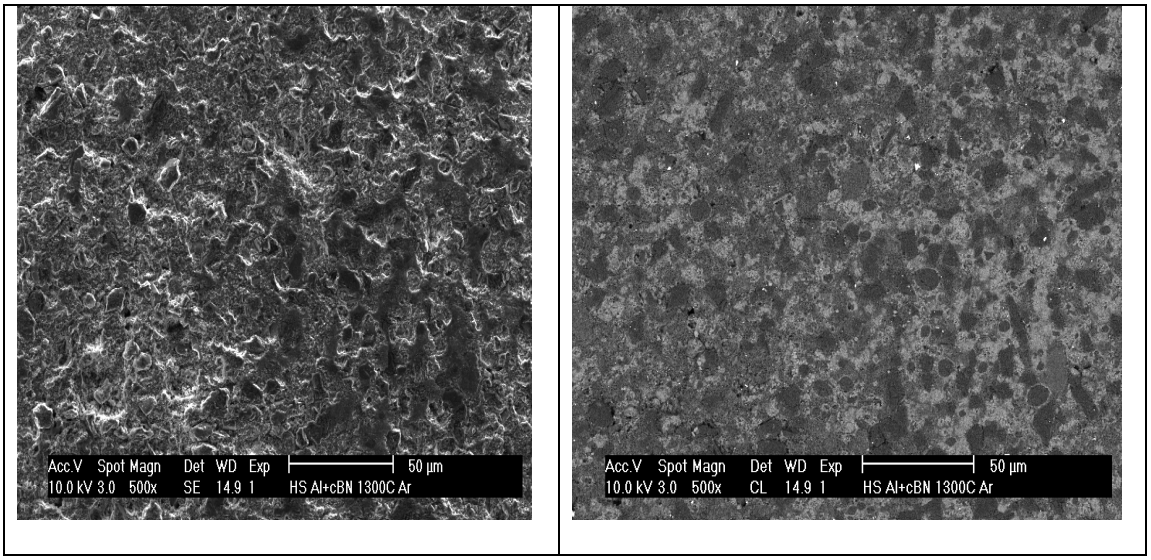

Figure 7.9: Secondary electron and backscatter images of the McBN30-N5 sample

Table 7.7: Samples prepared using multimodal powder mixtures (based on model 2) with their properties

Sample name	Al content Vol.(%)	Hot pressing conditions	Green density (g/cm^3)	Density after hot pressing (g/cm^3)	Porosity (%)	Open porosity (%)	Phase content
McBN30-N4	30	800 °C, 50 MPa, 10 °C/min	2.48	2.77	14	6	Al, cBN
McBN30-N5	30	800 °C, 50 MPa, 10 °C/min	-	2.71	17	12	Al, cBN
McBN30-N6	30	1 000 °C, 50 MPa, 10 °C/min	-	2.53	-	23	Al, cBN, AlN, AlB_2
McBN30-N7	30	1 100 °C, 50 MPa, 1 °C/min	-	2.37	-	22.5	Al, cBN, AlN, AlB_2
McBN30-N8	30	1 100 °C, 50 MPa, 50 °C/min	-	2.53	-	19.1	Al, cBN, AlN, AlB_2
McBN30-N9	30	1 000 °C, 50 MPa, 10 °C/min	-	2.37	-	-	Al, cBN, AlN, AlB_2
[2]McBN30-N10	30	800 °C, 50 MPa, 10 °C/min[2]	-	2.60	19	11.4	Al, cBN
[3]McBN30-N11	30	1 300 °C, 50 MPa, 10° C/min	-	2.59	20	10	cBN, AlN, AlB_{12}
McBN30-N12	30	1 750 °C,10 MPa, 10 °C/min	-	-	-	-	hBN, cBN, AlN, AlB_{12}
McBN50-N2	50	800 °C, 50 MPa, 10 °C/min	-	2.82	8	2.5	Al, cBN

2) coated with 5% Al compound, 3)hot pressed at 800°C for 30 min and heat treated at 1300°C for 60 min under pressure .

The mixing of the powders had been optimized, but the challenge of densifying the material remained. All the samples hot pressed using the optimized powder mixture are presented in Table 7.7. Sample McBN30-N6 was hot pressed at a temperature of 1 000 ^{o}C because higher temperatures should improve the wetting (Xue et al,1992). However, the sample was found to be porous with a density of 2.53 g/cm^3. Samples McBN30-N7 and McBN30-N8 were then hot pressed at 1 100 ^{o}C but different heating rates were used to achieve different ratios of densification and different reaction rates. The density of these samples is independent of the heating rate. Both samples were porous, but in both samples Al and cBN reacted.

In the quest to improve the densification of the material, the cBN particles were coated (using CVD methods) with Al which formed Al compounds at high temperatures, i.e. AlN and AlB_2 (samples McBN30-N9 and McBN30-N10). The optimum coating condition gave about 8% coating (coating procedure described in section 4.3.3). The Al compounds were supposed to protect the cBN particles and possibly improve the wetting. The results of the McBN30-N10 sample, however, showed an improvement of only 1% (from 12% to 11%) in open porosity.

Sample McBN30-N11 was prepared by hot pressing at 800 ^{o}C for 30 min. The temperature was increased to 1 300 ^{o}C under a constant pressure of 50 MPa. The open porosity measured in this sample was 10%. Another sample, McBN30-N12, was prepared differently. The powder was kept under a constant pressure of 10 MPa and the temperature was increased from 25 ^{o}C to 1 750 ^{o}C using a heating rate of 50 ^{o}C/min. The procedure followed in conducting this experiment was taken from the work done by Benko *et al* (1997) where they successfully hot press BN with Al as a metallic binder. In both cases the samples reacted with the graphite pot and could not be removed from the pot, and hence the density was not measured. Figure 7.10 shows photographs of the samples McBN30-N4, McBN30-N11 and McBN30-N12.

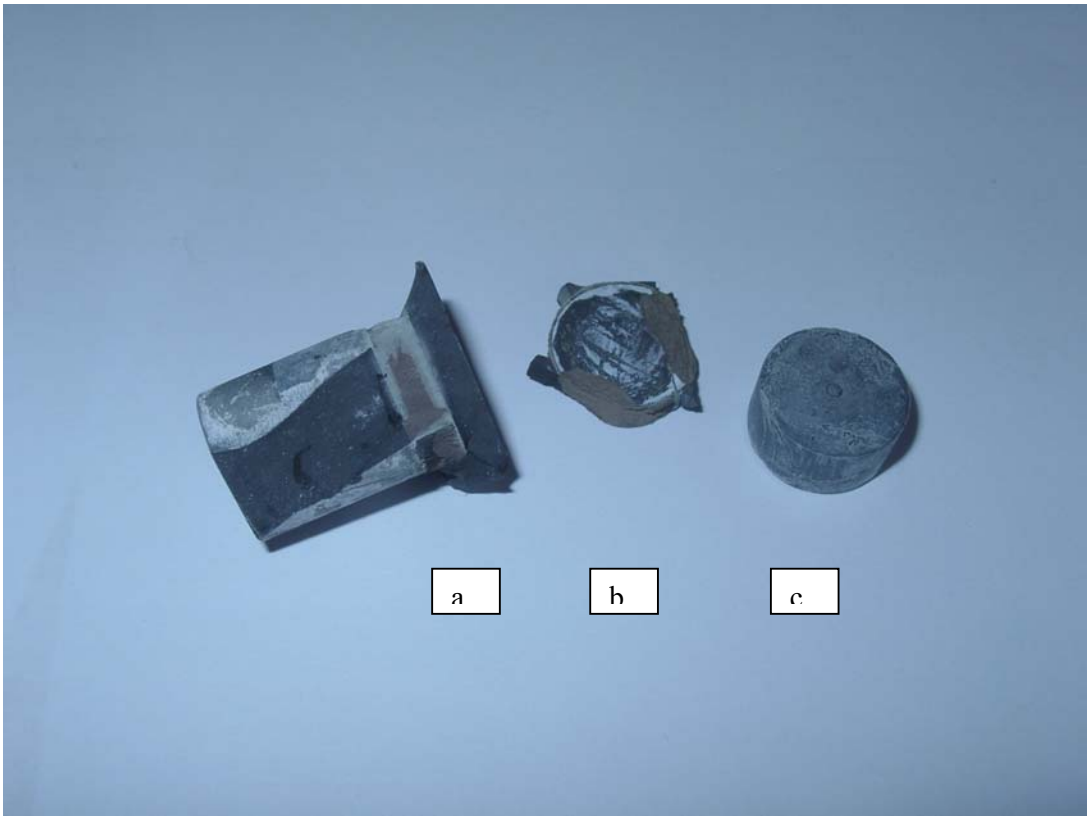

Figure 7.10: Photographs of samples (a) McBN30-N12, (b) McBN30-N11 and (c) McBN30-N4

Sample (c) of image 7.10 shows the dense McBN30-N4 sample. Sample McBN30-N11 7.10(b) and McBN30-N12 7.10(a) show different colours which are an indication of the porosity of the sample. This further supports the view discussed in the previous section that the densification process should be separated from the reaction process.

Sample McBN50-N2 with 50 vol. % Al showed only a slight increase in density. Hot pressing of the sample reduced the overall porosity to 8%, with an open porosity of 2.5%.

7.3.1 Phase composition of the hot-pressed and heat-treated samples

The XRD measurements revealed for all the samples hot pressed at 800 °C only the existence of Al and cBN. By contrast, the samples hot pressed at higher temperatures showed, besides cBN, the formation of AlN and AlB_2. Figure 7.11 shows the phases detected by XRD.

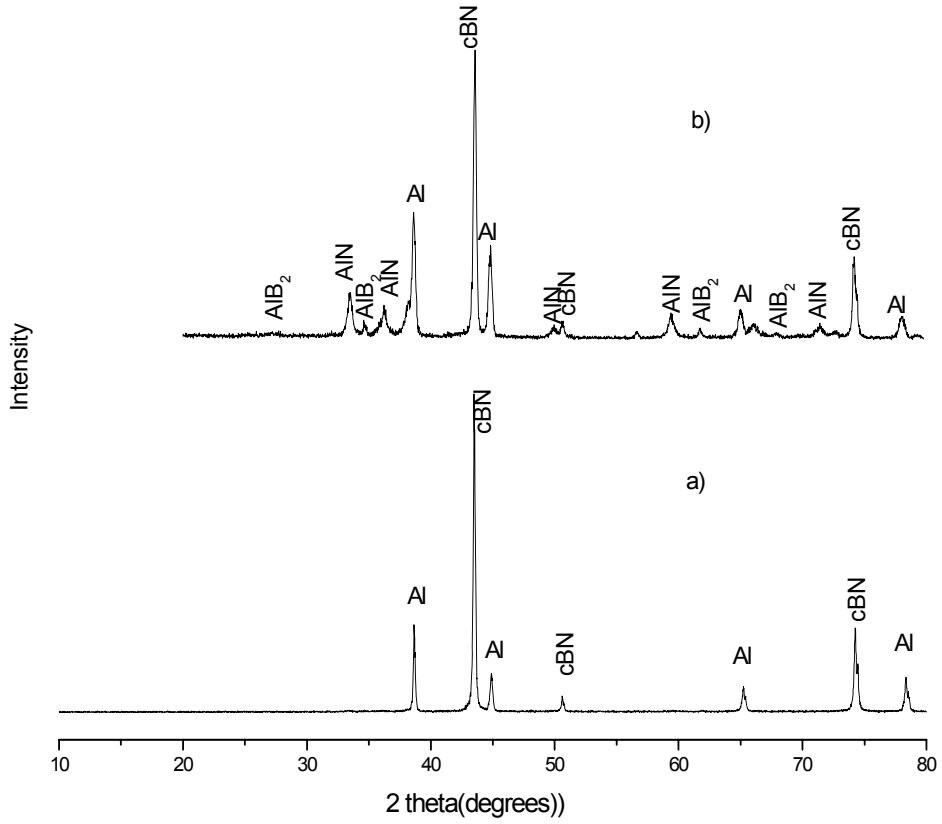

Figure 7.11: XRD results of the (a) McBN30-N5 and (b) McBN30-N7 samples

XRD phase quantification was performed on the McBN50-N2 sample heated to 1 300 ^{o}C for 1 h and the results are presented in the Table 7.8. The quantification was done using the Rietveld analysis technique (Krawidtz 2001).

Table 7.8: Phase quantification results for McBN50-N2HT13-1 sample

α-Al_2O_3	3.18 ± 0.4 wt %
AlB_{12}	19.9 ± 2.7 wt %
AlN	52.5 ± 2.2 wt %
cBN	24.4 ± 2.2 wt %

7.3.2 Vickers hardness of the sample

The McBN50-N2 sample heat treated at 1 300 ^{o}C for 60 min was metallographically polished to a mirror finish to prepare it for Vickers hardness testing and SEM analysis. The Vickers hardness Hv(30) measured was found to be 17.5 ± 0.8 GPa. (The hardness obtained was again related to the amount of Al added during powder mixing.) The expected hardness was 0.24 x 45 + 0.53 x 11 + 0.20 x 26 + 0.032 x 21 = 22 GPa (estimated using data from Table 7.8) and equation 3.5.

The amount of AlN present in the final material lowered the hardness, which was less than that obtained when using monomodal 3 μm cBN. The possible reason is that in the samples with monomodal cBN, the particle size distribution was smaller, while in the samples with multimodal cBN, larger particles were present which would also affect the hardness of the sample.

7.3.3 Thermal properties

The low hardness obtained for the near dense samples disqualified this material for cutting tool applications. Because of the high thermal conductivity of cBN and AlN, it may be possible to use the composites developed in this work as heat sinks. For that purpose it was important to measure the thermal properties of the best materials made in this work. Thermal diffusivity (see paragraph 4.5.5) was measured for the McBN50-N2HT13-1 sample and the value of 10.5 m^2/s was obtained. The value of 23.1 $W.m^{-1}.K^{-1}$ for the thermal conductivity was calculated using the equation below:

$$\lambda = \alpha \times \rho \times C_p \quad \text{.....(7.1)}$$

$$= 10.5 \times 2.82 \times 10^3 \frac{kg}{m^2} \times 10^{-6} \frac{m^2}{s} \times 46.8 \frac{J}{60 \times 10^{-3} kg.K}$$

$$= 23.1 Wm^{-1}K^{-1}$$

where

- λ = the thermal conductivity
- α = the thermal diffusivity
- ρ = the density
- C_p = the specific heat capacity (aluminium nitride used) under constant pressure.

Heat sinks have been in widespread use since the beginning of the transformer age and their use is growing. Table 7.9 below contains some of the key thermophysical properties of some representative heat sink materials. Included in table 7.9 is the material developed in this work for direct comparison.

Table 7.9 Thermal properties of commonly used heat sink materials

Material	Thermal Conductivity at 293K (W/m.K)	Thermal Expansion Coefficient at 293K (10^{-6}/K)
Polycrystalline Aluminium nitride (AlN) (Shaffer *et al*, 1989)	185	4.6
Polycrystalline beryllium oxide (BeO) (Shaffer *et al*, 1989)	240	7.6
Single crystal natural diamond Type 11a (Spear, 1989)	2000	~0.8
Polycrystalline CVD diamond (Wort *et al*, 1994)	840	1.0
Polycrystalline silicon carbide (α-SiC) (Munro, 1997)	114	1.1
Polycrystalline aluminium oxide (Al_2O_3) (Shaffer *et al*, 1989)	29	7.0
Developed material (McBN50-N2HT13-1)	23.1	-

In our material there is significant amount of AlN (with a thermal conductivity of 185 $W.m^{-1}.K^{-1}$) present which can contribute to the overall thermal conductivity of the material. The fine-grained AlN contains oxygen and some boron. These defects strongly reduce the thermal conductivity of the composite. The presence of aluminium oxide (with thermal conductivity of 29 W/mK) will also have a negative effect in the thermal conductivity of this material. The overall porosity of 9% present in the sample contributed in lowering the thermal conductivity. The developed material has thermal conductivity much lower than that of AlN, which is the most widely used ceramic material in heat sink applications.

7.4 Densification by hot pressing of 12 µm cBN

Hot pressing of the 12 µm cBN with 50 vol. % Al produced an almost dense material with open porosities of less than 3%. Table 7.10 shows the samples hot pressed at 800 ^{o}C for 30 min under a pressure 50 MPa. All the samples were mixed using the tubular mixer with an initial Al concentration of 50 vol. %. The procedure in naming the samples was as follows: cBN12-50-N1HT13-1 means the first sample containing 12µm cBN powder was infiltrated with 50vol.% Al and heat treated at 1 300 ^{o}C for 1 hour

Table 7.10: Samples containing 50 vol. % Al with cBN (12 µm) heat treated at different temperatures and times

Sample name	**Density (g/cm^3)**	**Open porosity (%)**	**Phase content**
cBN12-50-N1HT10-2	2.96	2.2	AlN, Al, cBN, AlB_2
cBN12-50-N2HT11-0.5	2.95	2.0	AlN, Al, cBN, AlB_2
cBN12-50-N2HT11-1	2.95	2.0	AlN, Al, cBN, AlB_2
cBN12-50-N2HT11-2	2.92	2.0	AlN, Al, cBN, AlB_2
cBN12-50-N3HT12-0.5	2.92	2.0	AlN, Al, cBN, AlB_2, AlB_{12}
cBN12-50-N3HT12-1	2.93	2.2	AlN, Al, cBN, AlB_2, AlB_{12}
cBN12-50-N3HT12-2	2.92	2.0	AlN, Al, cBN, AlB_2, AlB_{12}
cBN12-50-N4HT13-0.5	2.96	1.8	AlN, Al, cBN, AlB_2, AlB_{12}
cBN12-50-N4HT13-1	2.95	2.2	AlN, Al, cBN, AlB_2, AlB_{12}
cBN12-50-N4HT13-2	2.95	2.0	AlN, cBN, AlB_2, AlB_{12}
cBN12-50-N5HT14-0.5	2.93	2.4	AlN, cBN, AlB_2, AlB_{12}
cBN12-50-N5HT14-1	2.93	2.2	AlN, cBN, AlB_{12}

The samples in Table 7.10 were metallographically polished on a 1 micron diamond wheel. The Vickers hardnesses measured in all the samples are shown in Figure 7.12.

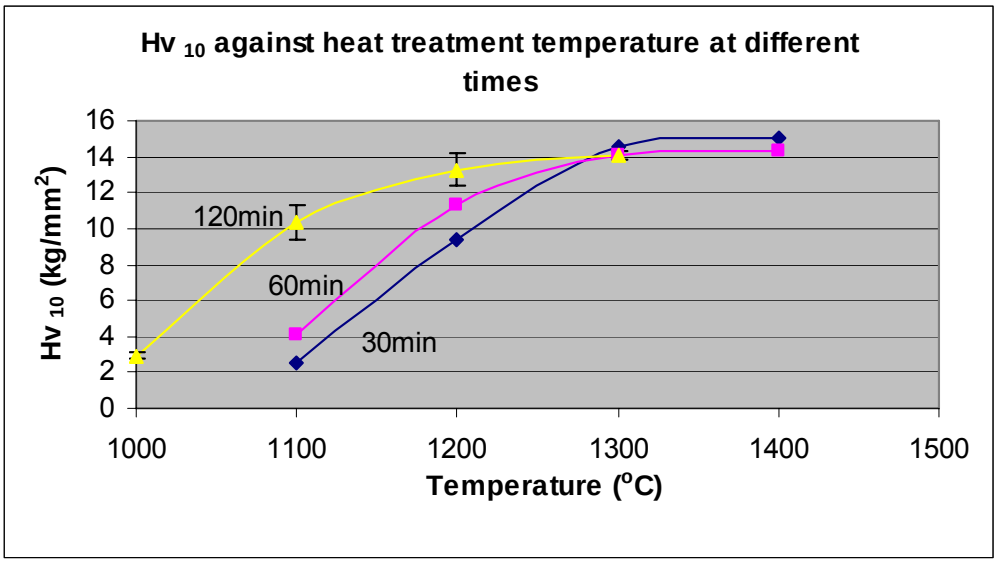

Figure 7.12: Vickers hardnesses of the samples initially containing 50 vol. % Al and cBN (12 µm) heat treated at different temperatures and times

The results in Figure 7.12 show that the Vickers hardness increases with increasing dwelling time. The hardness after 120 min at 1 100 ^{o}C is more than double that after 60 min at the same temperature. The change in hardness can be associated with the conversion of the soft Al phase to the harder phases (AlB_2 and AlN). As expected, the Vickers hardness increases with increasing temperature. At higher temperatures, Al converted faster and more completely into AlB_{12} and AlN. However, there is no visible change in hardness from 1 300 to 1 400 ^{o}C. The results suggest that further increase in temperature (above 1 300°C) did not improve the hardness to more than 15 GPa. This hardness is lower than the hardness measured for the sample containing 50 vol. % 3 µm cBN.

7.5 Discussion of the results from hot pressing

A number of different experiments were carried out using the hot press with different initial grain sizes of cBN powder, heating rates, densification temperatures, heat-treatment temperatures and times. Initially, hot pressing was done in an argon atmosphere. The relationship between density and hot-pressing conditions is presented in Figure 7.13 for samples using 3 µm cBN, pressed under argon and vacuum.. Hot pressing in vacuum resulted in better density compared with hot pressing in argon, and hence all subsequent experiments were done in vacuum.

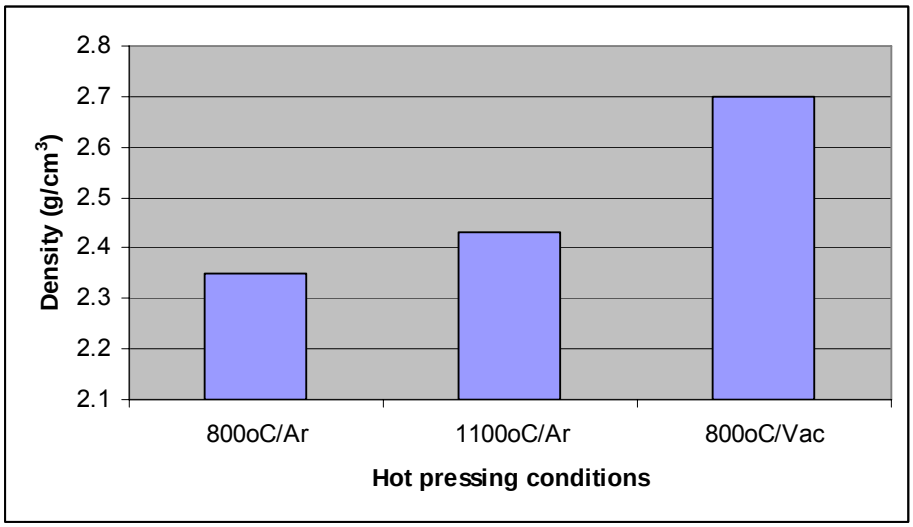

Figure 7.13: The relationship between density and hot-pressing conditions when 30 vol.% Al was used with 3 µm cBN.

(Samples used from table 7.1 and 7.2: cBN3-30-N1, cBN3-30-N2, cBN3-30-N4)

Although the density improved with hot pressing in vacuum, it was still low with a porosity of about 17%. Sinter forging of the sample did not improve the density. To obtain an optimum density, the Al concentration was varied from 20 to 50 vol. %. The relationship between the density and Al concentration is shown in Figure 7.14. The graph shows that the density increase due to reduction in porosity is almost directly proportional to the Al concentration. The highest density obtained, 2.80g/cm^3, when 50 vol. % Al was used, was 91.0% of the theoretical density. The amount of Al used during hot pressing has a direct effect on the mechanical properties of the final material, e.g. a high amount of Al will result in low hardness (refer to Chapter 3).

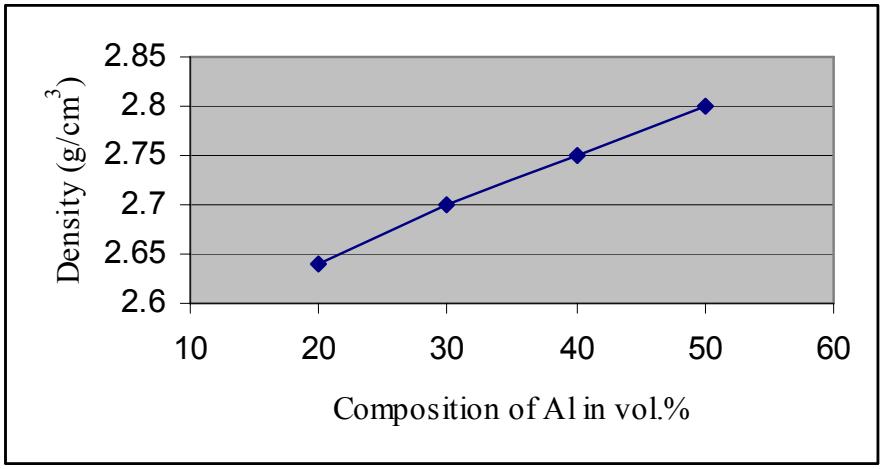

Figure 7.14: Graph showing the relationship between the density and Al concentration of the samples hot pressed at 800 ^{o}C for 30 min under 50 MPa

(Samples used from table 7.2: cBN3-20-N2, cBN3-30-N4, cBN3-40-N3, cBN3-50-N1)

To improve the density of the hot-pressed samples while using minimum Al content, the green density of the powder mixture was optimized. Four different grades of cBN crushed powders were mixed together to obtain an optimum green density. Green densities of about 70% were achieved. The graph in Figure 7.15 shows the densities obtained when 30 vol. % Al was mixed with multimodal crushed cBN powders. The results showed that the samples cold pressed before had better densities. The samples hot pressed at higher temperatures had even higher porosities. The XRD results show that the reaction rate of Al and cBN to form AlN and AlB_2 increases from 1 000 ^{o}C upwards. The formation of these phases further retards the densification, and hence porous samples result.

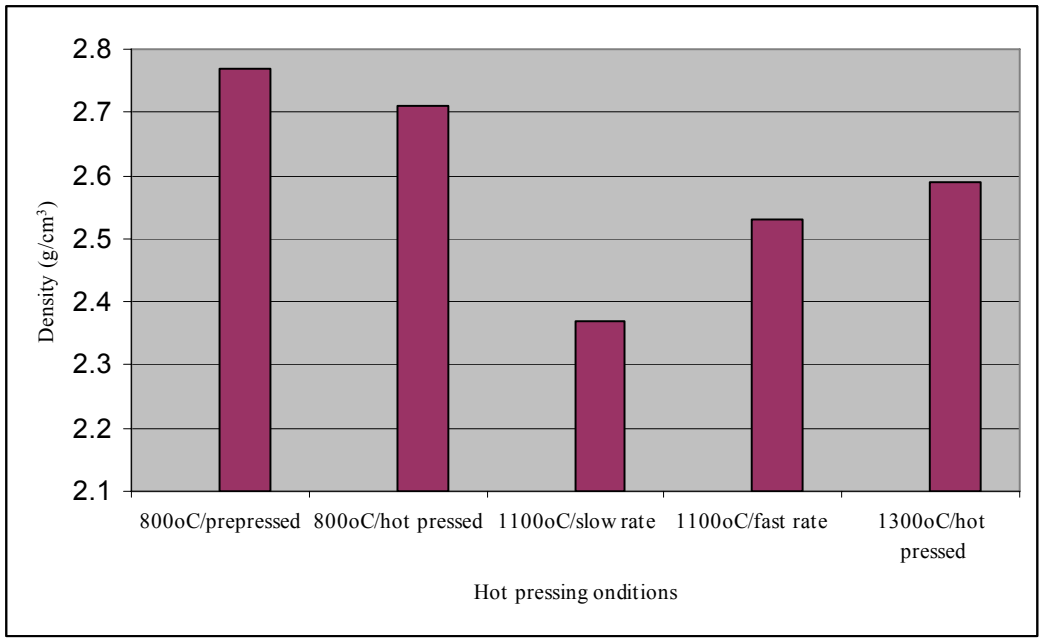

Figure 7.15: Graph of the densities of the samples containing 30 vol. % Al hot pressed under different conditions

(Samples used from table 7.7: McBN30-N4, McBN30-N5, McBN30-N7, McBN30-N8, McBN30-N11)

Although the green densities were more than 70%, Figure7.16 shows that the densities of the hot-pressed samples were not improved in comparison with the corresponding monomodal cBN samples. The effectiveness of using multimodal cBN would be clearer if a smaller amount of Al, i.e. less than 15 vol. %, was used. In this case some of the open pores could be closed by the fine cBN grains present in the multimodal system. When a high amount of Al, i.e. 30 vol. % is added, the densification during prepressing and hot pressing is controlled by the plastic deformation or

viscous flow of Al. Hence the differences in density of the samples made from monomodal or multimodal cBN are minor.

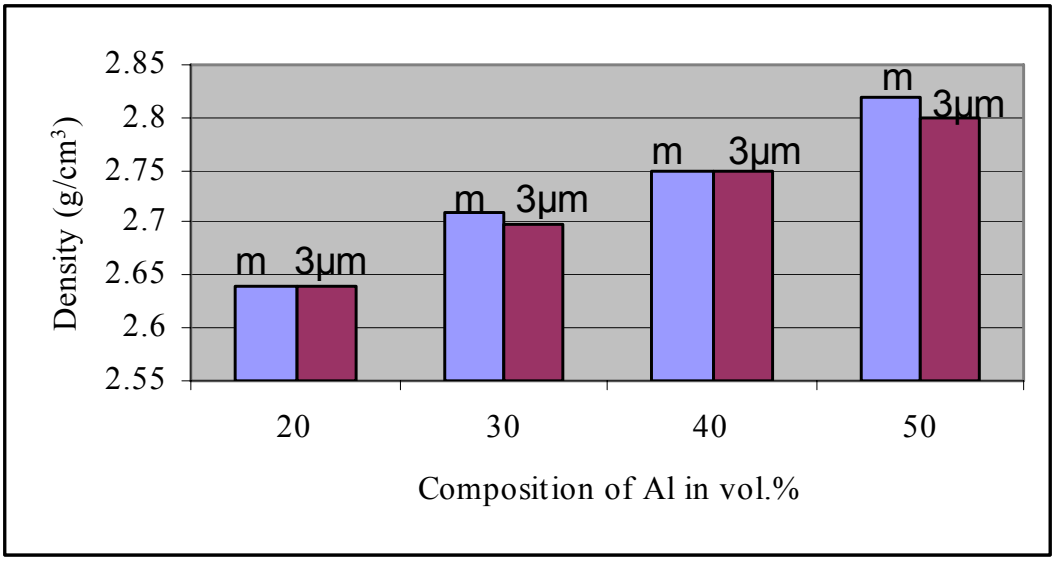

Figure 7.16: Graph showing the densities as a function of Al concentration for both monomodal and multimodal cBN hot pressed at 800 ^{o}C for 30 min under 50 MPa.

(Samples name from left to right: McBN20-N1,cBN20-N2,McBN30-N1,cBN30-N3, McBN40-N1,cBN40-N3, McBN50-N2 and cBN50-N1) (NB: m = multimodal)

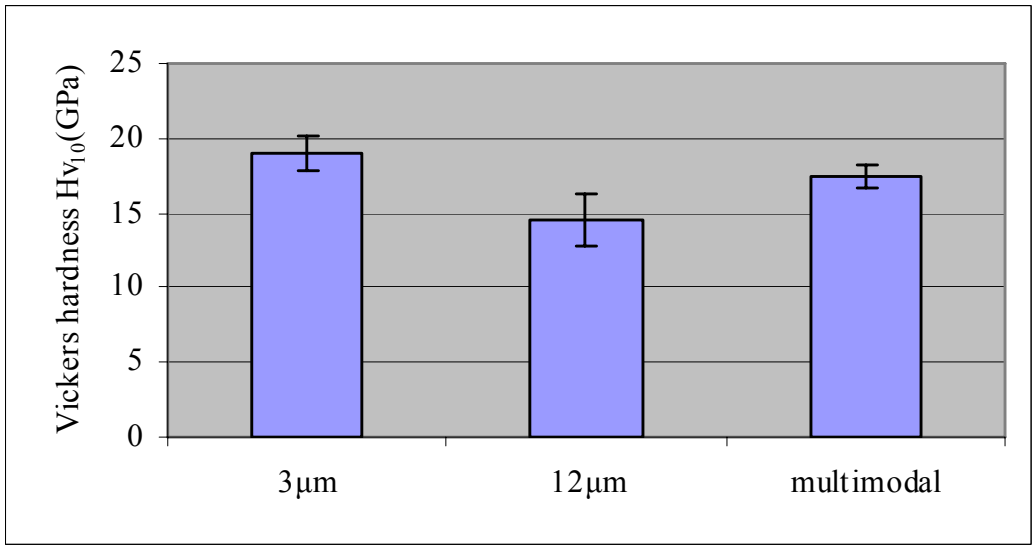

Figure 7.17: Vickers hardness measured on the hot-pressed samples annealed at 1 300 ^{o}C for 60 min

(Sample name from left to right: cBN3-50-N1HT13-1, cBN12-50-N1HT13-1, McBN50-N1HT13-1)

The Vickers hardness measured on the annealed samples is shown in Figure 7.17. The lowest hardness was measured on the cBN12-50-N1HT13-1 sample, while the cBN3-50-N1HT13-1 sample showed the highest hardness. This was expected since the hardness increases with decreasing particle size. The use of multimodal cBN did not improve the hardness. Since the densities of monomodal and multimodal cBN were similar, the hardness of multimodal cBN could be lowered due to the coarse cBN particles present.

The hardness obtained in Fig. 7.17, which was below 20 GPa, is low for a material to be used in the wear industry. Thus there was a need to determine the cause of the problem and how it could be overcome. SEM analysis (e.g Figure 7.4) shows that the material is composed mainly of the AlN phase, instead of the cBN phase. Since 50 vol. % of Al was added initially, this Al reacted with the cBN to form AlN. This is a problem since the initial 50 vol. % cBN would be reduced through its reaction with Al, and hence the higher amount of Al present initially would result in more cBN reacting and less of the cBN phase being present in the final material (e.g. 20 vol. % of Al will react with 9 vol. % of cBN shown in Figure 3.2). Aluminium nitride has a low hardness than cBN and this may be the reason for the low hardness present in the final sample. This assumption is supported by the calculation of the amount of the cBN phase used up during the reaction (Chapter 3). It is evident that there is a great need to reduce the amount of the initial vol. % of Al to improve the hardness of the material. The main problem was that reducing the amount of Al resulted in materials with low hot-pressed density. Use of the multimodal cBN mixture did not improve the density, as discussed above. When 30 vol. % Al was added (expected to fully densify material since green density of more than 70% was obtained), the open porosity of the final material was measured to be about 12%.

The results showed that there is poor wetting of the cBN by Al at a hot-pressing temperature of 800 °C. At higher temperatures, the reaction of Al with BN starts and this retards the densification. These findings are in agreement with the wetting angles of Al on hBN observed by Xue *et al.* (1992). The measured wetting angle in the Al-hBN system at 800 ^{o}C is about 140°. The angle decreases as the temperature increases. The infiltration of Al into BN will begin to take place spontaneously when the wetting angle becomes less than 90° at temperatures above 950 ^{o}C. However, the samples hot pressed at higher temperatures, e.g. 1 000 ^{o}C, showed some Al remaining, but also the presence of the AlN and AlB_2 phases. These phases prevent the Al from

spreading and can form bridges between the BN particles, reducing the rearrangement of cBN. It is thus important to allow densification to take place at 800 ^{o}C before reaction.

To change the wetting angle in this system, the cBN powder was coated with 8 vol. % Al compound. However, the the sample hot pressed had an open porosity of 11% (McBN50-N7) . This means that the coating did not improve the wetting. The Al compound coating the cBN consists mainly of AlN. Fujii *et al.* (1993) reported that the Al-AlN is also a non-wetting system. The contact angle between liquid Al and AlN is approximately 130°, as shown in Figure 7.18. Included in this figure is the relationship between the contact angle and the temperature in the Al/BN system. This may be the reason why the coating of cBN by the Al compounds did not improve the wetting of the cBN particles by Al, and hence the densification of the green compact did not improve.

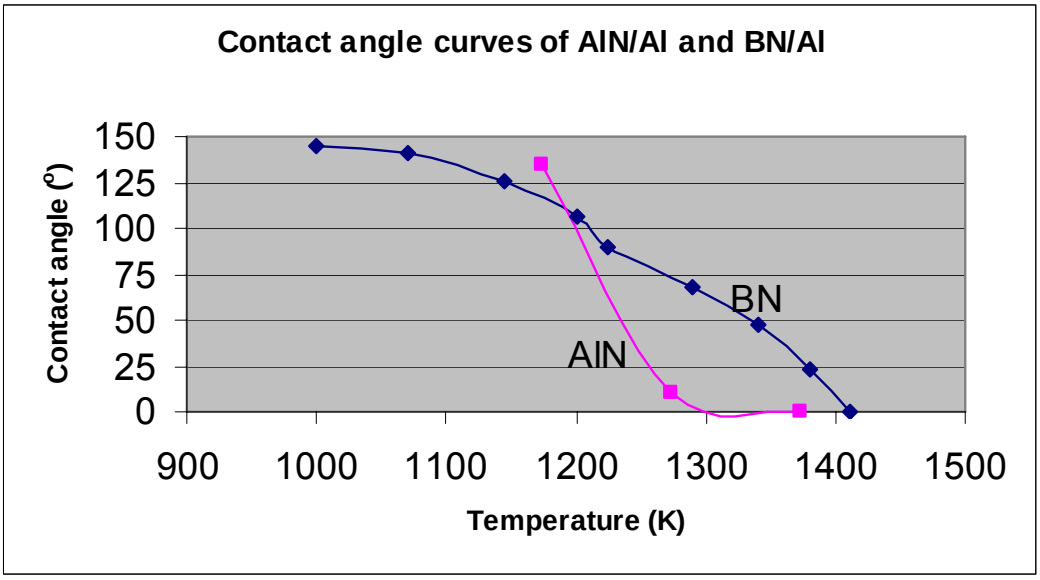

Figure 7.18: Contact angle curves of the Al/AlN [Fujii *et al.* (1993)] and Al/BN systems [Xue *et al.* (1992)]

To understand the wetting and the interaction of Al and BN, a sample McBN30-N1 was polished using an ion beam technique. It was necessary to use this technique since the polishing of the sample containing the hard BN and the soft aluminium metal by metallographic methods resulted in the pulling out and destruction of the soft Al phase.

SEM images of the microstructure of sample McBN30-N1 hot pressed at 800 °C are shown in Figures 7.19a to 7.20. Clearly visible are the dark phase of cBN and the light phase of Al homogeneously distributed throughout the sample. The amount of Al added seems to be enough

to fill all the pores. However, larger magnifications (Figures 7.19b and 7.20) reveal the existence of porosity in different areas. The EDX analysis indicates that at the interface between Al and BN, and between Al and the porous oxide phase containing different amounts of Al and B, in some cases silicon is also formed. The boron detected could be coming from the neighbouring BN grains or it could be part of the oxide phase. Figure 7.20 shows that between the cBN grains a glassy phase probably being formed containing alumina, boron oxide and silica. Alumina is also found within the aluminium phase, as labelled in Figure 7.20.

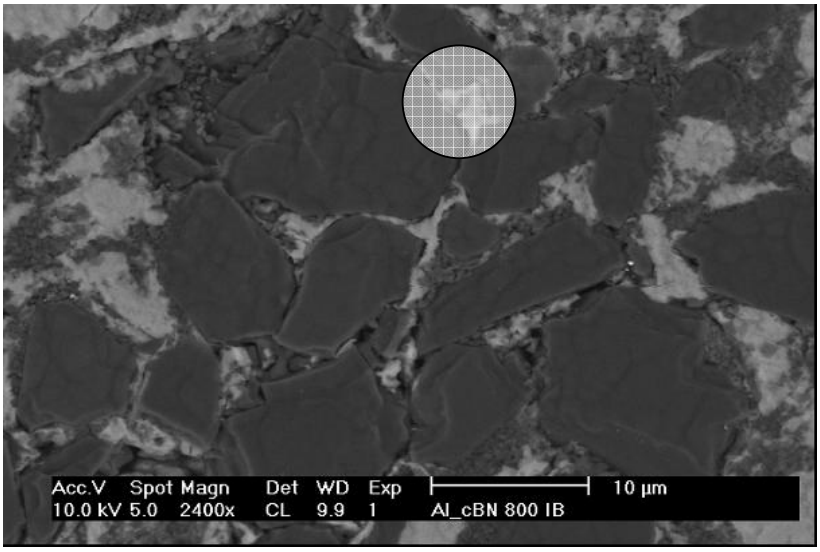

Figure 7.19a: McBN30-N2 sample as hot pressed at 800 ^{o}C

The dark phase is cBN and the light phase is Al. (Area in the circle enlarged in Figure 7.20b.)

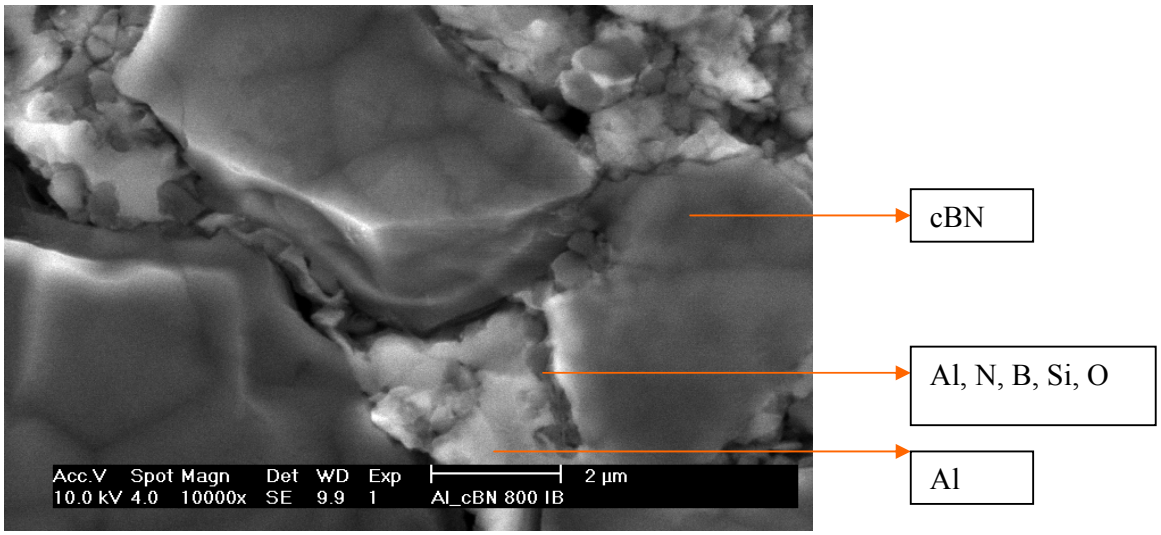

Figure 7.19b: McBN30-N2 sample as hot pressed at 800 ^{o}C

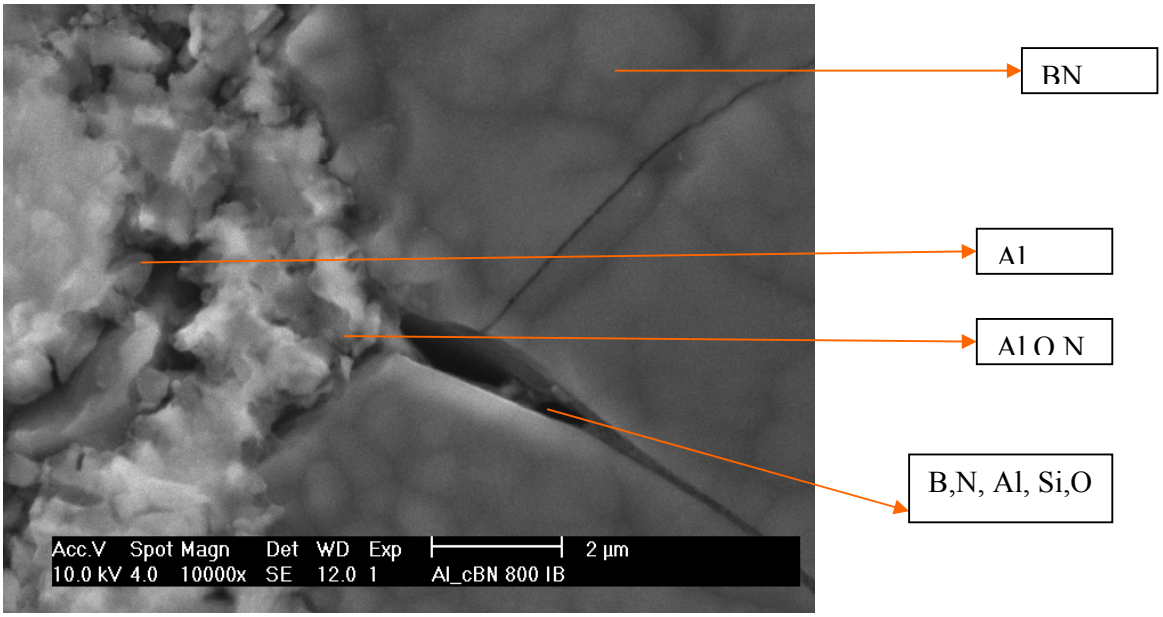

Figure 7.20: McBN30-N2 sample as hot pressed at 800 ^{o}C

There is a microstructural evidence of poor wetting between the Al and cBN. In order to control this, additional pressure of about 50 MPa was applied during hot pressing. This pressure was supposed to be sufficient to force the Al through the cBN. There is also evidence that the wetting is strongly affected by the oxide phase found in the boundary between Al and BN The observed oxide phases block the path of liquid Al during densification. Fujii e*t al.* (1993) reported that an aluminium oxide film formed on the aluminium surface (due to oxidation) which seems to prevent the interface of Al with hBN from advancing and the contact angle from decreasing to low values. Therefore, it is likely that both the aluminium and silicon aluminium oxide layers which were found in the boundary between Al and cBN have a decisive influence on the densification, retarding the spreading of Al between the cBN grains. No alumina was found in regions where segregations of the small cBN particles occur.

The influence of these oxide layers is greatly reduced when coarse Al powders are used. The reason for this lies in the fact that coarse powders have a lower specific surface area compared to fine ones, and therefore the amount of aluminium oxide in them is expected to be less Also, the influence of the oxide layers is further reduced by large pores available in coarse powder. Hence, the much coarser hBN powder (above 40 µm) densified to almost 100% of the theoretical density.

CHAPTER 8 CONCLUSIONS AND FUTURE WORK

The reaction of Al and cBN was investigated using samples containing 50 vol. % Al and 50 vol. % cBN (12 μm) hot pressed at 800 ^{o}C (chapter 5). The prepared samples were allowed to react isothermally at temperatures between 1 000 ^{o}C and 1 400 ^{o}C under nitrogen (N_2) and argon (Ar) atmospheres. The effects of both atmospheres on the reaction kinetics in the Al-cBN system were investigated. It was found that the degree and rate of the reactions increased with increasing temperature in both the N_2 and Ar atmospheres. The rate and degree of aluminium nitride (AlN) formation was considerably higher under N_2 than under Ar. The difference in the formation of AlN between the two atmospheres was attributed to the partial nitridation of Al due to the nitrogen. This process takes place because of the open porosity. The amount of aluminium diboride (AlB_2) that was formed at 1 100 ^{o}C increased as the temperature was increased to 1 200 ^{o}C. However, the amount of AlB_2 decreased above 1 300 ^{o}C as the aluminium dodecarboride (AlB_{12}) increased.

The study of the infiltration of an hBN matrix with molten aluminium was successful (section 6.1). This was done at a temperature of 800 ^{o}C and a pressure of 12 MPa. The SEM microstructure of the sample shows that the Al phase is homogeneously distributed in the hBN matrix. The lowest optimum temperature for the reaction between Al and hBN was found to be 1 300 ^{o}C for a period of 1 h. The amount of the AlN phase increases with increasing temperature, although very little increase was observed above 1 300 ^{o}C. This must be due to the depletion of the free aluminium present above 1 300 ^{o}C. All the composite materials prepared were found to be more than 97% dense. From this study it was concluded that 1 300 ^{o}C will be used as an optimum temperature in the reaction of Al and BN.

The heat treatment of the 12 μm cBN powder at 1 350 ^{o}C after soaking for 12 h revealed that about 40% hBN phase formed on the surface of the cBN powder (section 6.2). The infiltration of the partially hexagonalized cBN matrix with molten aluminium was equally successful under the same conditions used for the hBN matrix. The sample that initially contained 40 vol. % hBN and 60 vol. % cBN was found to be 98% dense. At temperatures below 1 300 ^{o}C, the amount of the hBN phase decreases due to its reaction with aluminium. However, above 1 300 ^{o}C, the volume of the hBN phase increases again, resulting in poor hardness of the final material. The conclusion reached was that to improve the mechanical properties no hBN phase must be present in the material.

Cubic boron nitride powder (12 μm) without hBN was also infiltrated with Al (section 6.3). The Al reacted with the cBN and no hBN was observed at temperatures below 1 400 ^{o}C. The resulting product showed improved hardness compared with that obtained with the partially hexagonalized cBN matrix. However, the infiltration of the 3 μm cBN powder was not successful (section 6.4).

The density achieved for the hot pressed cBN composite material was 91% of the theoretical density and it was obtained in a composite containing 50 vol. % Al (chapter 7). When the finer cBN particle sizes were used, the densities achieved were independent of the different particle sizes of cBN used (3 μm, and broad multimodal distributions). However, in the case of the monomodal 12 μm cBN powder, the density was more than 96% of the theoretical density.

There is clear evidence of poor wetting between Al and cBN at low temperatures and of relatively fast reaction between Al and cBN at higher temperatures. Both occurrences reduce the densification. The evidence from SEM showed that the poor wetting is probably caused by the oxide layers that form on the surface of the Al particles. The oxide layers, identified as silica and alumina, block the path of the Al, resulting in poor densification.

It was concluded that the infiltration of cBN by Al without mixing of the two powders resulted in better wetting. The success can be attributed to the use of Al sheets instead of Al powder. The Al sheets have less oxide since they have less surface area than the Al powder. For future work, Al powder with larger particles should be used during hot pressing. The use of larger particles with a smaller surface area should reduce the Al_2O_3 on the Al powder.

It was found that it is more difficult to infiltrate fine cBN powder than coarse cBN powder. As the surface area of 3 μm cBN powder is high compared with that of 12 μm cBN powder, it is to be expected that the 3 μm cBN powder will have a higher amount of oxygen trapped inside it than the 12 μm cBN powder. This will result in the formation of a passive alumina layer between the Al and BN, thus blocking the path of the Al into the open pores. The small pores present will make infiltration even more difficult. In future, the cBN powder should be washed prior to infiltration or hot pressing. Methods for washing cBN powders do exist. The best method used at our laboratory involves the use of methanol. This treatment will remove the B_2O_3 oxide layers which may be present on the surface of the powder.

The use of multimodal cBN powder did not improve the density of the hot-pressed samples. Thus, in future, powders of less than 3 μm should not be used because finer powders will not improve the densification. In addition, faster interaction with the Al is expected.

The samples initially cold pressed showed better densification. In future experiments, samples cold pressed under high pressure (~500 MPa) should be used. This may result in improved densification.

Hot pressing of the sample at 800 ^{o}C and heat treatment under pressure was not explored enough. Heat treatment under pressure, as in sinter forging (explained in section 7.1), needs to be explored.

The hardnesses measured on the samples containing 50 vol. % Al after heat treatment at 1 300 ^{o}C for 1 h were 14.5 ± 1.8 GPa, 17.5 ± 0.8 GPa and 19 ± 1.2 GPa for 12 μm cBN, multimodal and 3 μm cBN respectively. The graph in Figure 3.2 shows that the maximum hardness to a first approximation that can be obtained from the 50/50 compositions is 20 GPa. For future work, the maximum amount of 30 vol. % Al should be used to achieve a respectable Vickers hardness of about 30 GPa. To improved densification while using lower Al content a reduction of the oxide content of the green samples is required.

REFERENCES

Avner, S.H.(1974) *Introduction to Physical Metallurgy*, 2nd edition, Macgrow Hill publication.

Bartl, A., Bohr, S. Haubner, R. and Lux, B. (1996) A comparison of low-pressure CVD synthesis of diamond and cBN, *International Journal of Refractory Metals and Hard Materials*, **14:** 147-157.

Benko, E., Morgiel, J. and Czeppe, T. (1997) BN sintered with Al: Microstructure and hardness, *Ceramics International*, **23:** 89.

Bezhenar, B.N.P, Bozhko, S.A., Belyavina, N.N. and Markiv, V.Ya. (1999) Point defects in crystal lattices of cubic boron nitride and aluminium nitride depending on conditions of sintering cBN-AlN composite materials, *Journal of Superhard Materials*, **21:** 72.

Bhaumik, S.K., Divakar, C. and Singh, A.K. (1993) Processing, properties and application of Polycrystalline Cubic Boron Nitride (PCBN) cutting tools, *Metals materials and processes*, **3**:199.

Bodkin, R. and Liversage, J. (2003) Guide to using the hot press, *University of Witswatersrand*,SA.

Bodkin, R. (2005) A Synthesis and Study of $AlMgB_{14}$, *University of Witwatersrand*, SA.

Dove, S.B. (2001), UTHSCSA Image Tool, ddsweb@uthscsa.edu

Element Six (2000), Cubic Boron Nitride abrasives, www.e6.com

Endo, T., Fukunanga, O. and Iwata, M. (1981) The synthesis of cBN using $Ca_3B_2N_4$, *Journal of Materials Science*, **16:** 2227.

Eremets, M.I., Takemura, K., Blank, V.D., Sato, Y. *et al*. (1998) Disordered state in first order phase transitions: Hexagonal-to-cubic and cubic-to-hexagonal transitions in boron nitride, *Physical Review B*, **57:** 5655.

European Patent: EP 0598 140 A1, Mitsubishi Materials Corporation.

Fujii, H., Nakae, H. and Okada, K. (1993) Interfacial reaction wetting in the boron nitride/molten aluminium system, *Acta Metallurgica et Materialia,* **41:** 2963.

Fukunanga, O. (2000) The equilibrium phase boundary between hexagonal and cubic boron nitride, *Diamond and Related Materials,* **9:** 7.

Fraunhofer Institute, Germany on www.iaf.fgh.de

German, R.H. (1996) *Sintering Theory and Practice*, John Wiley and Sons Inc., New York.

Hao, X.P., Cui, D.L., Shi, G. X., Yin, Y.Q., Xu, X.G., Wang, J.Y., Jiang, M.H., Xu, X.W., Li, Y.P. and Sun, B.Q. (2001) Synthesis of cBN at low-temperature and low pressure conditions, *Chemistry of Materials*, **13:** 2457.

Hara, A. and Yazu, S. (1979) Sintered Cutting Tool and Manufacturing Process, Japan Patent Application Number 21633.

Krawitz, A.D. (2001) Introduction to Diffraction in Materials Science and Engineering, John Wiley and Sons, USA.

Larsson, P. Axen, N., Ekstrom, T., Gordeev, S., Hogmark, S. (1999) Wear of a type of diamond composites, *International journal of refractory metals and hard materials*, **17**:453.

Luyckx, Prof. S. (2004), University of Witwatersrand , Private communication.

McCulloch, D.G., McKenzie, D.R and Coringe, C. M. (2000) *Ab initio* study of structure in boron nitride, aluminium nitride and mixed aluminium boron nitride amorphous alloys, *Journal of Applied Physics,* **88:** 5028.

Munro, R.G. (1997), Material Properties of a Sintered α-SiC, Journal of Physical and Chemical Reference Data, **26**, 1195

Nakano, S., Ikawa, H.I, Fukunaga, O. (1992) Synthesis of cubic Boron Nitride by decomposition of magnesium boron nitride, *Journal of American Ceramic Society*, 240.

Osipova, I.I.and Shvedkov, E.L. (1992) Cutting ceramics 1985-1990, *Soviet powder metallurgy and metal ceramics*, **31**:751.

Porter, A and Easterling, K.E. (1992) Phase transformations in metals and alloys , 2nd edition., CRC Press.

Reed, J.S. (1995) *Principles of Ceramics Processing*, 2nd edition, John Wiley and Sons Inc., New York.

Rizzoli, C., Salamakha, P.S., Sologub, O.L. and Bocelli, G. (2002) X-ray investigation of the Al-B-N ternary system: isothermal section at 1500°C: Crystal structure of the $Al_{0.185}B_6CN_{0.256}$ compound, *Journal of Alloys and Compounds***, 343:** 135.

Rogl, P. and Schuster, J.C. (1992) Phase Diagrams of Ternary Boron Nitride and Silicon Nitride Systems, *The Materials Information Society*, USA.

Rong, X.Z. and Fukunaga, O. (1993) Cubic BN-WC-Co composite sintered at high pressures and high temperatures, *Diamond Film Technology*, **3:** 65.

Rong, X.Z. and Fukunaga, O. (1994) Sintering of cubic boron nitride with added aluminium at high pressure and high temperatures, *Transactions: Materials Research Society of Japan*, **14B:** 1455.

Rong, X.Z., Tsurumi, T., Yano, T. and Fukunaga, O. (2002) High-pressure sintering of cBN-TiN-Al composite for cutting tool application, *Diamond and Related Materials*, **11:** 280.

Schmid H.K.(1993), TEM-Studies on the microstructure/micro-chemistry of Boron Nitride cutting tool materials, *CSIR Report*.

Shaffer, P.T.B., Schorr, J.R and Hexemer, R.L. (1989), Green Light to Aluminum Nitride, Ceramic Industry, **132**, 25.

Simelane, T.N. (2004) University of Johannesburg, Private communication.

Skeleton Technologies (2000) Materials for the Future, info@skeleton-technology.com.

Smith, D.M. and Stermer, D.L. (1987) Powder Technology, **53**, 23.

Solozhenko, V.L. (1994) New concept of BN phase diagram: an applied aspect *Diamond and Related Materials*, **4:** 1.

Spear, K.E. (1989), Diamond - Ceramic Coating of the Future, Journal of the American Ceramic Society, **72**, 171

Standish, N. Yu, A.B. and Zou, R. P. (1991) *Optimisation of coal grind for maximum bulk density, Powder Technology*, **68**: 175.

Sumitomo Electrical Industries (2000) http://www.sei.co.jp

Sumitomo Patent: EP 0 386 338 A1.

USA patent No: 5 151 107, Norton Company.

USA Patent: PCT/US96/07014.

Vaben,R., Forester, J., Stover, D. (1995) Toughening of SiC ceramics by a bimodal grain size distribution produced by hipping ultrafine and coarse grained SiC powders, *Nanostructured Materials*, *6*: 889.

Walnsley, J.C. and Lang, A.R. (1987) A transmission electron microscope study of a cubic boron nitride-based compact material with AlN and AlB_2 binder phases, *Journal of Materials Science*, **22:** 4093.

Wentorf, R.H. and Bundy, F.P. (1980) Sintered Superhard Materials, *Science*, **208:** 873.

Wentorf, R.H. (1961) Synthesis of the cubic form of boron nitride, *Journal of Chemical Physics*, **34:** 809.

Wort, C.J.H., Sweeney, M.A., Copper, G.A. and Sussmann, R.S.(1994), Thermal Properties of Bulk Polycrystalline CVD Diamond, **3**, 1158.

Xue, M., Wang, J.T. and Zhao, F.M. (1992) Penetration and adhesion behaviour of boron nitride by liquid aluminium, *Journal of Materials Science Letters*, **11:** 199.

Yazu, S., Kohno, Y.,Satu, S. and Hara, A. New cBN-TiN composite sintered under ultra high pressure, *Sumitomo electric Industries limited.*

Yu, A.B. and Standish, N. (1993) A study of the packing of particles with a mixture size distribution, *Powder Technology*, **76**: 113.

Zhang, W.J. and Matsumoto, S. (2000), The influence of experiment parameters on the growth of cBN films by bias-assisted direct current jet plasma chemical vapour deposited, Materials Research Society, **15**, 2677.

APPENDICES

Appendix A

Raw data used to plot reaction kinetics graph shown in chapter 5.

Table A.1 shows the data used to calculate the volume percentages of the different phases present in the material. The results shown in Table A.2 were obtained using five different peaks for AlN, four for Al, three for AlB_2 and one each for AlB_{12} and cBN. The reason for using average absolute intensities was to avoid the problem of texture which was more evident in the case of aluminium.

The first column in Table A.1 contains the angles at which the peaks occurred. The second column shows the absolute intensities obtained from the powder cell normalized with regard to volume. Some of these values were taken from Table 4.4, which includes the I_{JCPDS} card numbers. The values from the third to the sixth column are the experimental absolute intensities at different times. The last rows in these columns show the normalized average absolute intensities. To show how these values were calculated, an AlN phase obtained after 30 min is used:

$$\frac{I_{AlN}}{I_{Abs}^{AlN}} = \frac{1}{n}\sum_{i=1}^{n}\frac{I_{measured}^{angle}}{I_{Abs}^{angle}} \quad \text{.....} A1$$

$$= \frac{1}{5}\left[\frac{263.85}{384.48} + \frac{173.34}{240.24} + \frac{247.9}{361.23} + \frac{221.95}{233.88} + \frac{195.5}{208.08}\right]$$

$$= 0.796$$

From these values V% can be calculated using an equation similar to 4.7 which is described in Section 4.2.2.

$$V_{AlN} = \frac{\frac{I_{AlN}}{I_{Abs}^{AlN}}}{\frac{I_{AlN}}{I_{Abs}^{AlN}} + \frac{I_{Al}}{I_{Abs}^{Al}} + \frac{I_{cBN}}{I_{Abs}^{cBN}} + \frac{I_{AlB_2}}{I_{Abs}^{AlB_2}} + \frac{I_{AlB_{12}}}{I_{Abs}^{AlB_{12}}}} \times 100 \quad \text{.....} A2$$

$$= \frac{0.796}{0.796 + 0.182 + 1.07 + 0.059 + 0.32} \times 100 = 32.8\%$$

Table A.1: Data used to calculate the volume percentages shown in Table A.2 below

Angle 2θ (°)	Absolute I	30 min	60 min	120 min	180 min
AlN					
33.5	384.5	263.9	278.2	293.1	388.1
36.3	240.2	173.3	158.6	190.9	238.4
38.2	361.2	247.9	261.4	275.4	364.6
59.9	233.9	221.9	293.7	252.4	206.3
66.6	208.1	195.5	143.7	219.5	166.7
		0.797	0.811	0.891	0.939
Al					
38.5	916.0	76.7	119.9	142.4	50.7
44.7	443.1	18.7	62.9	30.7	1.4
65.1	281.2	134.0	65.7	45.4	27.3
78.2	325.5	40.4	25.5	51.3	17.0
		0.182	0.146	0.136	0.0520
AlB_2					
34.3	195.3	10.9	9.58	10.8	11.3
44.5	611.8	34.2	30.0	33.8	35.5
61.6	156.9	10.2	8.54	10.9	6.26
		0.0589	0.0508	0.0600	0.0520
cBN					
43.3	358.0	383.0	328.5	308.0	301.0
		1.07	0.918	0.860	0.841
AlB_{12}					
21.4	22.1	7.13	8.69	9.09	11.6
		0.322	0.393	0.411	0.522

Table A.2: Volume percent of the different phases obtained after the heat treatment of the samples at a temperature of 1 200 ^{o}C (used to plot the graph in Figure 5.4)

	30 min	60 min	120 min	180 min
AlN	32.8	35.0	37.8	39.0
Al	7.48	6.31	5.77	2.16
AlB_2	2.43	2.19	2.55	2.16
cBN	44.0	39.6	36.5	35.0
AlB_{12}	13.3	16.9	17.4	21.7

Table A.3: Volume percent of the different phases obtained after the heat treatment of the samples at a temperature of 1 100 ^{o}C (used to plot the graph in Figure 5.3)

	30 min	60 min	120 min	180 min
AlN	23.0	32.1	35.1	45.5
Al	10.3	9.89	6.21	1.96
AlB_2	9.57	7.99	4.51	2.48
cBN	57.1	50.0	45.1	38.8
AlB_{12}	0	0	8.70	10.9

Table A.4: Volume percent of the different phases obtained from the heat treatment of the samples at a temperature of 1 300 ^{o}C (used to plot the graph in Figure 5.5)

	30 min	60 min	120 min	180 min
AlN	43.3	45.5	46.1	51.0
Al	7.24	5.40	5.37	1.14
AlB_2	2.38	1.81	1.85	1.58
cBN	32.6	30.8	28.9	25.3
AlB_{12}	15.4	16.4	17.8	21.0

Table A.5: Volume percent of the different phases obtained from the heat treatment of the samples at a temperature of 1 400 ^{o}C (used to plot the graph in Figure 5.6)

	30 min	60 min	120 min	180 min
AlN	51.7	52.8	-	55.0
Al	2.01	1.38	-	0.228
AlB_2	1.59	1.27	-	0.879
cBN	29.4	26.2	-	24.3
AlB_{12}	15.2	18.4	-	19.6

Table A.6: Volume percent of the different phases obtained from the heat treatment of the samples at a temperature of 1 100 ^{o}C (used to plot the graph in Figure 5.8)

	30 min	60 min	120 min	180 min
AlN	17.6	24.3	27.6	30.5
Al	7.34	4.64	4.40	2.76
AlB_2	5.71	5.18	4.66	4.40
cBN	55.9	51.0	47.9	44.1
AlB_{12}	13.5	14.9	15.5	18.2

Table A.7: Volume percent of the different phases obtained from the heat treatment of the samples at a temperature of 1 200 ^{o}C (used to plot the graph in Figure 5.9)

	30 min	60 min	120 min	180 min
AlN	26.0	21.3	27.8	31.7
Al	3.61	1.45	1.46	0.832
AlB_2	4.63	6.96	4.66	3.46
cBN	48.8	37.1	43.0	38.7
AlB_{12}	17.0	33.2	23.1	25.3

Table A.8: Volume percent of the different phases obtained from the heat treatment of the samples at a temperature of 1 300 ^{o}C (used to plot the graph in Figure 5.10)

	30 min	60 min	120 min	180 min
AlN	31.9	32.9	34.0	34.5
Al	1.36	1.01	0.656	0.706
AlB_2	4.77	4.34	3.81	3.56
cBN	42.3	37.2	32.0	30.2
AlB_{12}	19.7	24.5	29.6	31.0

Table A.9: Volume percent of the different phases obtained from the heat treatment of the samples at a temperature of 1 400 ^{o}C (used to plot the graph in Figure 5.11)

	30 min	60 min	120 min	180 min
AlN	36.1	37.1	39.1	40.2
Al	1.26	0.972	0.925	0.435
AlB_2	2.67	2.25	2.02	1.69
cBN	39.6	36.6	32.8	28.5
AlB_{12}	20.4	23.0	25.1	29.3

Appendix B

UTHSCSA Image Tool used to perform image analysis (see Section 5.4)

UTHSCSA Image Tool is an image processing and analysis program for Microsoft Windows 95 or Windows NT.It was written using Borland's C++ version 5.0.2. Image Tool can acquire, display, edit, analyze, process, compress, save and print gray scale and color images. Image analysis functions include dimensional (distance, angle) and gray scale measurements (point,line and area histogram with statistics). Image Tool supports standard processing functions such as contrast manipulation, sharpening, smoothing, edge detection, median filtering and spatial convolutions with user-defined convolution masks. Image Tool also has built-in scripting capabilities which make it possible to record repetitive tasks and playback saved scripts to automate image analysis.

Image Tool provides for geometric transformations such as rotate, flip vertical and horizontal and magnification up to four levels. All analysis and processing functions are available at any magnification factor. The program is a multiple document interface application supporting any number of windows (images) simultaneously. In addition, spatial calibration is available to indicate measurements such as millimetres, microns, miles for linear and area.

The capabilities provided by the Image Tool (as described above) led to the conclusion that such program is suitable to be used in this work. Moreover, the program is available at no cost.

Appendix C

Fundamental concepts explaining the meaning of the results obtained from the Mastersizer 2000.

To understand the meaning of the results from the Mastersizer it is important to provide an explanation for a number of fundamental concepts. These fundamental concepts are:

- The results are volume based.
- The result is expressed in terms of equivalent spheres.
- How the distribution parameters are derived.

Volume based results

The first and probably most important point to remember in interpreting results is that the fundamental size distribution derived by this technique is volume based. This means that when the results indicates, that 15% of the distribution is in the size category 4.6-6.5 microns, this means that the total volume of all particles with diameters in this range represents 15% of the total volume of all particles in the distribution. This can be illustrated by using the following example: Suppose, for simplicity, that a sample consists of only two sizes of particle; 50% by number having a diameter of 1 micron and 50% by number a diameter of 10 microns. Assuming that the particles are spherical, the volume of each of the larger particles is 1000 times the volume of one of the smaller ones. Thus, as a volume distribution, the larger particles represent 99.9% of the total volume.

The Malvern software allows the results to be converted to distribution forms other than volume (such as a number distribution for exmple), but it should be remembered that the initial measurement is volume based and any subsequent conversions are liable to introduce systematic errors.

Equivalent spheres

Mie theory (described in section 4.1) presumes that the particles you are measuring are perfect spheres. In practice the situation is different since most particles have irregular shape. This causes a problem in the definition of the term “measure the particle size”. One way to describe the irregular shaped particle is to compare some feature of the actual particle to an imaginary spherical particle. Some typical methods of doing this are:

- Equivalent surface area. The diameter of the theoretical sphere that has the same surface area of the original particle can be calculated.
- Equavalent maximum length. This is where the diameter of a theoretical sphere is the same as the maximum dimension of the original particle.
- Equivalent minimum length. This is where the diameter of a theoretical sphere is the same as the minimum dimension of the original particle.

There are many other methods available to do this. This technique is known as "equivalent spheres". The Mastersizer uses the volume of the particle to measure its size.

Derived distribution parameters

The third point is that the analysed distribution is expressed in a set of size classes which are optimised to match the detector geometry and optical configuration giving the best resolution. All parameters are derived from this fundamental distribution.

Distribution parameters and derived diameters are calculated from the fundamental distribution using the summation of the contributions from each size band. In perfoming this calculation the representative diameter for each band is taken to be the geometric mean of the size band limits:

$$\sqrt{d_{i-l}d_i} \qquad \text{(C.1)}$$

This number will be slightly different to the arithmetic mean:

$$\frac{d_{i-l}+d_i}{2} \qquad \text{(C.2)}$$

For example, the size band 404.21-492.47 microns has a geometric mean of 446.16 microns and arithmetic mean of 448.34 microns. In most cases the difference is small but the geometric mean is chosen in these calculations as more appropriate to the logarithmic spacing of the fundamental size classes.

Appendix D

Model multimodal powder compositions (combination of different grades) derived from the packing model program

The packing model program (used in section 7.2) calculates the packing density of a mixture of powders where each has its own size distribution. The size distributions used should be volume size distributions. This program uses the linear-mixture packing model (Yu and Standish, 1993; Standish et al, 1991). The program allows one or more of the fractional solid volumes to be fixed. The program will allow the other values to change during the optimisation, but keep the ones specified fixed. The results obtained from this program are shown in table D1. Some of these results are shown in table 7.4.

Table D1: Calculated possible ratios of the cBN powders to obtain a maximum density

Model	Grade 1	Grade 2	Grade 4	Grade 9	Density (%)
1	0.2	0.334	0.332	0.134	76
2	0.2	0.36	0.183	0.257	77
3	0.563	0	0.261	0.176	78.2
4	0.549	0	0.322	0.129	78
5	0.589	0	0.118	0.293	77.9
6	0.44	0.123	0.224	0.213	78.1
7	0.518	0.043	0.288	0.151	78.1
8	0.552	0	0.41	0.038	78
9	0.552	0	0.343	0.105	78.2
10	0.2	0.351	0.234	0.216	77
11	0.55	0.044	0.005	0.4	77.9
12	0.522	0.039	0.254	0.185	78.2